



National Technical University of Athens
School of Electrical & Computer Engineering
Information Transmission Systems and Material Technology

*Development and Assembly of
Measurement Setup for Assessing
the Magnetic Behavior of
SpaceWire Links*

Thesis

Alexandros D. Bechrakis Triantafyllos

Alexandra P. Mavropoulou

Supervisor:

Prof. Christos N. Capsalis

Athens, April 2020



National Technical University of Athens
School of Electrical & Computer Engineering
Information Transmission Systems and Material Technology

*Development and Assembly of Measurement
Setup for Assessing the Magnetic Behavior of
SpaceWire Links*

Thesis

Alexandros D. Bechrakis Triantafyllos

Alexandra P. Mavropoulou

Supervisor:

Prof. Christos N. Capsalis

Approved by the three - member Inquiry Committee

A handwritten signature in blue ink, appearing to be 'X. Capsalis', written over a dotted line.

.....

Christos Capsalis

Professor NTUA

A handwritten signature in blue ink, appearing to be 'P. Cottis', written over a dotted line.

.....

Panagiotis Cottis

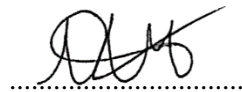
Professor NTUA

A handwritten signature in blue ink, appearing to be 'G. Fikioris', written over a dotted line.

.....

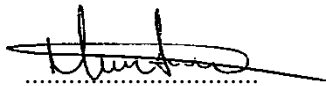
George Fikioris

Professor NTUA



Alexandros D. Bechrakis Triantafyllos

Diploma in Electrical and Computer Engineering NTUA



Alexandra P. Mavropoulou

Diploma in Electrical and Computer Engineering NTUA

Copyright © Alexandros D. Bechrakis Triantafyllos, 2018

Copyright © Alexandra P. Mavropoulou, 2018

All rights reserved.

It is prohibited to copy, store and distribute this work, in whole or in part, for commercial purposes. Reproduction, storage and distribution for a non-profit, educational or research nature are permitted, provided the source of origin is indicated and the present message maintained. Questions about the use of the work for profit should be directed to the author.

The views and conclusions contained in this document are those of the authors and should not be construed as representing the official positions of the National Technical University of Athens.

Abstract

An infeasible part of any space mission design is the interconnecting wiring of the mission's units. As a result, any emissions produced by the latter are of vital importance regarding the Electromagnetic Compatibility of the whole spacecraft design. The development of the SpaceWire standard has proven very advantageous for the space industry as it aims to standardize the process of creating a wired network in a spacecraft. The former, enhances the reusability of already developed components, making them compatible with new missions and therefore reducing their cost. Nevertheless, the widespread implementation of the SpaceWire standard has also increased the importance of assessing the potential for electromagnetic interference produced by a SpaceWire network. Towards this goal, within the context of the project "Modeling Electromagnetic Emissions of Space Equipment for EMC and Cleanliness Purposes" realized by the Wireless and Long Distance Communication Laboratory (WLDCL) of the School of Electrical & Computer Engineering of the National Technical University of Athens, the current thesis aims to develop a setup for measuring both the static and the ELF magnetic field emissions caused by the operation of a full-duplex SpaceWire link. Through these measurements, the potential for magnetic field emissions from the link will be evaluated and a thorough examination will be made to identify any correlation between the emissions' level and some of the transmission's characteristics. For the formation of the SpaceWire link, a suitable cable assembly is utilized in conjunction with an instrument simulating the interconnected nodes. The magnetic field emissions of the link are monitored, for several sets of link characteristics, with the use of two triaxial fluxgate magnetic field sensors. Any low frequency magnetic field emissions produced by the operation of a SpaceWire link can be attributed, inter alia, to alternating currents flowing through the ground loop, caused by the termination of the outer shield of the cable assembly. These currents can be induced to the conductive shield through inductive couplings between the latter and the signal carrying twisted wire pairs. Nonetheless, for a more complete analysis, several additional potential emission mechanisms will be discussed. The lack of any specialized magnetic shielding in the area of the measurements will be negated by the employment of a suitable measuring technique, in order to differentiate between the ambient field's components and any emissions caused by the operation of the link. Overall, an assessment of the behavior of the link regarding its static and ELF magnetic field emissions will be presented and some additional tests for future analysis will be proposed.

Keywords: Electromagnetic Compatibility, Low Voltage Differential Signalling - LVDS, Magnetic field measurements, SpaceWire

Table of Contents

ABSTRACT	5
1. THE SPACEWIRE STANDARD	8
1. INTRODUCTION	8
2. NETWORK LAYER.....	9
3. DATA LINK LAYER	10
4. ENCODING LAYER	12
5. PHYSICAL LAYER.....	14
i. Cables.....	14
ii. Inner Conductors.....	14
iii. Twisted Pair.....	14
iv. Complete cable.....	15
v. Shield details.....	16
vi. Connectors	17
vii. Cable Assemblies	17
viii. Low Voltage Differential Signalling	19
6. SPACEWIRE PORT	21
2. MEASURING LAYOUT & EQUIPMENT	22
1. INTRODUCTION	22
2. MEASUREMENTS.....	24
3. MEASURING EQUIPMENT.....	25
i. Magnetometers	26
ii. Power supply units	27
iii. Data acquisition unit (DAQ)	28
iv. iSAFT SpaceWire Simulator	30
4. EUT'S LAYOUT	37
3. EMISSION MECHANISMS & POTENTIAL EMISSION SPECTRUM	40
1. EMISSION MECHANISMS.....	40
i. Capacitive coupling	40
ii. Inductive coupling	41
iii. Shield grounding	42
2. CURRENT'S FREQUENCY SPECTRUM	47
i. Current's Waveform	47
ii. Fourier Analysis & Frequency Spectrum.....	51
iii. Frequency Spectrum for Undefined Payload.....	53
iv. DC component – Payload Correlation	55
4. MEASUREMENTS RESULTS.....	58
1. MEASURING LAYOUT.....	59
2. DC MAGNETIC FIELD EMISSIONS	61
3. AC MAGNETIC FIELD EMISSIONS	68
i. Discrete noise components in the low frequency range.....	68
ii. SpaceWire link's low frequency emissions	70
iii. Spectral power density axial distribution	84
iv. Emission Amplitude.....	86

CONCLUSION	87
BIBLIOGRAPHY	88

1. The SpaceWire Standard

1. Introduction

The existence of a global standard governing the connection methods between units and subsystems in the space industry would greatly enhance the cost-effectiveness and reliability of all designs. The potential for a designer to reuse a component enables the performance of more research with a smaller budget, whereas utilizing already developed and tested equipment can improve the reliability of the design. This prospect led the European Cooperation for Space Standardization (ECSS) to develop the SpaceWire standard. The first attempt was made in 2003 [1] and since then the standard has been reissued twice, in 2008 [2] and 2019 [3]. The aim of this standard is to define the properties of the links, nodes, routers, and networks used in the spacecraft design process. Since its inception, the SpaceWire standard has been adopted by many space agencies, such as ESA, NASA, JAXA and ROSCOSMOS. Some notable space mission utilizing this standard are Gaia, ExoMars, Bepi-Colombo and James Webb Space Telescope.

The main aim of this thesis is to measure the magnetic field emissions produced by the operation of a link designed with respect to the SpaceWire standard, or simply a SpW link. The latter is a point to point, full-duplex and bidirectional connection between two nodes of a spacecraft's network, so that both can receive and transmit simultaneously at rates from 2 Mbps to 400 Mbps. Even if the purpose of this thesis is to study SpW links, at this stage, a brief overview of the SpaceWire standard will be provided, based on the latest issue ECSS-E-ST-50-12C Rev.1 [3]. The overview aims to introduce the reader to the basic concept of the standard while emphasizing the aspects that concern this thesis, namely cable assemblies, signalling method, port architecture etc. It is without saying that the following should not be taken as a complete analysis of the standard.

The SpW standard can be partitioned in the following layers (**Figure 1-1**), as proposed by ECSS-E-ST-50-12C Rev.1 [3], in order to simplify its analysis.

- **Network layer:** Defines the structure of a SpW network (nodes, routing switches etc.) and the packets used.
- **Data Link layer:** Defines the link's state, the flow of information and error recovery.
- **Encoding layer:** Defines the encoding and serialization of the information to be sent in a state suitable for transmission in the physical

layer, as well as the decoding and deserialization of the signal received from the physical layer.

- **Physical layer:** Defines the physical components of the link (cables, connectors, drivers and receivers).
- **Management information base:** Defines the management of the user application's requests, as well as the monitor and control of the SpW layers.

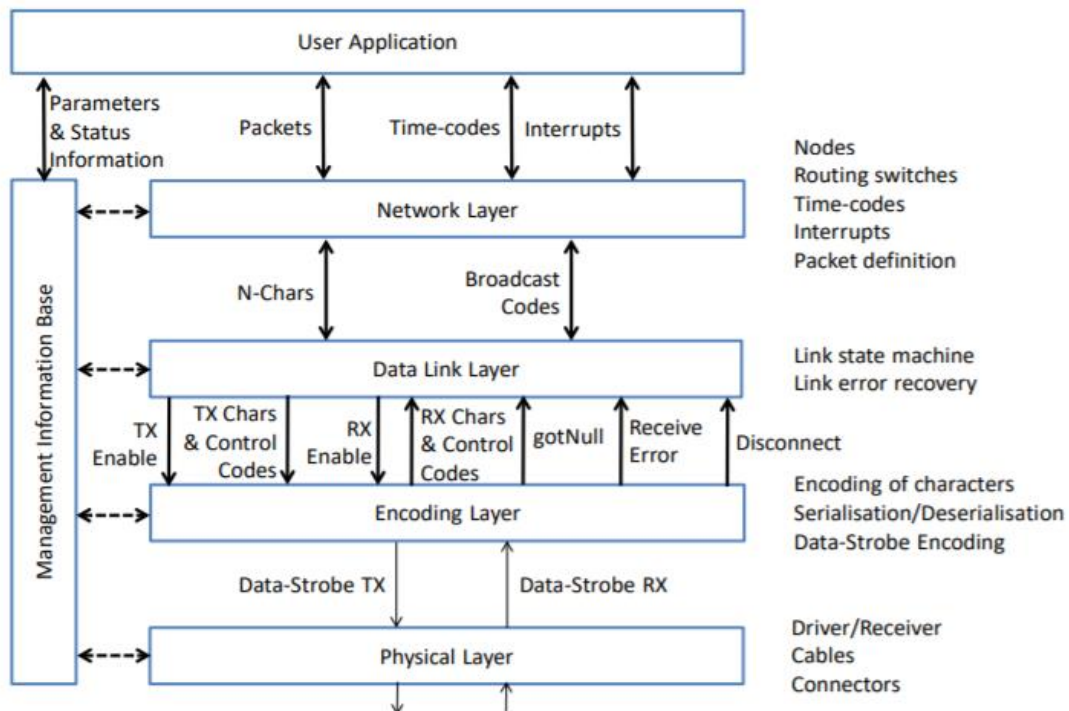


Figure 1-1. SpaceWire protocol stack, [3].

2. Network Layer

The SpW network is comprised of point to point links and routing switches, with each routing switch featuring no more than 31 ports. Data transmission through a SpW network is achieved using distinct packets. Each packet consists of the "Destination Address", the "Cargo" and the "End of Packet" or "Error End of Packet" (EOP or EEP), as illustrated in Figure 1-2.

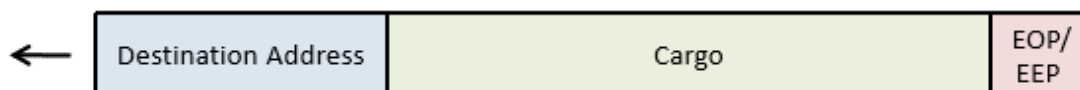


Figure 1-2. SpaceWire packet format [3].

The destination address is used to route a packet through a network, either by path or by logical addressing. If path addressing form is used, the

destination address consists of a path to be followed so that the packet can reach its final destination. The leading data character defines the port (0 to 31) the packet must take at the next routing switch and when used, it is removed from the destination address. In the case of logical addressing, the destination address is the destination's identifier. The identifier is in the range from 32 to 255 and every routing switch has a table matching each identifier with the port the packet has to take in order to reach the desired destination. The Cargo of a SpW packet consists of the data to be transferred, while the End of Packet (EOP) or the Error End of Packet (EEP) signal the packet's end. When EOP is used it implies the correct transmission of the packet and it signifies the beginning of the next one. On the other hand, if an error occurs while the Data Link Layer is at the "Run" state (see **clause 1.3**), an error recovery mechanism is activated. This mechanism terminates the packet in which the error was detected with Error End of Packet (EEP).

3. Data Link Layer

The Data Link Layer acts as an intermediate between the Network Layer and the Encoding Layer, controlling the flow of information over a SpW link as well as its establishment and its re-establishment after a disconnection. Additionally, the Data Link Layer is responsible for providing information about the status of each port, such as its state (Started, Connecting, Run, Error Reset, Error Wait, Ready), the values of the transmit and receive credit counters¹ for each port and the type of error occurred, if any has been detected (Error flags).

The state of a port, also called link's state, defines the operations that each port can perform (transmission, reception etc.). As already mentioned, a SpW link connects two ports, therefore it has two link states, the combination of those states governs the operation of the SpW link. All the possible states of a SpW link and their interconnections are depicted in the following state diagram (**Figure 1-3**).

It is worth mentioning the reaction of a SpW link to an error occurrence (the types of errors are listed in **Table 1-1**). When an error detection is triggered, regardless of its current state, the link's state changes to "Error Reset". At this state, the transmission and reception are ceased, via de-asserting the "Transmit/Receive Enable" control flags used to control the Encoding Layer's operation. If after 6.4 μ s all ports are enabled, the link state machine moves to the "Error Wait" state, where the reception is enabled, though without storing any received data. After 12.8 μ s, the state changes to "Ready" and builds up to

¹ Transmit and receive credit counters are utilized in a SpW port to implement the flow control mechanism.

“Run”, as shown in **Figure 1-3**. If an additional error occurs during this process, the state moves once again to “Error Reset” and the aforementioned procedure is repeated.

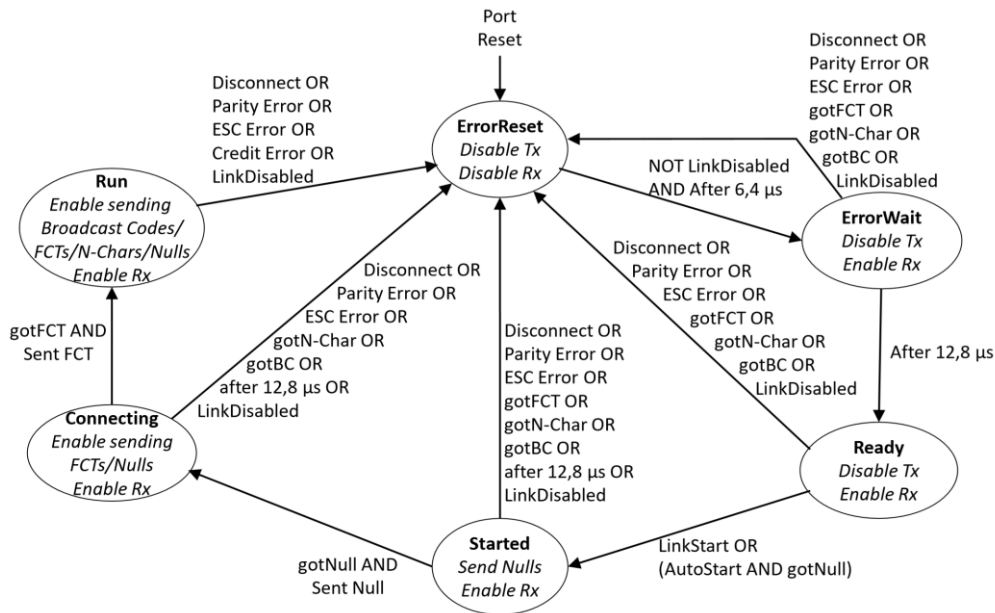


Figure 1-3. Link initialization behavior [3].

Error Types

Error	Detection method
Disconnect	The length of time since the last reception or transmission through the link is longer than a defined threshold.
Parity Error	The parity is not odd (an even number of bits is set to ‘1’).
ESC Error	An invalid combination of control characters is detected. Such combinations are: ESC-ESC or ESC-EOP or ESC-EFP.
Credit Error	Signifies an otherwise undetected error, noticed by unexpected values in the receiver’s or transmitter’s counter of a SpW port.
Link Disabled	A specified SpaceWire port is disabled.

Table 1-1. Error types and detection methods

An error occurrence while the link is at the “Run” state, triggers an error recovery mechanism. The recovery state machine moves from “Normal” to “Recovery” state, where an Error End of Packet (EEP) is written to the receive FIFO and the cause of the error is recorded. This allows the transmitter to identify the data that needs to be resent, thus ensuring reliable transmission. The state diagram of the error recovery process is depicted in **Figure 1-4**.

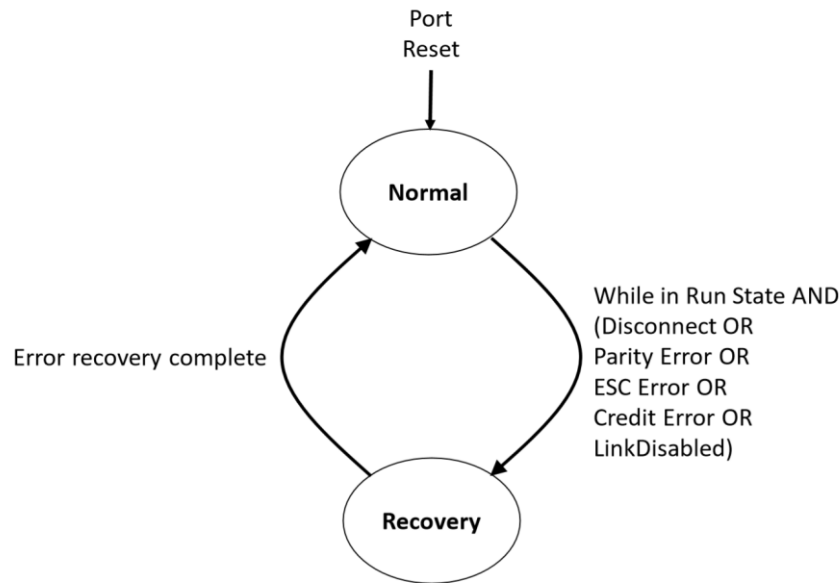


Figure 1-4. Link error recovery behavior [3].

4. Encoding Layer

The encoding layer encodes/decodes the characters into symbols, serializes/de-serializes the symbols into a bit stream and encodes/decodes the bit stream utilizing the data-strobe technique. The encoding layer uses two kinds of characters, data and control characters. Data characters consist of 10 bits, a parity bit, a data-control flag and 8 bits of data (Figure 1-5), while control characters consist of 4 bits, a parity bit, a data-control flag and 2 control bits (Figure 1-6).

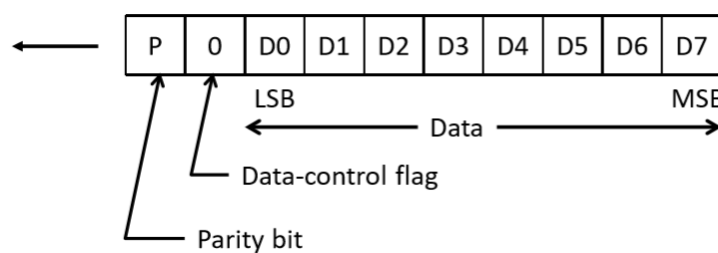


Figure 1-5. Data character encoding [3].

The parity bit assigned to each character is set to produce odd parity and is used to detect parity errors, while the data-control flag is used to differentiate between a data and a control character. Specifically, the data-control flag is set to zero in a data character and one in a control character. While data characters are utilized for data transmission, control characters are used either individually or to form control codes. There are four types of control characters, namely “Flow Control Token (FCT)”, “End of Packet (EOP)”, “Error End of

Packet (EEP) and “Escape (ESC)”, with their two-bit control types as defined in Figure 1-6.

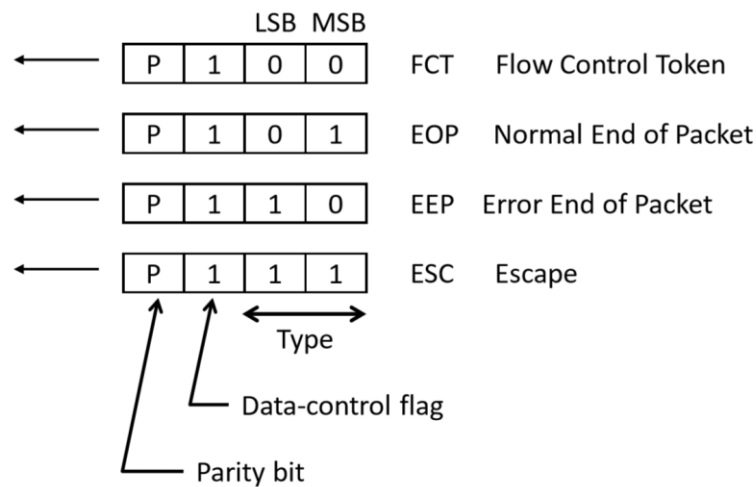


Figure 1-6. Control character encoding [3].

While EOP and EEP mark the normal or unforeseen termination of the transmission of a packet, FCT and ESC are incorporated in control codes. Specifically, ESC followed by FCT comprise the Null control code, which is used to keep the link active whenever data is not being sent. The Null control code due to its aforementioned use, acts as the indicator for a link’s disconnection. Additionally, ESC control character followed by a data character form a broadcast code (BC) which is used for time-codes and distributed interrupt codes. In addition to forming control codes, flow control tokens are used to control the flow of packets over the link. By sending FCTs, the one end of the link signifies to the other end that it is ready to receive more data.

After the characters are encoded into symbols and the former are serialized, data-strobe encoding produces the final serial bit stream to be transmitted. The Data signal, which is used to transmit the data, is set to high when the data bit is logic 1 and to low when the data bit is logic 0. On the other hand, the Strobe signal is used to incorporate the clock signal in order to allow the synchronization of the receiver. The Strobe signal changes state whenever the next data value is the same as the last one transmitted. Therefore, with a simple XOR operation between the logic values of the Data and the Strobe signals, the receiver acquires the Clock signal. As evident by the way the strobe signal is produced, the simultaneous transition of both the data and the strobe signals is not a normal part of DS encoding. For this reason, when the link is to reset, there should be a delay between the reset of the strobe and data signals to avoid possible damage to the receiver. When the length of time since the last transmission on either the data or strobe lines exceeds a certain time value, automatic disconnection of the link occurs. To prevent this, if no information is due to be sent, Null codes are transmitted to keep the SpW link active.

5. Physical Layer

The physical layer of the SpaceWire standard defines the structure of the cables, connectors, cable assemblies, line drivers and receivers that comprise the physical medium.

i. Cables

There is a variety of SpW cables as described in ECSS-E-ST-50-12C Rev.1 [3], specifically a low mass variant as well as a typical design that are described in ECSS 3902/004 [4] and ECSS 3902/003 [5], respectively. There is also the possibility to utilize application-oriented SpW cables, designed specifically to achieve certain characteristics. This type of SpW cable is categorized as Type B cable and it can be incorporated in Type B cable assemblies. The current analysis focuses on the typical design of a SpW cable specified in ECSS 3902/003 [5].

A typical SpW cable consists of four twisted pair wires each with its shield and jacket as well as an additional overall binder, shield and jacket. Every twisted pair is used to carry one signal utilizing low voltage differential signalling. The DS encoding method used, demands the use of two signals (Data and Strobe) for each direction of the SpW link; therefore, comprising a full-duplex link, the SpW cable consists of four twisted wire pairs. There are two varieties of a typical SpW cable, one using 28 AWG² signal wires and another using 26 AWG. These two varieties are structured in the same way with the only difference being that the 26 AWG variant features slightly larger dimensions [4]. The dimensions mentioned below concern the 28 AWG variant as described in ECSS-E-ST-50-12C [2].

ii. Inner Conductors

Every one of the signal wires is 28 AWG and comprises of seven strands of 36 AWG high-strength copper alloy with a silver coating of minimum thickness 2.0 μm . Utilizing low voltage signalling (LVDS), a twisted pair should minimize the voltage degradation as the signal traverses the conductor, therefore the maximum acceptable DC resistance of the inner conductor is 256 Ohm/km. The insulation for each signal wire is a white, expanded, microporous PTFE.

iii. Twisted Pair

Each twisted pair comprises of a conducting part (inner conductor), a filler, a braided shield, and a jacket, as shown in **Figure 1-7**. The filler has a diameter of 1.0mm and is made of expanded microporous PTFE. Its use aims to provide

² AWG: American Wire Gauge

a uniform diameter under the shield, contributing to uniform impedance throughout the twisted pair. Every twisted pair is designed to provide 100 ± 6 Ohms characteristic impedance between the two inner conductors of the wire pair. The lay-length of the insulated conductor pair is between 12 and 16 times the outside diameter of the unshielded twisted pair, providing a lay-length of 32-41 twists/m [4]. The braided shield used for each twisted pair is of push back type providing not less than 90% coverage. The jacket for each twisted pair is a white layer of extruded fluoropolymer PFA with a nominal wall thickness of 0.15 mm.

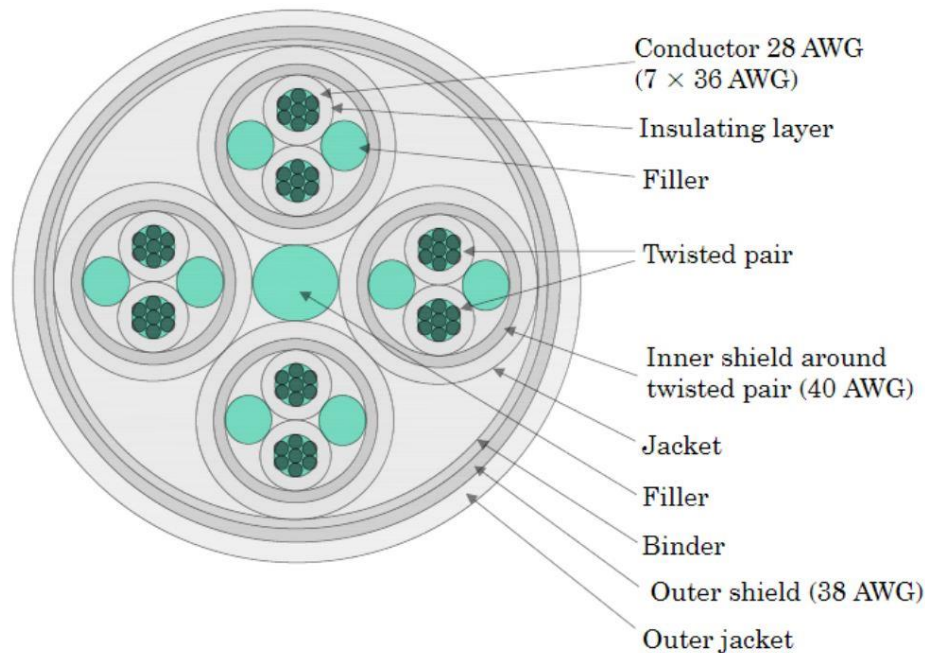


Figure 1-7. SpaceWire cable construction [1].

iv. Complete cable

The complete SpW cable has a maximum diameter of 7 mm and a maximum weight of 80 g/m. The four differential pairs of the cable should be twisted together between 12 and 16 times the outside diameter of two shielded differential pairs, providing a 55-77mm lay-length. The filler in the middle of the differential pairs is made of a microporous PTFE, has a diameter of 1.0 mm and aims to achieve a uniform diameter, thus a uniform impedance over the cable. Additionally, a binder of the same material, as the filler, is wrapped with 50% maximum overlap over the differential pairs to keep them and the filler in a fixed position, further adding to constant impedance over the cable. A braided shield of push-back type covers the binder providing not less than 90% coverage. It should be noted that the shields of the differential pairs and the outer shield do not make contact. The jacket covering the shield is a white layer of extruded fluoropolymer PFA with a nominal wall thickness of 0.25 mm [2]. It should be noted that the outer jacket bears no identifying marking to avoid

applying pressure to the cable in the construction process and therefore disrupting its electrical properties.

The intra-pair skew, i.e. the difference between the expected and actual positions of the rising or falling edges of the signal in a twisted pair, is less than 0.1ns/m. The inter-pair skew, i.e. the difference between the actual positions of the respective bit streams' transitions for a data-strobe signal pair, may be more than 0.1 ns/m, provided that the cable assembly meets the overall skew requirements of the SpW link [3]. It should be noted that these parameters are met only for the cable and not the cable assembly because most of the crosstalk, skew and jitter of the signals is due to the connectors.

v. Shield details

The shield for the twisted wire pairs consists of 40 AWG wire, whereas the outer shield of the cable consists of 38 AWG wire. The strands used in the construction of both shields are soft or annealed oxygen-free, high conductivity copper with a silver coating of 2.5 μm minimum thickness. Although the braided shielding does not give 100% coverage, it provides plenty of flexibility and strength to the cable. This leads to a cable resilient to harsh conditions, which are frequently met in space missions.

The minimum shield effectiveness as defined by ESCC No.3902/004 [4] is depicted in **Figure 1-8**.

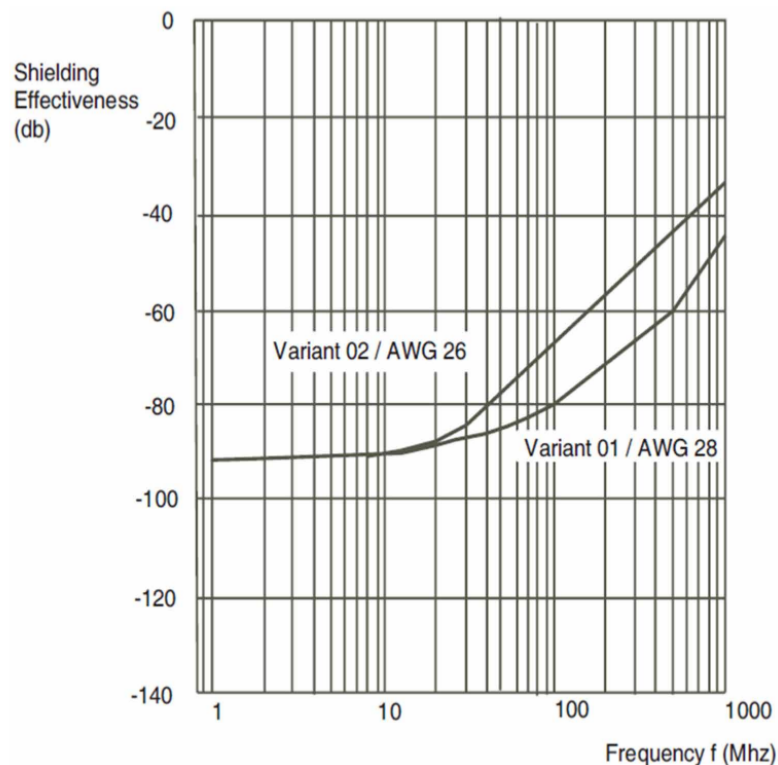


Figure 1-8. Minimum Shielding Effectiveness [5].

vi. Connectors

There are two types of connectors for SpW cables, namely Type A and Type B. Type B defines a wide range of custom connectors that must conform to certain design characteristics given in 5.3.3.1c-5.3.3.4.2 of ECSS-E-ST-50-12C Rev.1 [3]. This type of connector can be constructed to achieve specific properties oriented towards a certain application and should be supplier-defined. Usually, such connectors are used on type B cable assemblies.

The typical connector used in a SpW cable assembly is a micro-miniature D-type connector with nine crimp contacts (**Figure 1-9**), labeled as type A connector. Type A connectors with female contacts shall be used on unit assemblies and connectors with male contacts on cable assemblies. The electrical resistance between two mated connectors is less than 10mOhm at DC. Any connector that is attached to SpW cable has the wire conductors directly soldered or crimped to the contacts. To accommodate the connection of each wire conductor to its respective pin, the wire pair is left untwisted near the connector. For connectors with female contacts, a conductive gasket is also included to improve their EMI immunity. In addition, a low impedance connection exists between the connector's body and the unit's ground (usually the unit chassis) of less than 10mOhm at DC (ECSS-E-ST-50-12C Rev.1 [3]).

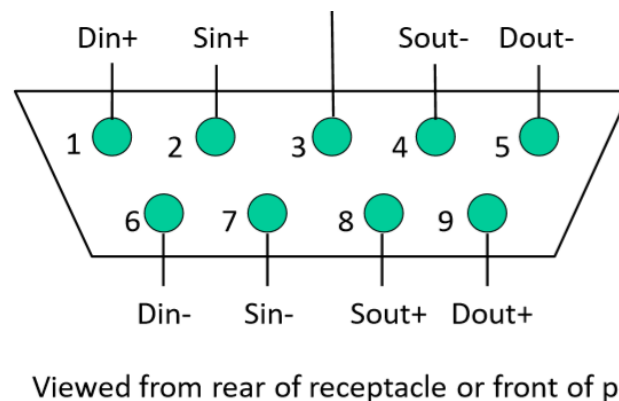


Figure 1-9. SpaceWire connector contact identification [3].

vii. Cable Assemblies

SpaceWire cable assemblies are categorized as type A and type B. A cable assembly using type B custom cables and connectors, is also labeled as type B and should conform to the guidelines given in 5.3.4.4 of ECSS-E-ST-50-12C Rev.1 [3]. The typical SpW cable assembly, labeled as type A, consists of two type A connectors and a length of cable. Specifically, each connector features a metallic backshell which is utilized as a 360 degrees termination for the outer shield of the cable. This creates a continuous conductive barrier between the signal wires and any interfering source, further adding to the cable's electromagnetic immunity. Additionally, the main body of the connector is

connected to the backshell via a low impedance connection of less than 10mOhm, at DC [3].

To adjust the maximum length of cable that can be used, data to strobe skew, jitter and signal attenuation requirements of the SpW link should be considered. Longer cables can usually be used at lower data rates provided that the signal attenuation, the system jitter and the skew limits are not violated at the operating data signalling rate [5]. The maximum intra-pair skew for a cable assembly is less than 0.5 ns, whereas the maximum intra-pair skew added by the connectors at both ends is less than 0.07ns. In addition, the insertion loss for each differential pair is less than 7 dB at frequencies up to 1.5 times the data signalling rate [3].

The latest revision of the standard has made an alteration in the design of type A cable assemblies. Therefore, typical SpW cable assemblies conforming to older versions of the standard are labeled as Type AL (L stands for Legacy), while the ones conforming to the latest version are labeled as Type A, their only difference is the way the inner shields of the four twisted pairs are terminated at each end. Though seemingly unimportant, this alteration can have significant effects on the electromagnetic emissions and immunity of a SpW link. It should be noted that Type AL cable assemblies are not recommended for new designs.

In this type of cable assembly, the inner shields of the two wire pairs carrying the transmitted signals D and S (Dout, Sout) at each end of the cable, are connected together and via pigtail, to pin 3 of the connector as shown in **Figure 1-10**. The pairs of inner shields that are matched together at each end, are isolated from one another and the outer shield.

On the contrary, in a type A cable assembly, the inner shields are connected to the connector shell and pin 3 is left unconnected as shown in **Figure 1-11**. Leaving pin 3 unconnected does not pose an ESD threat, as an isolated conductor would. As mentioned earlier, a type A female connector has its pin 3 connected to circuit ground, therefore the contact of the male connector is not isolated.

The cable's signal wires cross over in both type A and type AL cable assemblies in order to achieve the necessary transmit-to-receive interconnection. As most of the crosstalk is due to the connectors, differential far end and near end crosstalk (FEXT and NEXT) for the cable assembly between any two pairs are more lenient than the ones concerning only the cable ([3], clause 5.3.2.6). For both type A and AL cable assemblies, FEXT and NEXT is not more than -20 dB up to 1 GHz.

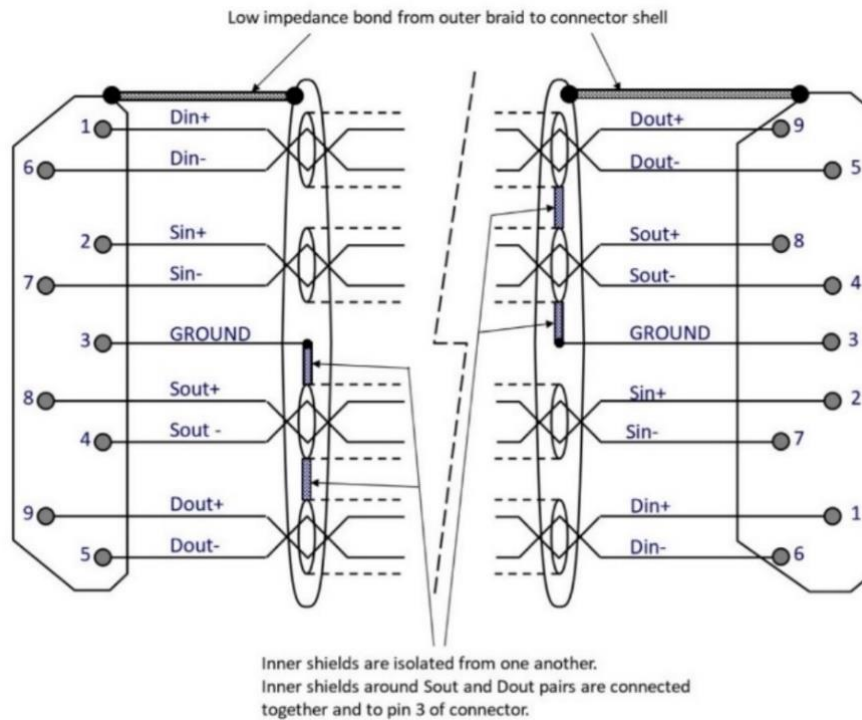


Figure 1-10. SpaceWire cable assembly Type AL [3].

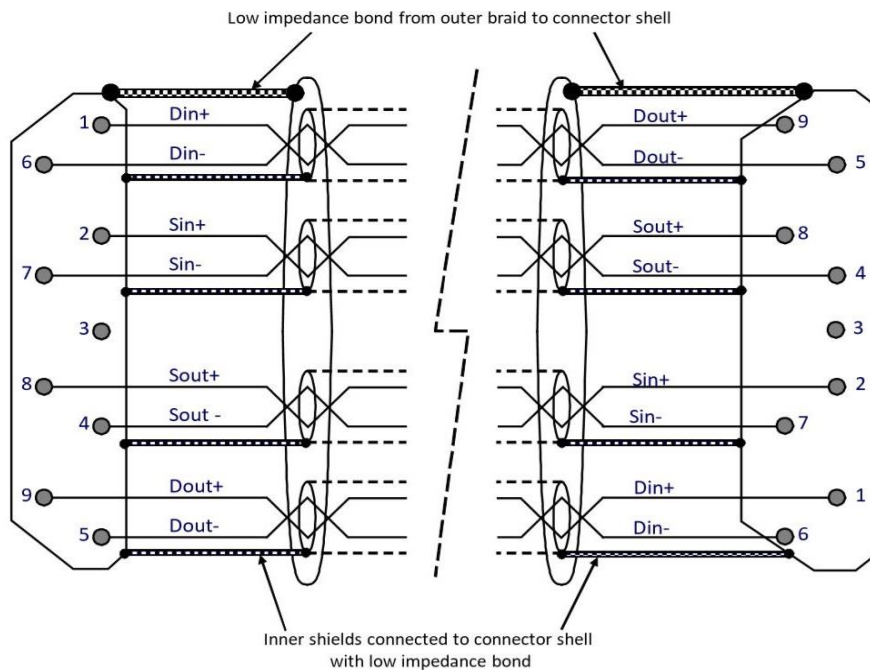


Figure 1-11. SpaceWire cable assembly Type A [3].

viii. Low Voltage Differential Signalling

The method used to drive signals through a SpW link is Low Voltage Differential Signalling - LVDS (Figure 1-12). The LVDS technique provides sufficient noise margin thus enabling the use of low voltages, leading to high link speed with low power consumption. LVDS uses balanced or differential

signals with a voltage swing around 350mV. Additionally, being a method of differential signalling, it provides immunity to variations of local ground at each end of the cable.

Every data or strobe signal that is driven through a SpW cable consists of the positive (OUT_P) and the negative (OUT_N) side, both using a common-mode voltage in the range from 1.125 V to 1.45 V and amplitude from 124mV to 227mV ($|OUT_{P/N} - V_{CM}| \in (124mV, 227mV)$). The differential LVDS output signal (OUT_P - OUT_N) should have the characteristics shown in **Figure 1-13** regarding its rise and fall time, ringing, monotony, and amplitude. The wire pair shall be terminated at the receiver by a 100 Ohm $\pm 1\%$ resistor to avoid reflections.

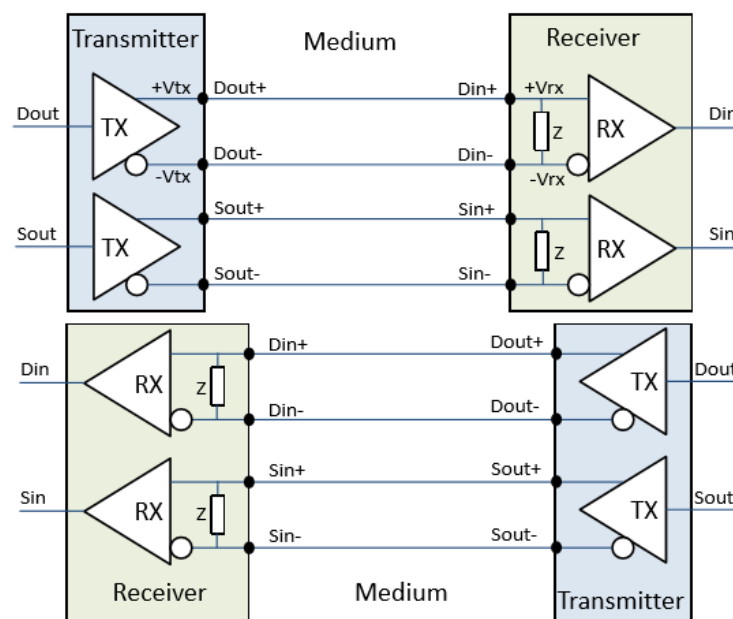


Figure 1-12. SpaceWire LDVS [3].

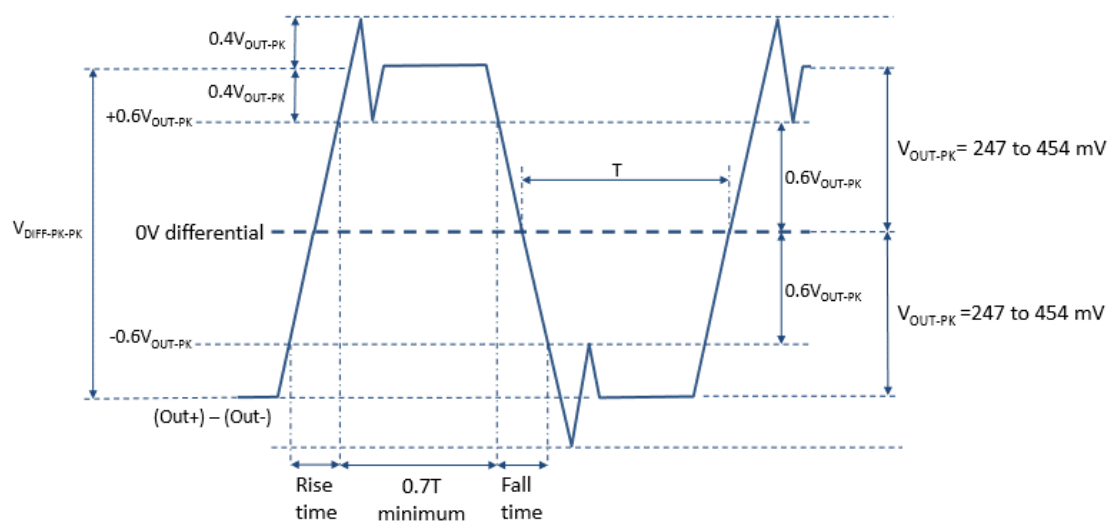


Figure 1-13. LVDS line driver differential output signal [3].

When the positive received signal (IN_P) is greater than the negative one (IN_N) by more than 100 mV, the receiver's output is a logic 1. On the contrary, when the differential input signal at the receiver is less than -100 mV, a logic 0 shall result at the line receiver output. The line receiver is designed to operate correctly with an input voltage in the range of 0 to 2.4 V and a differential input voltage up to 600 mV. Furthermore, the LVDS line driver and receiver circuits are designed to be resilient to a variety of possible fails that may occur, such as the outputs to be open or short circuit or even shorted to local ground.

The main advantage of the LVDS method, which also interests this thesis, is the low magnetic emissions produced. Specifically, due to the small equal and opposite currents flowing through the twisted pairs, the generated magnetic fields are weak and tend to cancel each other out. In addition, the twisting of each wire pair as well as the twisting of the four twisted wire pairs, further reduces the cable's emissions.

To conclude the analysis of the SpW standard the SpW port will be briefly examined. The former is an inseparable part of any SpW link and thus, for reasons that will become clear in following chapters, its architecture will be presented.

6. SpaceWire Port

To begin with, a SpW port possesses two FIFO queues, a transmit (TX) FIFO and a receive (RX) FIFO, where data is stored until transmitted over the link or read by an application respectively. Additionally, each port incorporates a flow control manager, responsible for preventing overflows, i.e. transmissions from the far end of the link when the port's receive FIFO does not have adequate space. This is achieved by managing the movement of data over the link using flow control tokens (FCTs). Furthermore, the port is provided with a transmitter, receiver and two pairs of line drivers and live receivers. The transmitter is responsible for creating the data and strobe signals transmitted over the link. The latter is achieved by encoding the characters to be sent into symbols, which are then serialized, and the produced bit stream is encoded into the data and strobe signals. Finally, the line drivers, using the data and strobe signals provided by the transmitter, generate the LVDS signals which are then transmitted over the SpW link. The received LVDS signals are converted into data and strobe signals by the line receivers which are then decoded by the receiver. The initialization, as well as, the error recovery of the link, are controlled by the link's state machine. An illustration of the aforementioned architecture is presented in **Figure 1-14**.

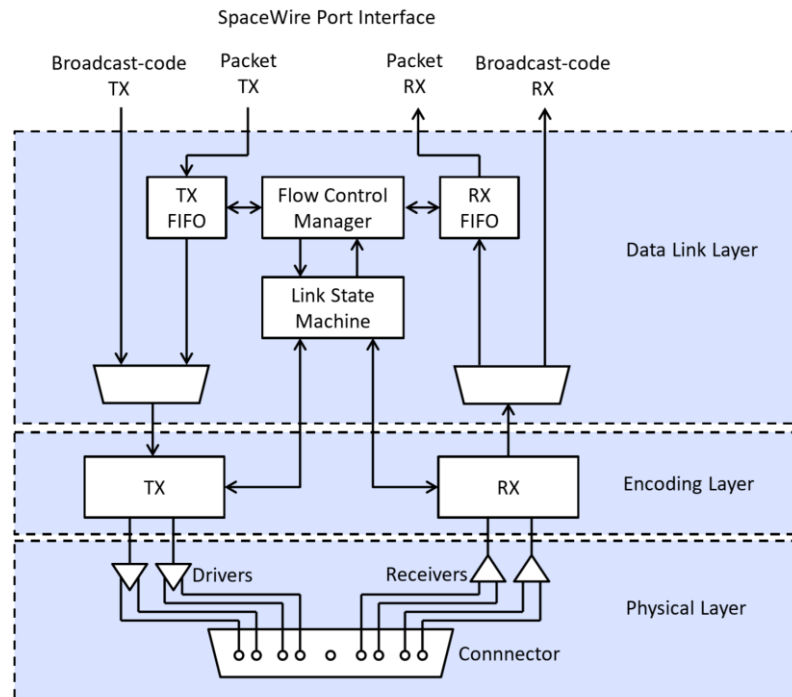


Figure 1-14. SpaceWire Port Architecture [3].

At this point, an important comment will be made that will be employed latter in this thesis. As already mentioned, the SpW standard utilizes broadcast codes, FCTs, N-Chars³ and Nulls (“NULL” control codes) to achieve the flow of information through the SpW link. When the link is operating, the sending priority from highest to lowest is as follows: broadcast codes, FCTs, N-Chars and finally Nulls. The point of interest is that if no broadcast codes, FCTs or N-Chars are due to be sent then Nulls are transmitted through the link to avoid a disconnect error from occurring.

After providing a brief overview of the SpW standard, the next subject to be discussed should be the measuring layout and equipment used to perform the measurements presented in this thesis.

2. Measuring Layout & Equipment

1. Introduction

Initially, to emphasize the importance and the possibilities offered by studying a SpW link’s magnetic field emissions, it is considered essential to describe the necessity and the difficulties of achieving “magnetic cleanliness” in a space mission. The need for magnetic field measurements is present in a

³ N-Chars or Normal Characters: the components of packets (data characters, EOP, EEP)

wide range of missions as they can be used to widen our understanding regarding the laws governing the universe, from planet formation to particle interactions. For example, they can be used to reveal crucial information about the structural composition of planets, as well as to study the interactions between the solar wind and planetary or interplanetary environments. The precision of the magnetic field measurements required by such missions is extremely high. Being able to acquire precise and accurate measurements, requires ensuring that the former are free from any spacecraft-induced interference. The latter is a very difficult task, as every electronic circuit on the spacecraft emits electromagnetic radiation, thus it is unavoidable that part of it will be measured by the magnetic field sensors. For this reason, a lot of effort is made in the design process to reduce the emissions of most instruments, either by specialized design techniques or by the addition of adequate shielding. For instance, both the use of twisted wire pairs and LVDS in the SpW standard are design choices which offer, between other advantages, low electromagnetic emissions from the cable. Due to the dramatic increase of the launch cost, deriving from increasing the weight of the spacecraft, in most space missions the ability to add electromagnetic shielding is limited. Consequently, in most cases, a combination of techniques is employed to achieve the desired signal to interference ratio (SIR) in the measurements. One such technique is to place the magnetic sensors in a boom, extending as far away as possible from the spacecraft, to increase the distance between the magnetic field sensors and the interference sources, therefore increasing the SIR in the measurements (**Figure 2-1**).

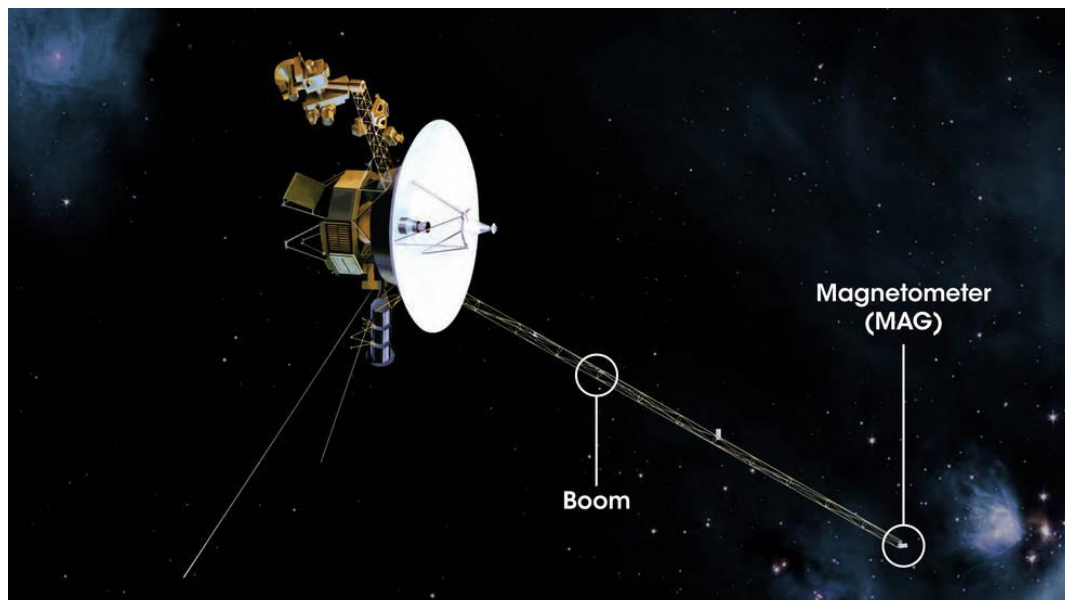


Figure 2-1. Illustration of NASA's Voyager spacecraft, with the Magnetometer (MAG) instrument and its boom displayed (NASA - The Voyage to interstellar space - Magnetometer <https://www.nasa.gov/feature/goddard/2019/the-voyage-to-interstellar-space>).

Though effective in reducing the level of interference, this method can be insufficient for some missions. Another technique is to define an emission model for every instrument of the spacecraft. If the latter is achieved, it enables the accurate prediction of the interference in the measuring point and therefore the subtraction of the unwanted part of the measurement. This option requires performing extensive on-ground testing for the magnetic emissions of every instrument in a space mission. Of course, modeling the emissions of any instrument is a very complex procedure and even more so, when the coexistence of all the instruments must be accounted for. A significantly simpler and equally worthwhile technique is to identify a low emissions operational mode for each instrument by comparing the measurements for various of its operating modes.

Following this thought process, it is the aim of this thesis to measure the magnetic emissions of an operating full-duplex SpW link and to investigate any possible correlation between their level and the characteristics of the link, such as link's rate, packet's payload size etc. This can offer valuable information concerning the potential interference caused by the spacecraft's wiring as well as define the link's parameters that lead to minimum magnetic field emissions. A network designed according to the SpW standard can be comprised of links with different characteristics. This flexibility in choosing and adjusting each SpW link's characteristics, if combined with knowledge concerning the level of the magnetic emissions from the spacecraft's wiring, can lead to the implementation of a low emissions mode for the inner communications of the spacecraft. This will offer the prospect of minimizing the interference level in the measurements by altering some simple variables of the interconnecting network in a spacecraft when it is required.

Having rendered the measurements goal clear, the layout and equipment used can now be thoroughly analyzed.

2. Measurements

The magnetic field measurements are performed inside a semi-anechoic chamber which is situated inside a Faraday cage. Although the former can cancel all external high frequency electromagnetic radiation, the same cannot be said for low frequency magnetic fields. For this to be achieved, either passive or active specialized magnetic shielding is required. Whereas active shielding makes use of specially positioned coils (e.g. Helmholtz coils), in order to create a field opposite to the ambient in the area of interest, therefore canceling it, passive shielding exploits some of the properties of magnetic materials to achieve "magnetic cleanliness". A brief summary of the most widespread methods for passive magnetic shielding is given below [6]. The most effective

method is superconductor shielding, which can completely isolate an area from external magnetic fields. This, though, is achieved at a very high cost both for its installation and its maintenance, as superconductor shielding requires cryogenic temperatures. Another option is to use sheets of metal alloys with high magnetic permeability such as Mu Metal, which offers great results at a much lower cost.

As for the semi-anechoic chamber, its specially designed ferrite inner walls are constructed to absorb all the incident high-frequency electromagnetic radiation generated in the interior of the chamber. Therefore, its presence ensures that there will not be any interference from secondary emitting sources in the measurements (reflections from the walls of the Faraday cage). However, this property of the semi-anechoic chamber is valid only for high-frequency electromagnetic radiation. Consequently, for low frequency magnetic fields, the presence of both the semi-anechoic chamber and the Faraday cage is irrelevant.

With the former in mind, to achieve the desired accuracy of the measurements, the ambient magnetic field needs to be removed with a suitable post process technique. In such a manner, the implementation of high cost passive shielding as well as the need for the compensating field from active shielding, is avoided. The employed technique aims to isolate the desired part of the measurements by comparing the measured signal with the background noise (measurement of the ambient magnetic field). For this reason, an additional measurement, with the link deactivated is performed before each desired measurement, to acquire the ambient magnetic field. The reliability of this method is based on the absence of fast-changing magnetic field sources at the frequencies of interest in the area of the measurements. Specifically, the interference at these frequencies is mainly caused by the Earth's magnetic field, the power grid (50 Hz) and potential components caused by the operation of the measuring equipment. Therefore, even if the ambient magnetic field slightly changes over time, it can be considered constant for the duration of the two consecutive measurements. To enhance the reliability of this method, the measurements are performed with the least possible delay between them (not exceeding 30 seconds). To conclude, with the implementation of this method, the magnetic emissions caused by the operation of a SpW link can be identified by comparing the frequency spectrums of these two measurements.

3. Measuring Equipment

The equipment used to perform the measurements consists of two triaxial fluxgate magnetometers, each with its power supply unit, and a data acquisition unit (DAQ) to complete the computer-based measuring system.

After being filtered and digitalized, the measuring data is exported through the DAQ to a PC to be processed further. A brief overview of each utilized instrument is presented below.

i. Magnetometers

The magnetic field sensors used are two “Bartington Instrument Mag690” packaged and circular connected magnetometers (**Figure 2-2**) [7]. Each magnetometer consists of three fluxgate sensors, positioned orthogonally to one another, providing a three-dimensional measurement of the magnetic field, with a measuring range of $\pm 100\mu\text{T}$ for each axis and a bandwidth (3dB) greater than 1.5 kHz. Each magnetic field sensor is powered by its own power supply unit, which provides it with a $\pm 12\text{V}$ voltage. The sensors return three unbalanced analog output signals to the power supply unit, one for each axis. The output voltage range of these signals is $\pm 10\text{V}$ with a scaling of $100\text{mV}/\mu\text{T}$. As the sensors can measure both the orientation and the amplitude of the magnetic field, it is evident that a 0V output corresponds to a complete absence of magnetic field.



Figure 2-2. Magnetometer “Mag 690” by Bartington Instruments.

Due to small variations in the positioning of the spirals of the sensing and driving coils for each fluxgate magnetometer, there is an offset in the measurement of the static (DC) magnetic field for each axis in the range of $\pm 100\text{nT}$. The existence of such an offset does not affect the credibility of the measurements, as it is present in both the ambient and the desired field measurements. Therefore, when comparing the static part of the two measurements, this offset will be subtracted as part of the ambient magnetic field.

An important aspect that should be considered in the positioning of the magnetic field sensors, is the ability to standardize the measuring process and rid it of any human inflicted errors. For this purpose, it is essential that the sensors’ positions are strictly defined by the operator and maintained for the

desired measurements. To accommodate such a prospect, a base has been specially designed and 3D printed to contain both magnetometers (**Figure 2-3**). This base is made of plastic so as not to affect the magnetic field measurements and offers three different arrangements for a two-sensor layout.

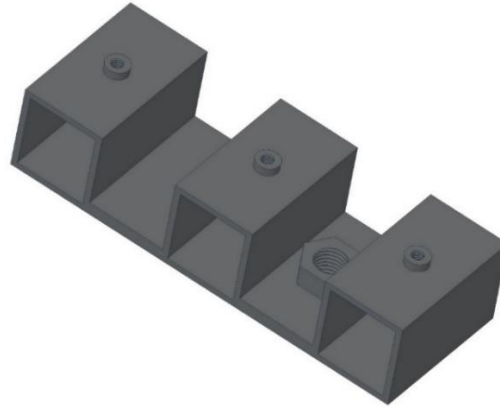


Figure 2-3. Magnetometers' base, designed in "Design Spark Mechanical" CAD software.

ii. Power supply units

For the power supply of the magnetometers, two "Bartington Instrument PSU1" (**Figure 2-4**) are used, one for each sensor [8]. Their purpose is to provide a battery packed power supply of $\pm 12V$ to each magnetic field sensor and to filter their analog output voltages.



Figure 2-4. Power Supply Unit "PSU1" by Bartington Instruments.

The filtered analog signals are then exported to three BNC connectors, one for each axis. The filtering process consists of a permanent low pass filter with a cut-off frequency of 9.5 kHz and an optional high pass filter with a cut-off frequency of 0.1 Hz. The activation-deactivation of the high pass filter is controlled by the DC/AC coupling button on the front side of the instrument. The PSU1 can operate both with balanced and unbalanced output

magnetometers after adjusting the respective setting. It should be noted that the filtered signals provided in the outputs of the PSU1 are single ended even if the output of the magnetic field sensor used is balanced. Additionally, the PSU1 can be powered both by an AC charging adaptor connected to the mains and by internal rechargeable batteries, the latter option though, lowers the internal noise added to the measurements by the instrument.

The settings of the PSU1 are adjusted to the characteristics of the magnetic field sensor Mag690 and the requirement of the measurements. Specifically, the magnetometer output type selector is set to “unbalanced” and the coupling to DC. Setting the coupling to DC deactivates the high pass filter, therefore the analog output voltages of the magnetic field sensors are filtered only by the low pass filter, thus removing the high-frequency noise from the signal.

iii. Data acquisition unit (DAQ)

The data acquisition unit is an indispensable part of any computer-based measuring system as it performs the digitalization and the transfer of the measurement information to a computer, therefore allowing its further analysis. The DAQ used in this measuring layout is the NI USB-6351 from National Instruments (**Figure 2-5**) [9], [10], a multifunction I/O device featuring 16 single-ended channels (or 8 differential) for analog inputs, 2 channels for analog outputs and 24 channels for digital I/O.



Figure 2-5. Data Acquisition unit NI USB-6351 by National Instruments.

The NI-DAQmx drivers accompanying this unit, enable automation applications such as customization and visualization of the data from a variety of supported programming languages. The platform currently used for processing and visualization of the measured data is “Matlab”. The NI USB-6351 offers an overall maximum sampling rate for multi-channel analog inputs of 10^6 samples per second. Furthermore, its analog to digital converter has a resolution of 16 bits, offering 65,536 different output codes, ensuring the accurate depiction of the analog measured signals. After converting the analog input signals to digital data, the latter is transferred via a USB signal stream to

the desired computer system. As mentioned earlier, the output voltages of each magnetometer are filtered by its corresponding power supply unit and then exported, as single-ended analog signals, through three BNC connectors, one for each axis. Therefore, in total, the data acquisition unit receives six single-ended analog signals which should be connected to six analog input channels. The connection of a signal to the corresponding channel for the NI USB-6351 is made by screw terminals by design. Consequently, the BNC connectors at the side of the cables to be connected to the DAQ are removed, making the inner conductors visible. The inner conductor embedded in the dielectric insulator material, carries the analog signal, whereas the cable's shield, carries the ground reference of the signal. The signal carrying conductors are connected to screw terminals corresponding to single-ended analog input channels. As for their ground references, each pair of wires carrying field measurements for the same axis but derived from different magnetometers, have their shields soldered together with the use of an additional wire and connected to an analog input ground channel, different for each pair. The NI USB-6351 Pinout and the connections made are visualized in **Figure 2-6**.

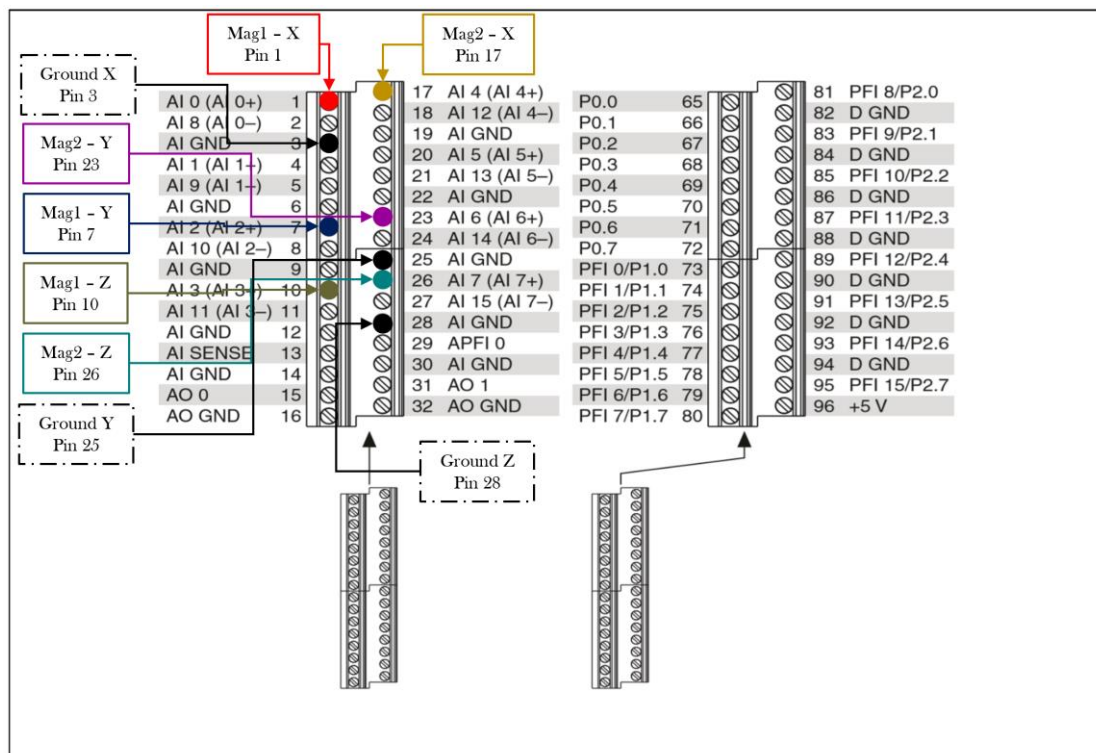


Figure 2-6. NI-USB 6351 Data Acquisition system's Pinout (NI 6351/6353 Specifications, National Instruments [9]).

In order to maximize the accuracy of the measurements, the instruments need to be left idle for some time after turning on the power, so their internal temperatures are stabilized. For this reason, the power supply for all instruments is turned on approximately 20 minutes before measuring.

iv. iSAFT SpaceWire Simulator

The equipment under test (EUT) that the aforementioned layout aims to measure, is a full-duplex SpW link. To create such a link, a SpW cable is needed as a physical interconnection, as well as an instrument that simulates the operation of the two connected nodes. The latter is achieved with the use of iSAFT SpaceWire Simulator [11], a platform designed to simulate devices or instruments acting as nodes in a SpW network. Each simulated node corresponds to a port of iSAFT's board and can generate or receive traffic over a physical interconnection. The interconnection of the nodes is performed by the user with the implementation of suitable wiring (SpW cable as defined in the standard). The characteristics of the SpW link can be defined via adjusting the parameters for the generated traffic from the nodes simulated by iSAFT (payload length, packet to packet delay time, link's speed etc.). Additionally, the user can record or preview the statistics for the operation of each node (transmitted packets, received packets, error occurrence etc.).

A platform like iSAFT, allows the simulation of a SpW network for on ground testing purposes, such as evaluating its reliability and electromagnetic immunity. It is comprised of the iSAFT Run-Time Engine (RTE) and various hardware components, that implement the SpW Simulator functionality. Furthermore, it possesses a graphical user interface and a remote-control server, allowing the operator to define the characteristics and manage the recording of the simulated SpW network, remotely, over a TCP/IP (Ethernet) link. A brief overview of its capabilities is provided below, with an emphasis on the features utilized in this thesis.

Board Configuration

The first aspect that the user confronts when interacting with iSAFT SpaceWire Simulator, is the board configuration. When connecting the remote server with the graphical interface, a display of the connected board and its available ports is presented. In this board type, four ports are provided and if one is connected, it is marked green. From this panel, the user can modify each port separately, through the port's configuration window, as well as enable or disable all the available ports simultaneously, through the board configuration window (**Figure 2-7**). Specifically, through the port's configuration window (**Figure 2-8**) the user can adjust important port characteristics such as enable the link's auto start (A) or packet sinking (G), as well as modify the link's rate (B), the maximum receive packet length (C), the maximum transmit packet length (D), the trigger out polarity (E) and the trigger signal pulse duration (F). If the link auto start is selected, the transmission from this port will start automatically when the link is connected. The packet sinking option refers to the management of the received packets from the current port and allows full rate reception. Specifically, it lets the port drop the received packets at the hardware level, enabling it to operate as a receiver under faster transmission

rates. Additionally, each port can be enabled or disabled separately through the port configuration window.

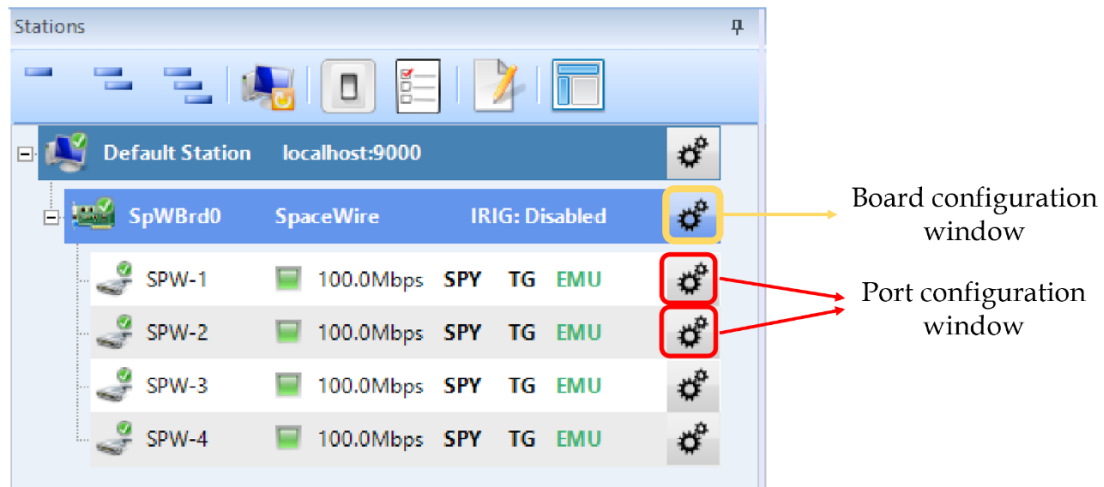


Figure 2-7. Board Configuration.

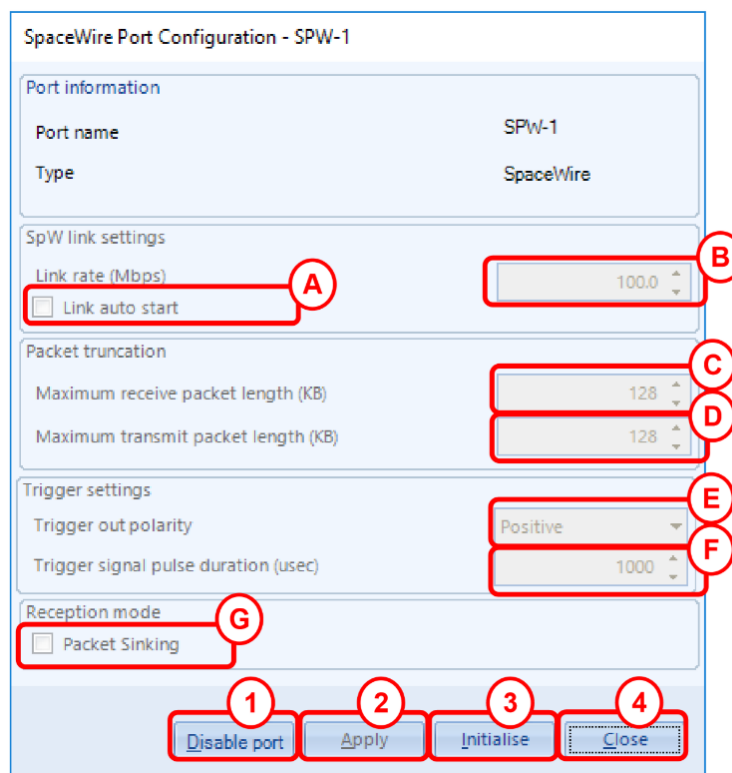


Figure 2-8. Port Configuration window [11].

To modify a port's transmission rate (link's rate), all the ports must first be disabled and re-enabled after applying the new rate. For the alteration of other characteristics, only the port to be edited should be disabled and then re-enabled. To categorize the operations that can be performed by iSAFT, the latter are separated into two broad categories, "Simulation" and "Recording".

Simulator

To generate traffic in a SpW network, the first aspect that should be defined is the traffic generated by each node. By pressing on the “SpW Simulation” button on the simulator ribbon group, under the iSAFT tab, the user can choose the port for which the traffic will be generated. Every port possesses its own Packet Library where the packets created by the user are stored. The simulator supports the creation of three packet types compatible with the SpW standard, namely, “SpaceWire”, “CPTP” and “RMAP” packets. The reason for such a demarcation is that there are several communication protocols (ECSS-E-ST-50-51C [12] & ECSS-E-ST-50-52C [13] & ECSS-E-ST-50-53C [14]) compatible with the SpW standard, providing a variety of services for on-board applications. In particular, the CCSDS Packet Transfer Protocol (CPTP) provides the ability to transfer different packet types by encapsulating them in SpW packets and isolating them only when they reach their destination. Such a procedure enables the transmission of packets with different features than the SpW packets, through a SpW network. The Remote Memory Access Protocol (RMAP) supports writing to and reading from memory in a SpW node. Specifically, these packets are used to gather information and data from SpW nodes as well as to control them and to configure the SpW network. In addition to the above, the configuration and control of routing switches is also achieved by RMAP packets. A protocol identifier is used at the beginning of each packet, in order to be processed accordingly upon its reception. Therefore, all the protocols can operate simultaneously in a SpW network without interacting with each other. The addition of a new packet to the Packet Library, for each supported type, is achieved by the indicators g, h and i (**Figure 2-9**). The main packet type used for data transmission in a SpW network and the one that will be utilized for this thesis is the “SpW packet”. The packet’s characteristics can be adjusted through the respective window when creating it (**Figure 2-10**). Specifically, for the “SpW Packet,” the user can define its name (A), terminator type (B) (EOP, EEP, Partial), packet to packet delay time (B) and payload length (D). The payload of each packet can be edited to be sequential from a user-defined start value, random or set by the user. The preview of the packet data is in hexadecimal. In addition, the platform provides the ability of error injection (C) into the generated packets in several different ways depending on iSAFT’s hardware. To measure the emissions of a SpW link, there is no need for error injection, therefore no further information is provided about this aspect and an interested reader should refer to the respective manual (iSAFT SpaceWire Simulator Operation Manual Version 1.7).

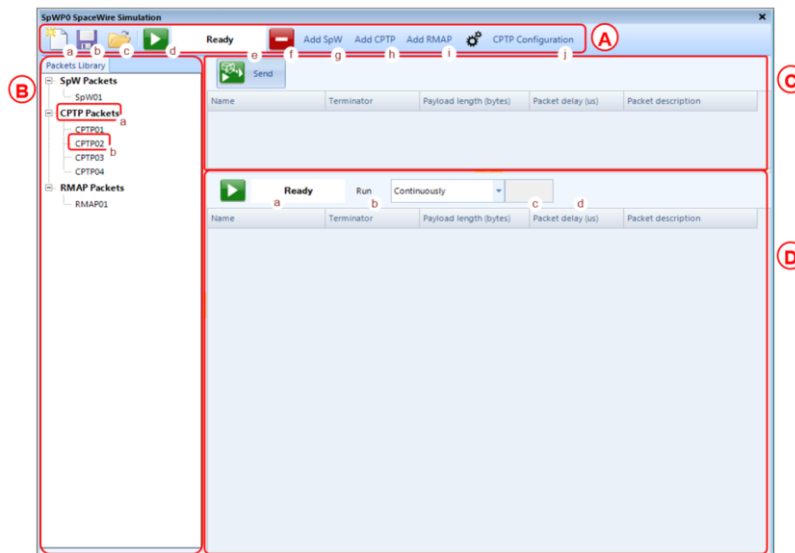


Figure 2-9. SpaceWire simulator panel [11].

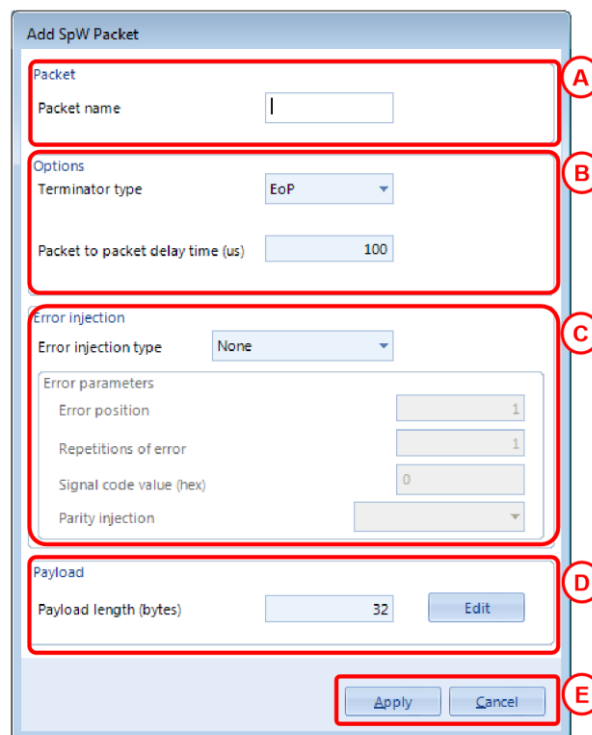


Figure 2-10. Add SpaceWire Packet window [11].

The next step, after creating the desired packets, is to form a transmission queue which consists of packets from the packet library. Such a queue can be transmitted either once or multiple times depending on the transmission group it belongs. The Asynchronous transmission group, illustrated in **Figure 2-11**, is used to transmit every packet of the queue once, sequentially. Therefore, every time the button “Send” is pressed one queue transmission occurs.

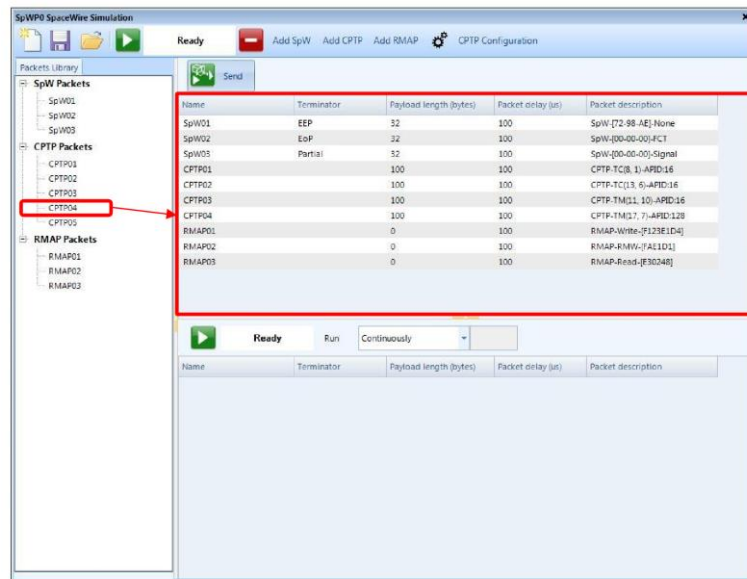


Figure 2-11. Asynchronous Transmission group [11].

On the other hand, if the transmission queue belongs to the Traffic Generation group (Figure 2-12), the queue is transmitted repetitively after the traffic generation is initiated. There is also an option defining the repetitions of execution (run continuously or run for a certain number of repetitions) and a Transmission Status Label, which changes depending on the status of the transmission (Ready, Running, Stopped). The former is altered by the “Start/Stop” button.

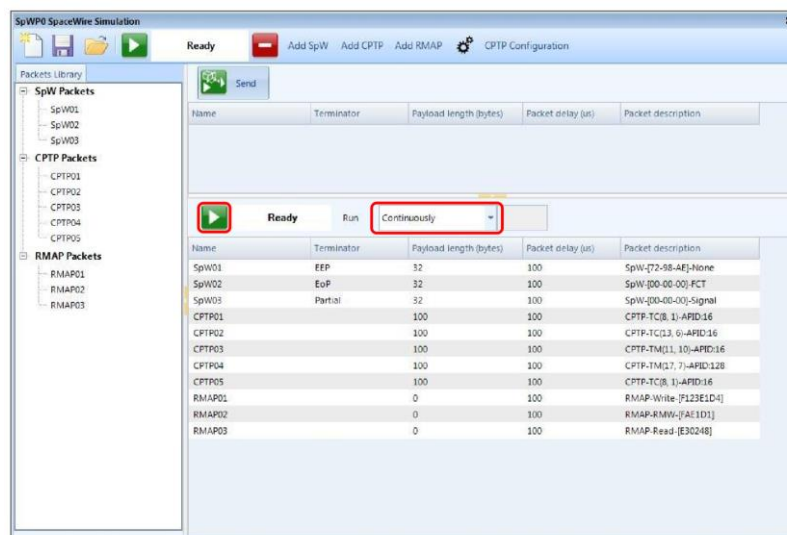


Figure 2-12. Traffic Generation group [11].

It is considered essential to mention that the reception status of a receiving port should be set to “Running” (Figure 2-9 d,e) before the respective transmitting port commences its transmission, otherwise the latter might be blocked.

Recorder

Another very important feature of iSAFT is its capability to record and store traffic data across the simulated network. By pressing the “SpW Monitoring” indicator, in the “Recorder” group, under the iSAFT tab, the user can enable the recording and define its parameters. Specifically, the condition on which the recording will begin as well as the criteria that the monitored data shall meet, are defined by the “Triggers” and “Filters” tabs, respectively, in the editing section for the recording parameters of each port (Figure 2-13, I). The recording is initiated by pressing the “Start” button (Figure 2-13, D). If a trigger is selected, the recording holds off until the triggering condition is met, otherwise it commences instantly. The status of the recording is presented in the respective indicator (Figure 2-13, F). Recording can be activated only for ports that support monitoring. The captured data are stored in a file or separated in multiple files generated by the recorder, depending on the selected setting.

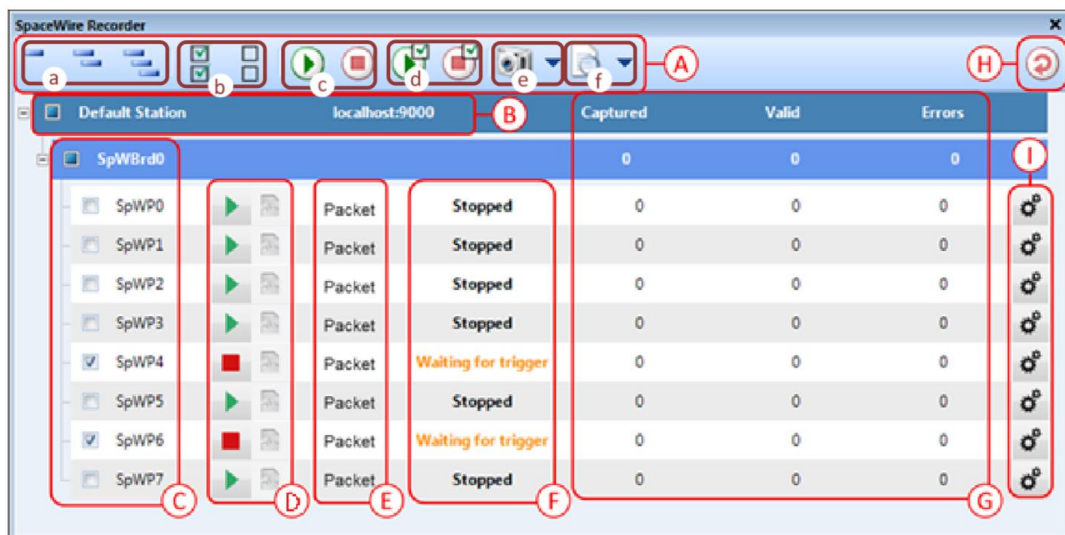


Figure 2-13. SpaceWire Recorder panel [11].

Although recording a network’s operation is a very important task, its relevance to the purposes of this thesis is negligible. Therefore, no further information about the recording functionality of iSAFT SpaceWire Simulator is provided at this stage.

Statistics

Both the simulator and recorder groups provide the capability of real-time preview of the statistics for the simulated and recorded data respectively. The user can preview these statistics, through the “SpW Simulation Statistics” indicators under each ribbon group. The statistics values provided by the two panels differ. Namely, the simulator’s statistics panel corresponds to the metrics from the physical ports during the simulation, while the recorder’s

statistics provide the statistic metrics, during a monitoring session. The respective panels are shown in **Figure 2-14** and **Figure 2-15**.

It should be noted that a port is displayed in the respective panel only if it supports simulation/monitoring functionality. These statistics can also be obtained by the user, either by creating a snapshot of the current state of the panel in Microsoft Excel format (**Figure 2-14 & Figure 2-15, A-c**) or by logging the data in a CSV file (**Figure 2-14 & Figure 2-15, A-e**).

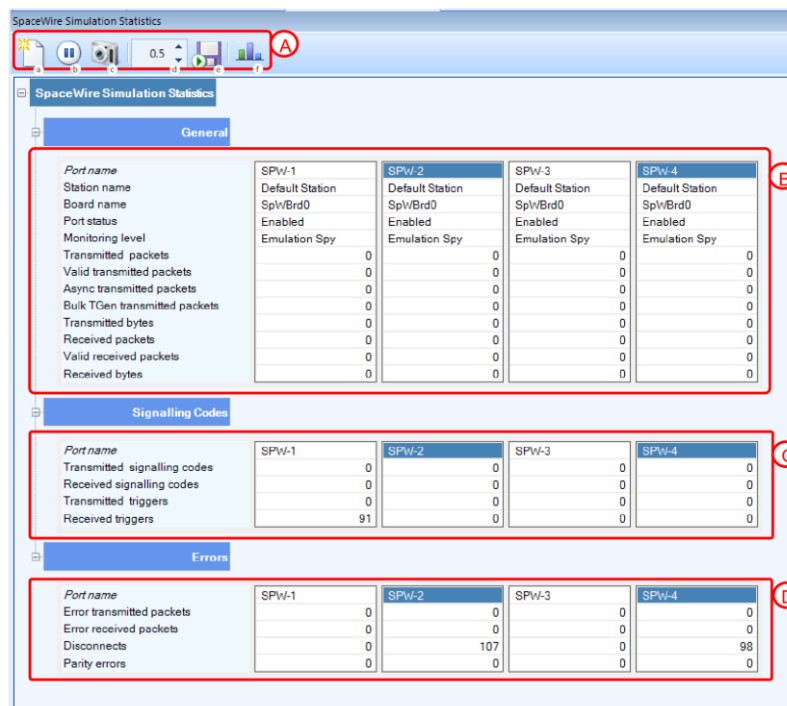


Figure 2-14. SpaceWire Simulator Statistics panel [11].

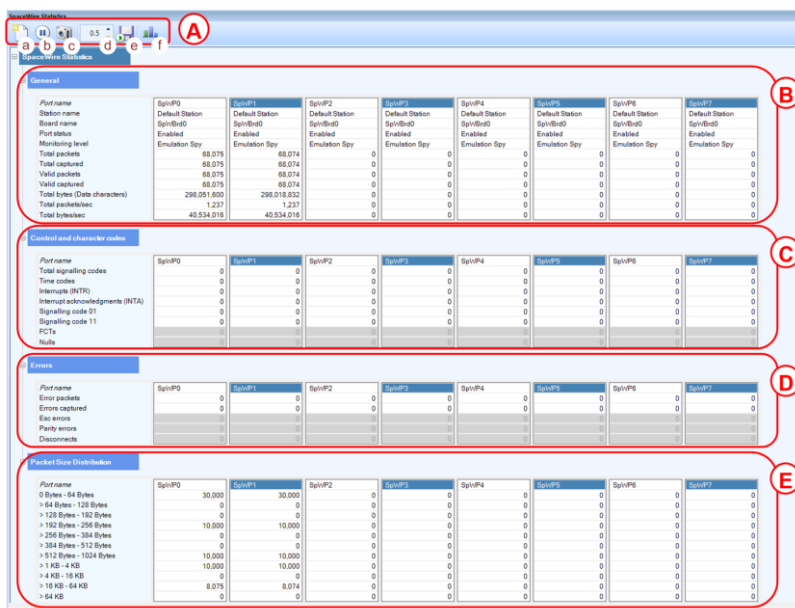


Figure 2-15. Recorder Statistics panel [11].

SpaceWire link's Generation

To create a full-duplex SpW link, two nodes need to be simulated using iSAFT SpaceWire Simulator. Therefore, only two ports are required from the four provided by the iSAFT's board. These ports are interconnected with the use of SpW cable. In order to simulate a full-duplex link, traffic must be generated and received in both ports. As described earlier, the link's speed can be altered from the board configuration panel by disabling the two utilized ports, editing the link's rate for both and re-enabling them. The packet size used for transmission will be the same for both ports and their payload content, as well as their length, shall be adjusted for each test.

From each port's simulator panel, a "SpW packet" is created and added to the port's traffic generation queue, so it can be transmitted repetitively. The packets used for transmission in both ports will have the same size and termination code, differing only in their content when the "Random" payload is used. At this point, the reception should be started for both ports. As mentioned earlier, if the reception is not started before the transmission is received, the latter might be dropped. Once starting both ports' reception, the traffic generation can begin. The transmission should continue until it is stopped by the operator, therefore the traffic generation indicator is set to continuously. After initiating the transmission for both ports, the operator can check that the link operates smoothly in both directions via the statistics simulator panel.

This thesis aims to study a SpW link's emissions for a variety of the link's characteristics (link's rate, packet's payload length, and content). Consequently, for every measurement setting, the characteristics of the link are set accordingly through the procedure described above. After verifying the correct operation of the link through the statistics panel, the measurement can be performed provided that the measuring layout is ready.

4. EUT's Layout

As mentioned earlier, the measurements are performed inside a semi anechoic chamber, all the interior surfaces of which, except for the floor, are covered by ferrite. The physical SpW link, iSAFT and interconnecting cable, is situated on top of a wooden table which is covered by a conductive layer. This layer simulates the ground plane and is electrically bonded to the chamber's floor by three conductive bond straps. The three bond straps are spaced apart less than a meter and have less than five to one ratio in length to width [15]. In order to simulate the link, the SpW cable has both its ends connected to two of the iSAFT's ports. The latter is placed on top of the table to avoid unnecessary length of cable being used. Furthermore, iSAFT is shielded with an L-shaped

conductive shield, which is electrically bonded to the conductive surface covering the table, as well as additional ferrites. The path created by the cable on top of the table's surface consists of two parts. The part with the greater importance for the measurements, is a 1.2m linear path of cable, 10cm from the table's edge, which is placed over a non-conductive standoff (a 1.2m x 10cm x 6.3cm piece of foam). The rest of the cable above the table is covered by conductive tape and its path is chosen in order to minimize its length. When possible, the cable travels under the conductive layer but far away from the magnetic field sensors. The magnetometers are placed close to the linear part of the cable's path which is situated over the non-conductive standoff. Similarly, the rest of the measuring equipment, consisting of the two PSUs and the DAQ, is also placed inside the semi anechoic chamber, but in the greatest possible distance from the EUT and the magnetic field sensors (over 3.5 meters). The specific magnetic field sensor layout used to obtain the measurements presented in this thesis will be thoroughly described in **chapter 4**. To summarize, the positioning of the Equipment Under Test (EUT) conforms with the regulations proposed by the Military Standard (MIL-STD-461G [15]). This setup, which is depicted in **Figure 2-16**, is designed for electric field measurements and its implications on low frequency alternating magnetic field measurements will be discussed in **chapter 4**.

All in all, the background noise measurement technique used, ensures that any static or low frequency magnetic field emissions caused by the operation of iSAFT or any other instrument of the measuring equipment will not be mistaken for magnetic emissions from the cable. In addition, the employment of two identical sensors can be used to indicate some properties of any arising magnetic field sources, as will be analyzed later in this thesis.

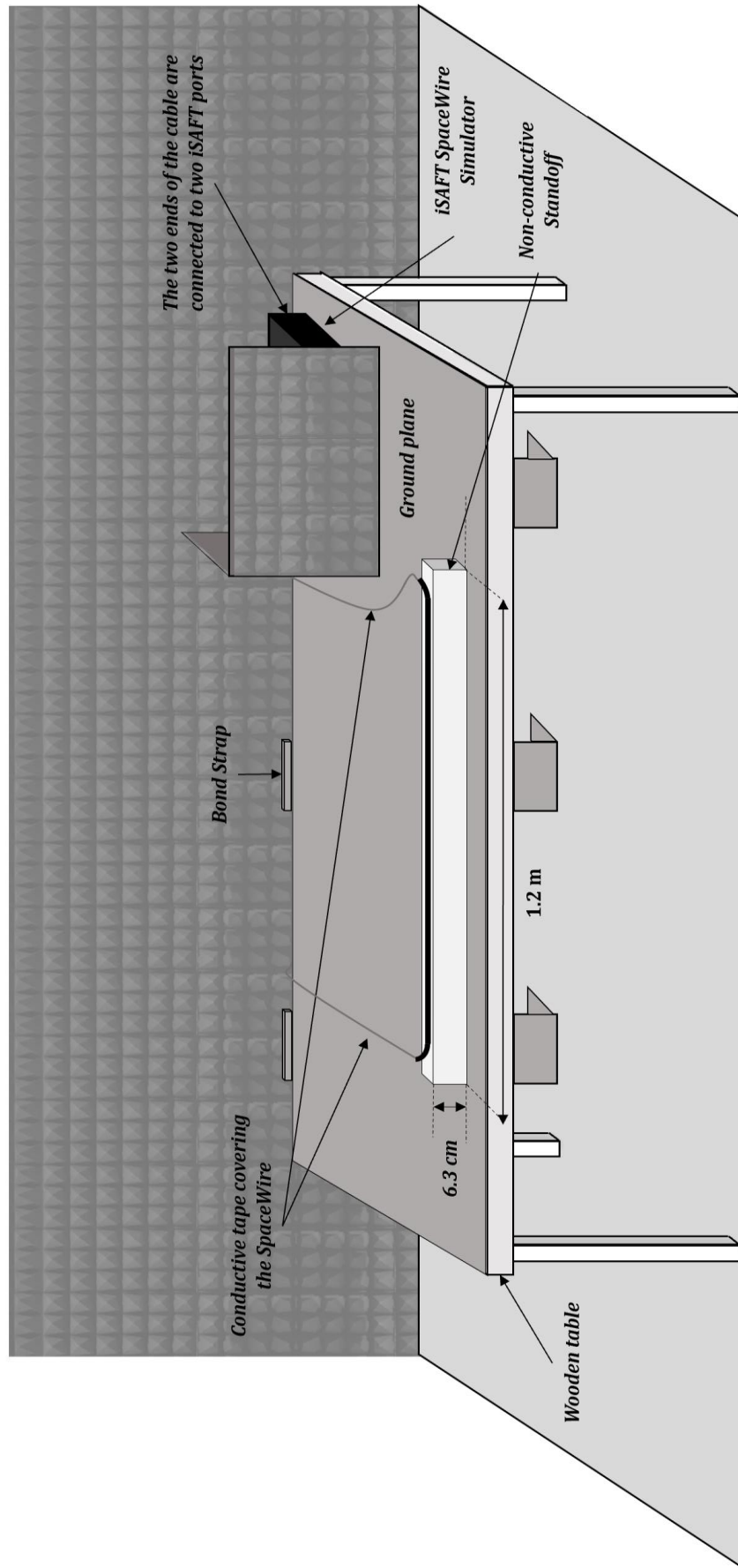


Figure 2-16. EUT's Layout [16].

3. Emission mechanisms & Potential

Emission Spectrum

The assumed undesired low-frequency magnetic field emissions that this setup aims to measure, are caused by low-frequency currents flowing through the inner and outer conductive shields of the SpW cable. These currents are induced to the cable's shields during the SpW link's operation through a plethora of coupling mechanisms between the conductive shields and the signal carrying conductors of the twisted pairs. Therefore, before presenting the measurement results, a brief analysis of the coupling mechanisms will be made so the emissions causes can be better understood. Whereas alternating currents can be induced to the conductive shields, the same cannot be said for DC currents. Specifically, any static magnetic field emissions produced by the operation of the link, are caused by DC currents flowing through the signal carrying conductors of the cable. The potential for such components in the wire pairs' currents will be examined later in this chapter.

1. Emission Mechanisms

i. Capacitive coupling

The existence of so many conductors inside the SpW cable, creates a very complex system of capacitive couplings between them; for instance, in the image below (Figure 3-1) all the mutual capacitances are drawn for only one of the conductors of one of the twisted pairs.

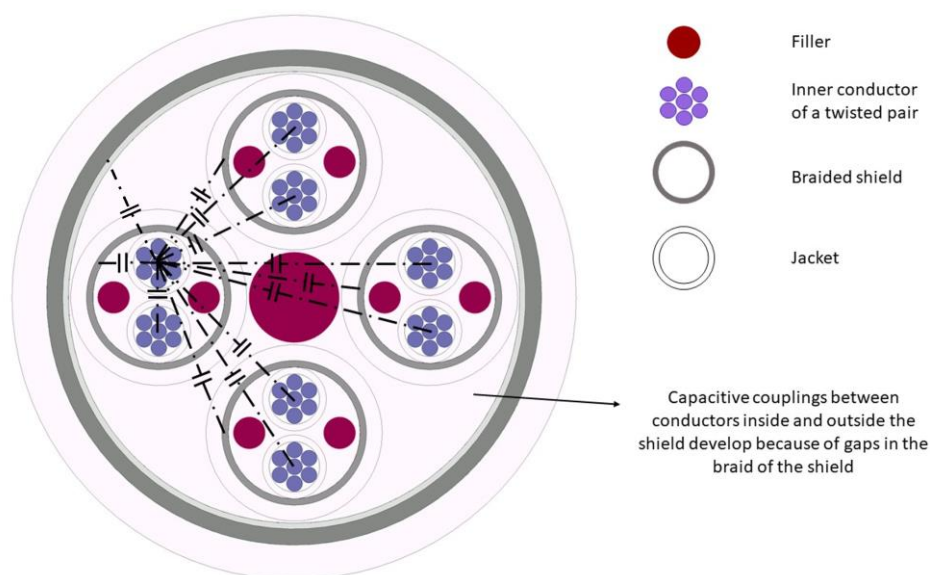


Figure 3-1. Capacitive couplings between conductors in a SpW cable.

Were the conductive shields completely covering each wire pair, there would be no capacitive couplings between conductors inside the shield and any conductors outside. Therefore, a simple grounding of the conductive shield would achieve complete cancelation of any induced noise through capacitive coupling. The use of braided shields cannot offer 100% coverage of the twisted pairs and this is the reason that so many capacitive couplings exist. It is important to note that due to the high quality of the material and the tightly woven braid of the shield, such couplings have relatively small capacitances.

Although the braided shield allows capacitive coupling between the interior and the exterior of the shield, it offers many advantages compared to a 100% coverage shield such as foil. For instance, it enables 360° termination of the outer shield, which is very challenging in a foil shield while also offering high flexibility and strain resistance to the cable.

To negate any induced noise through capacitive coupling to the shield, infiltrating the signal carrying conductors, the shield must be connected to ground. The grounding of the shield can be made either to the conductive enclosure of the connector and therefore to the conductive enclosure of the connected instrument or directly to the local circuit ground. The latter option makes sense only for cables in which unbalanced signalling is used and the shield is utilized as the reference for the received signal. In any other case it should be avoided because connecting the shield directly to the local ground at an instrument's input port, can potentially cause induced currents to flow to the local ground and as a result, cause interference [17].

ii. Inductive coupling

As was the case for capacitive coupling, inductive coupling also exists between each signal carrying conductor and any other conductor which is part of a closed-loop. As mentioned earlier, the magnetic emissions of the SpW link are caused by induced currents to the shields of the cable due to the operation of the link. The mutual inductance between two conductors depends on their geometry, their relative position and the magnetic properties of the medium between them.

In a SpW cable, each wire pair is twisted with itself and the four wire pairs are also twisted with each other. The complex geometry of any pair of conductors makes the definition of their mutual inductance a difficult process. Though it is hard to completely define any of these inductances, one can understand that the mutual inductance between any conductive shield and the two signal carrying conductors of a twisted pair, is different. As a result, even if the currents in the two wires of a pair are exactly equal with opposite directions, the total induced current in any conductive shield from an operating twisted pair will not be zero.

In general, the use of differential signalling theoretically prevents any magnetic emission from the wire pair, as the two conductors possess equal and opposite currents. However, either through transmission losses in the wire or by heat losses in the termination resistor, the two currents in a wire pair cannot be exactly equal. This adds up to the unequal inductances between the two wires of a pair and any conductive shield, making it safe to assume that the operation of a SpW link causes induced currents to flow in the cable's shields and therefore causes unwanted magnetic field emissions. The twisting of the wire pair greatly reduces its magnetic field emissions, but it cannot completely nullify them. [17]

iii. Shield grounding

In addition to the coupling mechanisms between nearby conductors, an important aspect to be considered when analyzing the emissions produced by the operation of a cable is the method used to ground the cable's shield.

When considering the shielding of a cable, it is usually more important to make certain design choices in order to increase its immunity to external interference than to avoid emissions. Towards this goal, it is necessary that the conductive shield is grounded, in order to protect the inner conductors from any noise induced through capacitive coupling to the shield. The grounding of the shield can be done either at one or at both ends of the cable, with each method providing certain advantages and disadvantages. Grounding the shield at only one end prevents the inclusion of the shield in any loop but allows it to act as an efficient straight wire antenna at certain frequencies, depending on the cable's length. Additionally, such a shield offers no protection against inductively induced noise, especially in higher frequencies. A simple conductive shield cannot block external magnetic fields and thus, in response to an external alternating magnetic field, an alternating current is induced in both the shield and the inner conductor. The inductively induced current to the shield, from the external interfering source, causes a secondary induced current to the inner conductor which cancels the directly induced current from the external interference source. This is essential in order to enable inductively induced noise cancellation for frequencies greater than the cut off frequency of the shield. Therefore, it is frequently preferable to ground the shield at both the wire's ends to enable the flow of current through it.

This though is not without consequences, because grounding the shield at both ends creates a conductive loop as the local grounds at the cable's ends are certainly connected through a conductive path (**Figure 3-2**). This loop can be detrimental to the performance of the system as the shield is part of a loop

antenna both picking up and radiating noise. The situation is significantly worsened if the ground loop has a physically large area.

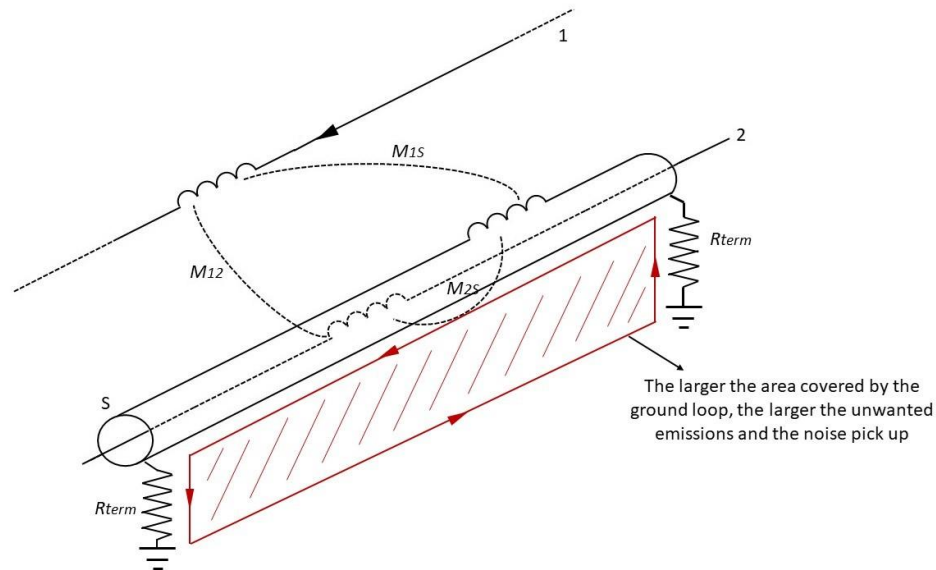


Figure 3-2. Mutual inductances between the inner conductor, the shield and an interfering conductor and the created ground loop.

It should be mentioned that for low-frequency currents, the cables are short compared to the wavelength and therefore the inductive couplings can be represented by lumped inductances.

At this stage, it is considered worthwhile to briefly analyse a major change that has been made in the “Physical Layer” of the SpW cable assembly in the latest version of the standard (ECSS-E-ST-50-12C Rev.1, 15 May 2019 [3]). Specifically, the cable assembly labeled as type AL (**Figure 1-10**) represents the cable assembly as it was defined up until the latest revision of the standard, whereas the one labeled as type A (**Figure 1-11**) defines the new type of cable assembly. The only difference between the two types is the way the inner shields of the twisted pairs are connected to ground. Based on the previous analysis of the coupling mechanisms and the shielding techniques used to protect the signal carrying conductors of a cable from induced noise, a short mention of the different properties of each cable assembly type is given below.

Type AL

In type AL cable assemblies, the inner shields are connected only at the transmitting end of each twisted pair, to pin 3 of the connector. In female connectors, this pin is connected to the local ground, therefore the inner shields are directly grounded to the local ground at the transmitting end. Though not allowing the formation of a loop, by connecting the shield only at one end, the shields can act as antennae for certain frequencies, both receiving and transmitting noise. Additionally, any induced currents to the shield will flow

to the local ground at an instrument's input port and thus potentially cause interference. Another problem with this method that hasn't been mentioned previously, is that stray capacitances are formed between any nearby conductors and the unconnected end of a shield. These capacitances maintain the separation of the conductors at lower frequencies but as the frequency increases, paths can be created for the induced current to flow through them to nearby conductors. This can lead to significant interference, as the nearby conductors can be signal carrying conductors. The phenomena described above are depicted in Figure 3-3.

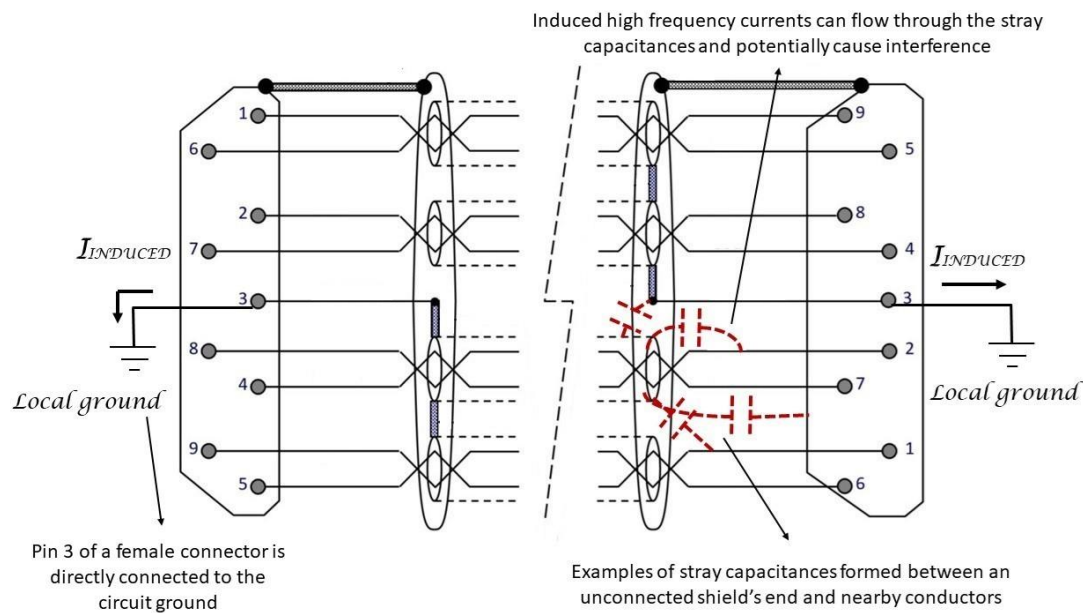


Figure 3-3. Type AL cable assembly.

Finally, another significant drawback of connecting a cable's shield to a connector's pin is the potential breach of the connected instrument's conductive enclosure. The purpose of a conductive enclosure is to act as a Faraday cage at high frequencies, blocking any external interference from entering and therefore from inducing noise to the inner sensitive electronic circuits of the instrument. This can be nullified if the pin where the shield was terminated, is connected via a wire (pigtail) to the local ground. If this method is used, any induced current to the shield runs through the pigtail to local ground and thus breaches the conductive enclosure of the connected instrument, acting as an interference source for the inner electronic circuits (Figure 3-4).

There are plenty of alternative techniques to mitigate this drawback, though because it is not specified in the standard which method is used to connect the ground pin of the connector to local ground, this potential problem is deemed worthy of mention.

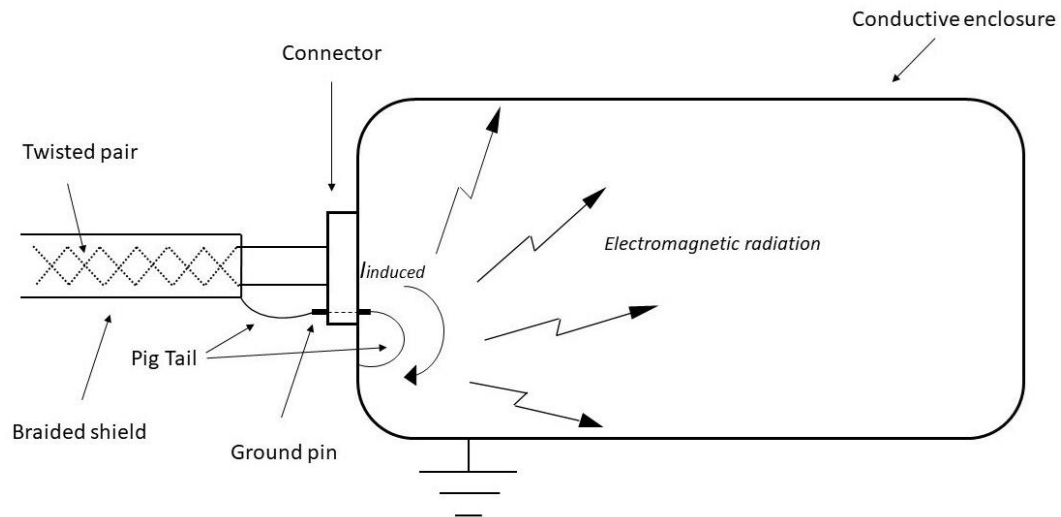


Figure 3-4. Ground pin connection to ground.

Type A

In the latest revision of the standard, the grounding method for the inner shields of the wire has been drastically altered. In type A cable assemblies, all the shields, inner and outer, are terminated to the conductive enclosure of the connector (**Figure 3-5**). The conductive enclosure of the male connector is connected to the enclosure of the female connector and therefore to the enclosure of the connected instrument. Grounding the shields through the enclosure, ensures that any induced currents to the shield will not cause interference in the system by flowing through the local ground at the instrument's port. This method of terminating the inner shields offers a plethora of advantages when compared with the one used for type AL cable assemblies.

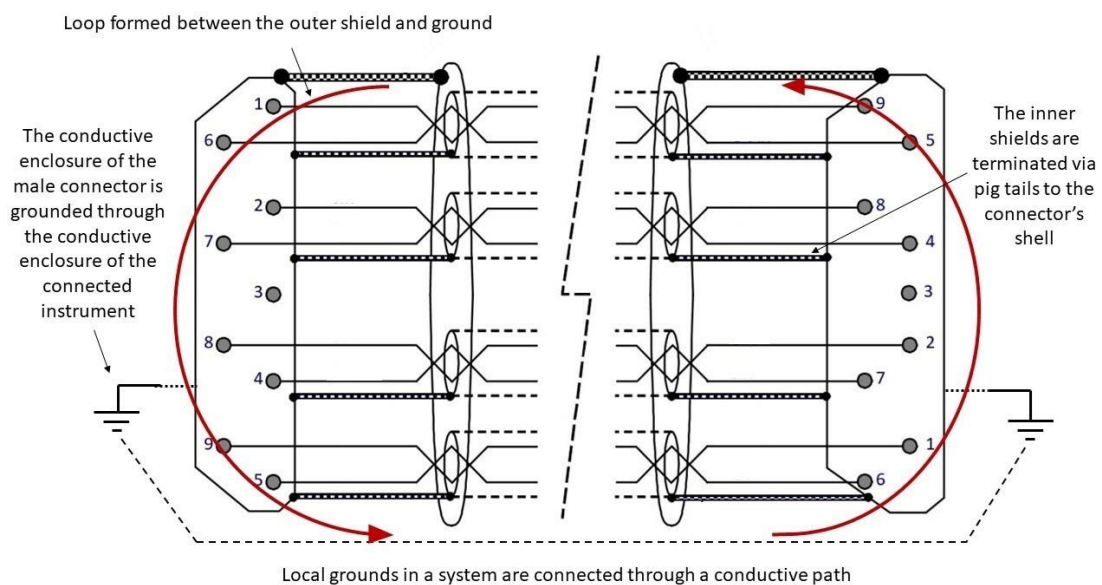


Figure 3-5. Type-A cable assembly.

In both types of cable assemblies, the outer shield of the cable is 360° terminated to the connector's conductive backshell at both ends of the cable. This is mainly done so that the outer shield completely engulfs the inner conductors, thus reducing the capacitances of the capacitive couplings between conductors inside and outside the shield. This area of the cable, near the connector, where the inner and outer shields are terminated, is responsible for the largest part of the emissions of the cable. As mentioned above, the outer shield is 360° terminated to the conductive backshell of the connector while the inner shields are connected via wires (Pig Tails) to either the ground pin (Type AL) or the connector's shell (Type A). Additionally, in order to connect the signal carrying conductors to their respective pins, the wire pairs must not be twisted near the connector. Therefore, an area is created where the signal carrying conductors are untwisted and unshielded from the inner shields and additional wires (Pig Tails) carry any induced current to the inner shields to either the connector's shell or the ground pin. This area is completely engulfed by a conductive layer formed by the outer shield and the conductive backshell of the connector (**Figure 3-6**). The untwisting of the wire pair and the wires that terminate the inner shields cause significantly more emissions at the aforementioned area than at any other point of the cable. The electromagnetic fields produced inside this conductive cavity induce currents in the outer shield which then pass through the ground loop and can lead to noticeable magnetic emissions.

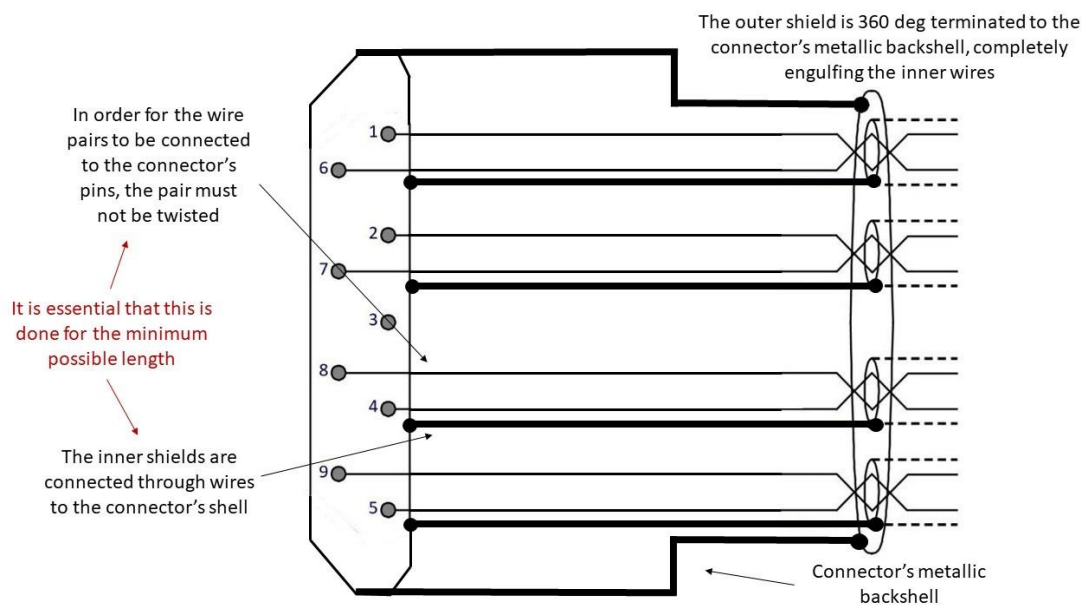


Figure 3-6. Cable's connection to the connector (Type A).

For this reason, it is of great importance in the design of the cable assembly that this area covers the shortest possible length, therefore the wire pair is untwisted for the minimum length required to make the connection and the wires used to terminate the inner shields are as short as possible. Despite those

efforts, the emissions caused by this design of the connector can be significantly more than those from any other mechanism described above.

This problem can be more noticeable at type A cable assemblies. Specifically, the grounding of the inner shields at both ends of the cable allows current to flow through them. This current can be either induced by the signal carrying conductors or caused by slight variations of the ground voltages at the cable's ends. The termination method used in type A cable assemblies increases the number of unshielded current-carrying conductors inside the conductive cavity formed between the conductive backshell of the connector and the outer shield. In return, this can lead to larger induced currents in the outer shield of the cable and therefore more noticeable magnetic emissions.

2. Current's Frequency Spectrum

As emphasized multiple times above, the main aim of this thesis is to measure the static and low frequency magnetic field emissions caused by the operation of a SpW link. The measured alternating magnetic fields are produced by AC currents flowing through the conductive shields of the SpW cable, which are in turn induced by the currents in the twisted pairs. For an alternating magnetic field of a certain frequency, there is an AC current with the same frequency in the outer shield. In turn this requires that the currents in the twisted pairs include this frequency in their spectrum. Furthermore, the induction mechanisms described above do not apply for DC currents, thus any static magnetic field emissions will be produced by DC components in the twisted pairs' currents. Therefore, in order to make a complete analysis for the potential of magnetic field emissions from the operation of a SpW link, the frequency spectrum of the currents flowing through the twisted pairs should be examined.

i. Current's Waveform

In order to examine the frequency spectrum of the currents flowing through a twisted pair, at first, the waveform of the current relative to the transmitted bit stream should be considered. At the receiving end, each wire pair is terminated by a 100 Ohm resistor and the differential output signal is obtained between the resistor's ends. As was thoroughly described in the overview of the standard's signalling layer, **clause 1.5.viii**, if the differential voltage's level is larger than 100mV, the received bit is deemed to be a one, whereas if the level is lower than -100mV it is deemed to be a zero. The current flowing through the termination resistor exhibits the same behavior as the voltage, with different high and low levels ($i(t) = \frac{v(t)}{R}$). A simple example, depicting the output voltage and current relative to the transmitted bit stream, is presented

in **Figure 3-7** (for the purposes of this analysis, no transmission errors are considered).

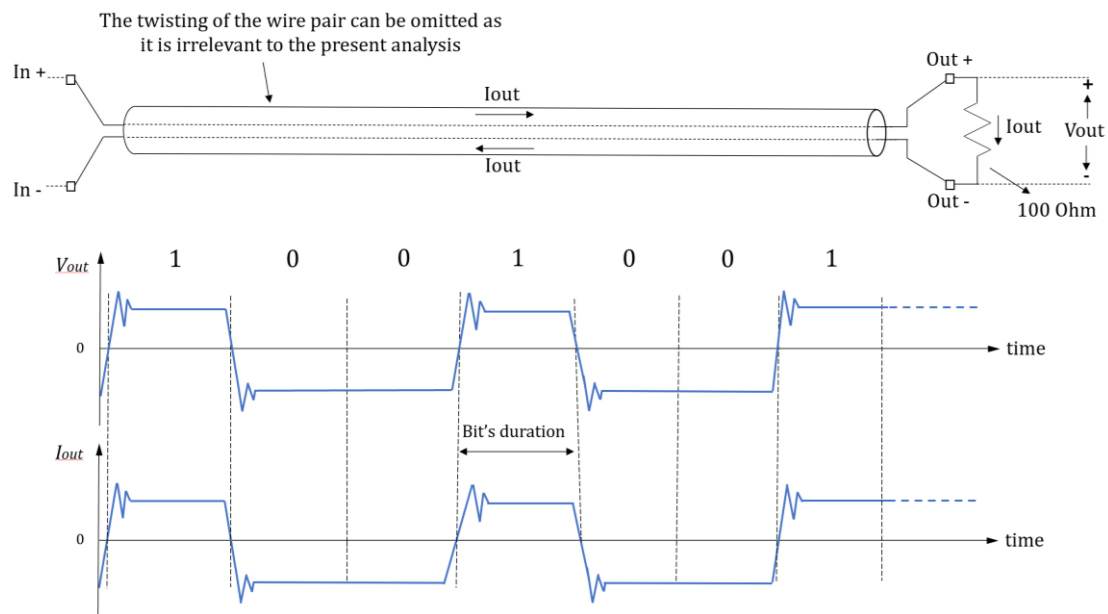


Figure 3-7. Output voltage and current relative to the transmitted bit stream.

The SpW cable consists of four twisted wire pairs, two of which are used for each direction of the link. The need for two signals arises from the use of the Data-Strobe encoding scheme in the SpW standard. The latter utilizes the Strobe signal to encode the clock of the transmitter and thus to enable the synchronization of the receiver. The Data signal is where the data bit stream is directly encoded, and it is used to convey the desired information through the link. In this particular analysis, the frequency spectrum of the current flowing through a data wire pair will be examined. This is mainly done to emphasize certain differences in the expected results for the different payload types used (“random” and “zeros”). It should be noted though, that studying only the data wire pair’s current, although offering great insight to the methods involved, does not consist a complete analysis for the potential spectral components of the induced current in the outer shield. For this to be achieved, the currents flowing through the Strobe wire pairs should also be examined. The transmission through the data wire pair is performed by sending SpW packets, Nulls⁴, FCTs⁵ and optionally broadcast codes, so in order to examine the current’s waveform, the role of these components in the case of this setup, will firstly be discussed.

⁴ Nulls→ Null control codes

⁵ FCTs→ Flow Control Tokens

SpW packet

A SpW packet consists of the header (destination address), the cargo (data characters) and the termination control character. In the case of a SpW link there is no need for a destination address as no routing switches exist. However, it is possible that iSAFT uses headers to differentiate between the different types of packets it can transmit (SpW, CPTP and RMAP packets). In any case, the existence of a header does not alter the following analysis, given that it has no reason to change between sequential packets. For the cargo to be constructed, a packet's payload is embedded in data characters, specifically, each byte of payload is integrated in a 10-bit data character (including a parity bit and a data control flag). After the data characters are serialized and the cargo is formed, the header is added before the first data character and a control character (EOP or EEP) after the last, thus completing the packet. The iSAFT's transmission mode used for the operation of the SpW link is "Traffic generation" (**clause 2.3.iv**), i.e. a single packet is transmitted continuously for each direction of the link. Additionally, the terminator type is a user defined parameter and, in this case, it is always set to EOP.

Flow Control Tokens

The data characters and the EOP and EEP control characters are the components of SpW packets and are labeled as N-Chars (Normal characters). The transmission of N-Chars across a SpW link is managed by the flow control mechanism and specifically by the transmission of FCTs. A SpW port possesses both a transmitter and a receiver and each of them has a counter which expresses the number of N-Chars that are allowed to be transmitted and are expected to be received respectively. When a N-Char is transmitted or received, the respective counter is decreased by one. The receiver's counter signifies the number of N-Chars for whom there is adequate space in the receive FIFO of the port and its maximum value is 56. If the receive FIFO can hold less than 56 N-Chars, the respective counter's maximum value can be smaller. The maximum value of the transmitter's counter is governed by the maximum value of the receiver's counter at the other end of the link. The FCTs are used to increase the values of these counters when required and each FCT corresponds to eight N-Chars. In particular, when there is enough space in the receiver's queue for another eight N-Chars and the respective counter has a value of eight or more, less than its maximum value, then a FCT is transmitted and the value of the receiver's counter is increased by eight. Likewise, if a FCT is received, the value of the transmitter's counter is increased by eight. When the latter becomes zero, N-Chars are not transferred to the transmitter until a FCT is received. If a N-Char is received and the value of the receiver's counter is zero, or if the transmitter's counter exceeds its maximum value, then a credit error is detected, signifying that another unknown error has occurred, and the link is reinitialized.

Null control codes

The packet to packet delay is set to the iSAFT's default value of 100 μ s. As was mentioned in **Table 1-1**, if the length of time since the last reception or transmission through the link is longer than a defined threshold (maximum 1 μ s), then a disconnect occurs. Following the disconnect, the link reinitialization begins. To avoid the latter, due to the relatively large packet to packet delay (100 μ s), when no packet is due to be sent, the transmitter sends repeatedly Nulls to keep the link active.

Broadcast codes

The time-codes and distributed interrupts formed by broadcast codes are used to transmit synchronization information and to signal events across a SpW Network respectively. Therefore, they are not used in the case of a point to point SpW link, such as the one currently examined.

In the case of traffic generation with identical packets, if no FCTs were being sent, the current's waveform in a data twisted pair would be a perfectly periodic signal, with a period of T, comprising of two states, packet and Null transmissions (**Figure 3-8**).

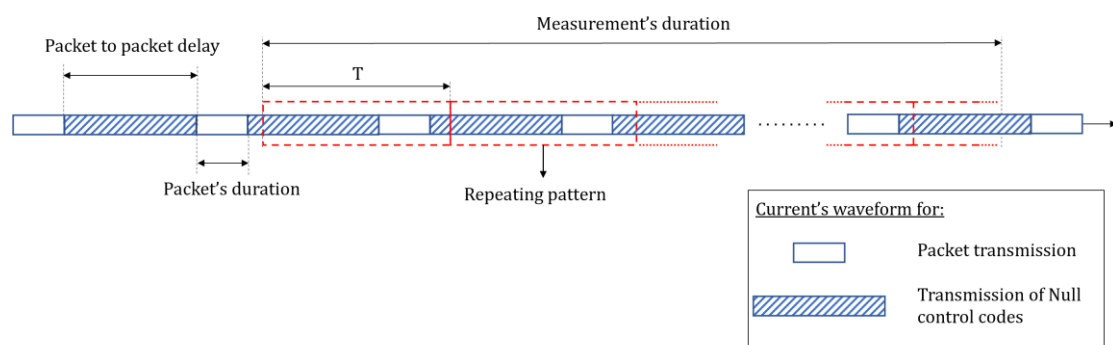


Figure 3-8. Current's waveform and patterns that emerge, without the presence of FCTs.

However, a port's transmitter will send FCTs when the same port's receiver acquires N-Chars. Therefore, the current's waveform for the data twisted pair for one direction of the link, depends on the data twisted pair's current for the other direction of the same link. If the packets' transmissions do not coincide for the two directions of the link, then the current's waveform would have a form like the one presented in **Figure 3-9**. When the one end of the link sends N-Chars, the other end will send a FCT for every eight N-Chars it receives. If FCT transmission is not required, either Nulls or N-Chars are sent, depending on the stage of the transmission and the sending priority.

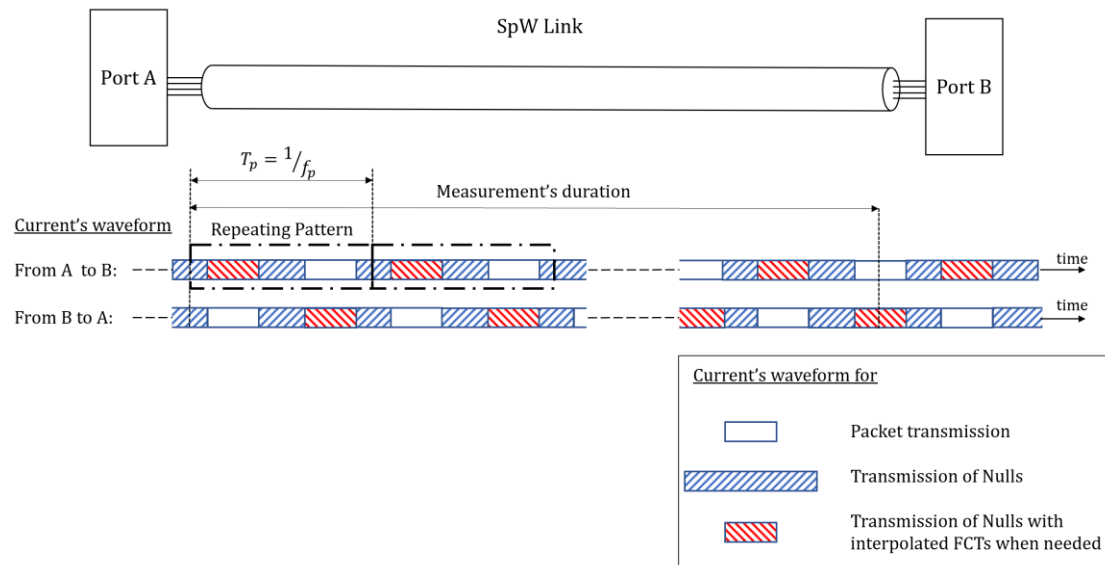


Figure 3-9. Data wire pair's current waveform and patterns that emerge, including the presence of FCTs.

It is impossible to completely predict the current's waveform, as the transmission is manually activated at both ends of the link and therefore, the relative positions of the packets' transmissions in the two waveforms cannot be known. The aforementioned case, i.e. when the packet transmissions for the two directions of the same link do not coincide, offers a simplified example where the repeating pattern is clear. If this is not the case, the current's waveform can become very complex as certain packets' durations may increase to accommodate the necessary transmission of FCTs. In general, it can be expected that patterns will emerge in the current's waveform of a data twisted pair. For example, a repeating pattern can be comprised of the packet's duration and the packet to packet delay as shown in **Figure 3-9**.

The case of inadequate room in the receive queue (Rx FIFO) and thus transmission delay, is not considered, as the iSAFT receiver's FIFO at each port is very large (8 Mbytes).

ii. Fourier Analysis & Frequency Spectrum

The frequency spectrum of an ideal periodic signal is an infinite sum of discrete spectral components. These components appear both in negative and positive harmonics of the signal's fundamental frequency as well as in DC. For the purpose of visualizing this behaviour, the periodic signal ($x(t)$) must be expressed by the equivalent Fourier series. The complex-exponential form of the latter is presented below (the expansion coefficients (c_n) are complex numbers and f_0 is the fundamental frequency of $x(t)$).

$$x(t) = \sum_{n=-\infty}^{+\infty} c_n e^{jn2\pi f_0 t} \quad [3.1]$$

$$c_n = \frac{1}{T} \int_{t_1}^{t_1+T} x(t) e^{-jn2\pi f_0 t} dt \quad [3.2]$$

$$c_{-n} = c_n^* \quad [3.3]$$

$$c_0 = \frac{1}{T} \int_{t_1}^{t_1+T} x(t) dt \quad [3.4]$$

c_0 is the average value of $x(t)$ for one period and is a real number

The form presented in [3.1] contains both positive and negative harmonics of the fundamental frequency. Considering [3.3], the Fourier series can be simplified to depict the one-sided spectrum of the signal [3.5].

$$x(t) = c_0 + \sum_{n=1}^{+\infty} 2|c_n| \cos(n2\pi f_0 t + \angle c_n) \quad [3.5]$$

From equation [3.5], it can be derived that the one-sided frequency domain representation of a periodic signal $x(t)$ is comprised of a DC part (c_0) and an infinite number of components in positive harmonics of the fundamental frequency. The amplitude and phase of these individual components depend on the respective expansion coefficients (c_n) and therefore on the signal's form for one period [3.5]. In most cases, especially for complex signals, the computation of the expansion coefficients (c_n) is a very challenging process. However, for the purposes of this chapter, such an estimation is not required. In order to indicate the potential for low frequency emissions caused by the operation of a SpW link, we need only prove that patterns will arise in the current's waveform, with large enough periods to simulate low frequency components in its frequency spectrum. Therefore, the analysis presented earlier about the existing patterns, is an interesting indication about the current's frequency spectrum and an adequate justification for performing the measurements.

Nevertheless, it should be emphasized that the existence of low frequency components in the twisted pair's currents does not necessarily mean that emissions will be observed in the same frequencies. For DC components, it is also required that there is a noticeable difference between the currents in the two wires of a pair, whereas for positive frequency components, that the mutual inductances between the outer shield and each wire of the pair have a detectable difference. In addition to the above, the currents in the Strobe twisted pairs can potentially have low frequency components of their own. Finally, without exactly identifying the patterns and computing the respective expansion coefficients, we cannot be sure about any emissions. However, the presented analysis is a decent indication that measuring the static and low frequency magnetic field emissions of an operating SpW link, is worthwhile.

iii. Frequency Spectrum for Undefined Payload

For low frequency components to arise in the frequency spectrum, it is not required that the transmitted bit stream and thus the current's waveform is perfectly periodic. That might actually be the case even when the transmitted packets are in theory identical as the potential transmission of a FCT between two sequential N-Chars may ruin the repeating pattern. Naturally, even if the Fourier analysis is implemented for a perfectly periodic signal, it does not mean that slight variations between sequential repetitions of the pattern or even random bit stream transmission cannot cause low frequency components. To further explain this, a brief description of a twisted pair's current frequency spectrum when the transmitted bit stream is unknown will be added at this stage. This being the case, the current's waveform cannot be completely defined, and it is an extremely challenging endeavor to calculate its frequency components, thus it will not be attempted. Nevertheless, some important comments about the procedure involved will be made.

Considering the bit stream as a random sequence of ones and zeros, one can understand that the current will be a random NRZ⁶ pulse waveform with level A corresponding to a bit of one and $-A$ to a zero bit. Although the exact waveform cannot be predicted, it is expected that patterns will emerge in the transmitted bit stream and therefore in the current's waveform, as shown in **Figure 3-10**.

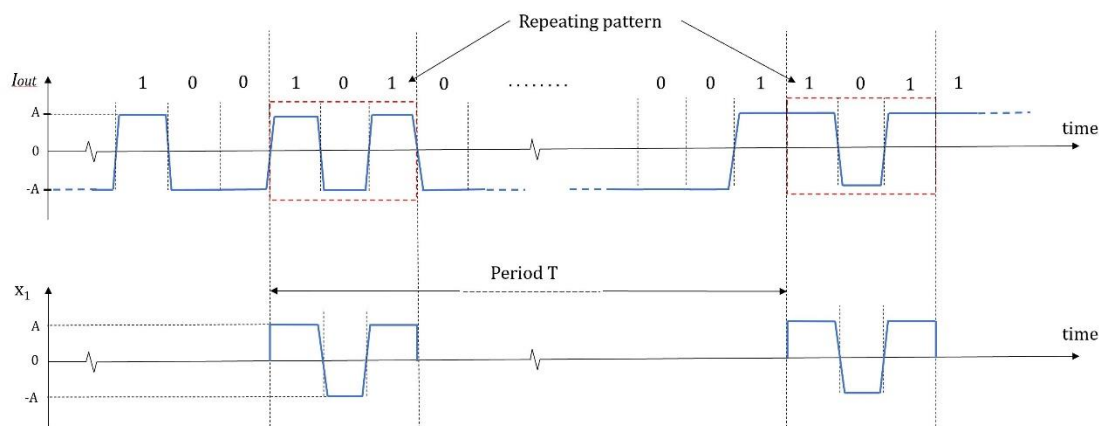


Figure 3-10. Current's waveform for transmission of a random bit stream.

The whole duration of the waveform can be analyzed to such components of repeating patterns. These components can be considered periodic signals with their contribution to the current's frequency spectrum focused around their fundamental frequency and its harmonics, as was presented in the earlier Fourier series analysis. As the transmitted bit stream is random, such patterns cannot be expected to appear during the whole time span of interest. This will only cause the reduction of the amplitude of their spectral components, which

⁶ NRZ: Non-Return to Zero

continue to appear in the spectrum even for a relatively short duration of the pattern in the signal. This argument will be verified by comparing the one-sided frequency spectrums for the three cases of a periodic signal presented below.

$$x_1(t) = 1 + \sum_{n=1}^{\infty} 2 \cos(2\pi n f_0 t), \quad \text{for } 0 \leq t \leq 3\text{sec}$$

$$x_2(t) = \begin{cases} 1 + \sum_{n=1}^{\infty} 2 \cos(2\pi n f_0 t), & \text{for } 0 \leq t \leq 1.5\text{sec} \\ 0, & \text{for } 1.5 \leq t \leq 3\text{sec} \end{cases}$$

$$x_3(t) = \begin{cases} 1 + \sum_{n=1}^{\infty} 2 \cos(2\pi n f_0 t), & \text{for } 0 \leq t \leq 0.5\text{sec} \\ 0, & \text{for } 0.5 \leq t \leq 3\text{sec} \end{cases}$$

where $f_0 = 100\text{Hz}$

For simplification purposes the amplitudes of all the expansion coefficients are set to one and their phases to zero:

$$\begin{pmatrix} c_i = 1 \\ \angle c_i = 0^\circ \end{pmatrix}, \quad \text{for } i = 0, 1, \dots, \infty$$

Additionally, only the first 5 harmonics are maintained in the presented spectrums (**Figure 3-11**, **Figure 3-12**) to facilitate the observations.

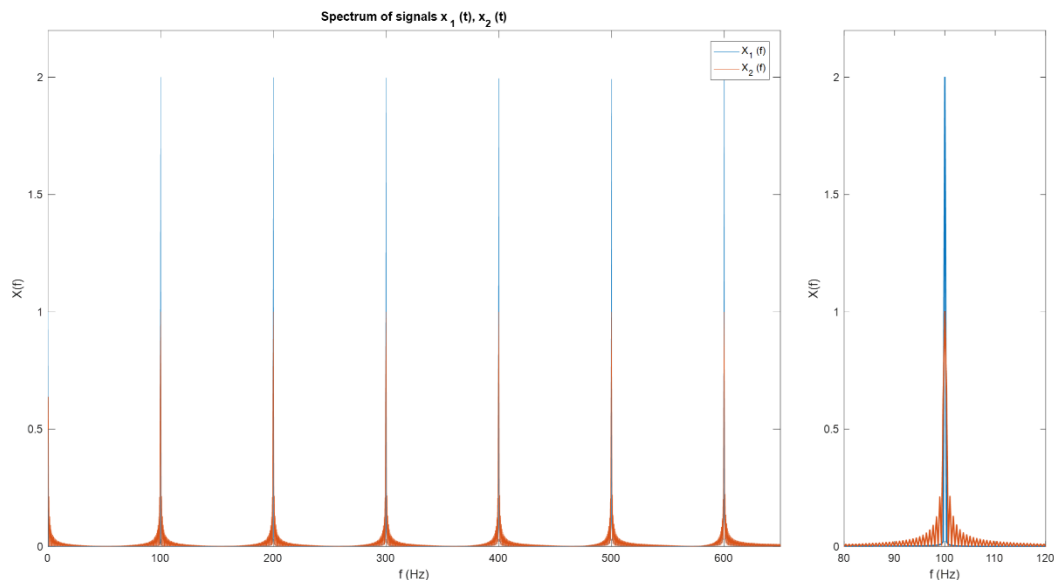


Figure 3-11. Spectrum of signals $x_1(t)$ and $x_2(t)$.

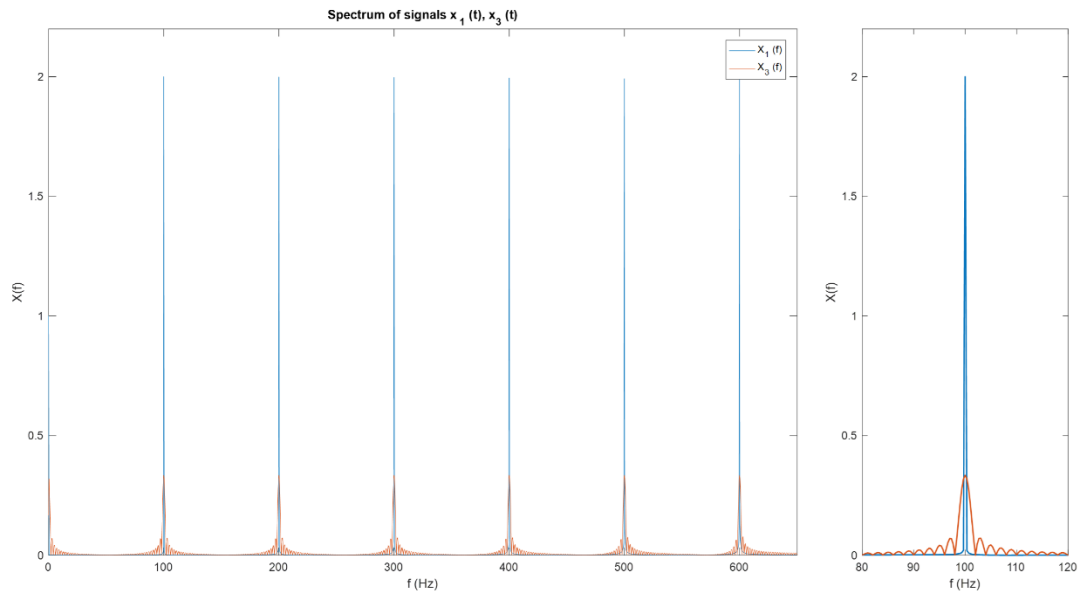


Figure 3-12. Spectrum of signals $x_1(t)$ and $x_3(t)$.

It can be observed that even when the pattern appears for only around 16% of the signal’s duration, though dampened, these frequency components are noticeable.

Bearing in mind the possibility for a multitude of such repeating patterns with different periods, it can be assumed that the frequency spectrum of the current will contain a large frequency range, including low frequencies. Therefore, there is the potential for low frequency emissions even when the transmitted bit stream is unknown. It should be emphasized again though, that the existence of such low frequency components in the twisted pair’s current does not necessarily mean that corresponding components will exist in these frequencies in the magnetic field.

iv. DC component – Payload Correlation

The use of different payload types (“zeros” and “random”), mainly aims to identify any differences between the measured static fields in each case. Specifically, there is an argument to be made that the DC component of the current in a data twisted pair will have a greater absolute value if a payload of zeros is used. This is due to the fact that a byte of zeros is integrated to a ten-bit data character containing minimum nine zero bits (the data control flag of a data character is always set to zero as shown in **Figure 3-13**).

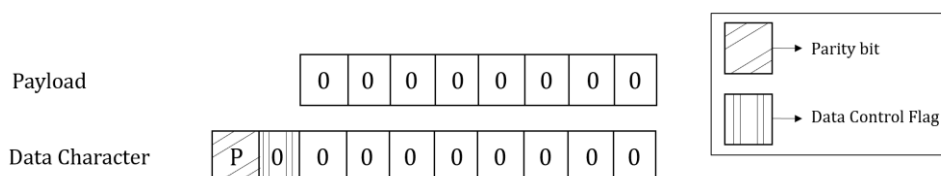


Figure 3-13. Data character and its payload.

The parity bits of sequential data characters with such payloads are set to ones, as shown in **Figure 3-14**.

Example of a 2-bytes packet

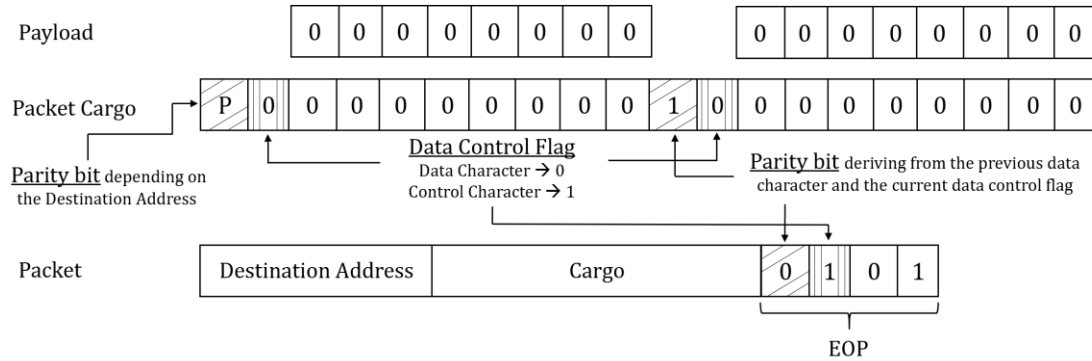


Figure 3-14. Example of a 2-byte packet.

Therefore, the cargo of a packet with a payload consisting of only zeros, is comprised of N_z zeros and N_0 ones (provided that all the parity bits, including the first, are ones).

$$N_z = 9 \times P$$

$$N_0 = P, \quad P = \text{payload length in bytes}$$

The potential transmission of FCTs between sequential data characters does not change this behaviour, as the parity bits of the data characters are already set to ones. In particular, the transmission of a FCT between two sequential data characters of this type, increases the number of zeros with respect to the number of ones ($N_z - N_0$), as can be observed in **Figure 3-15**.

Example of a 2-bytes packet with an interpolated FCT

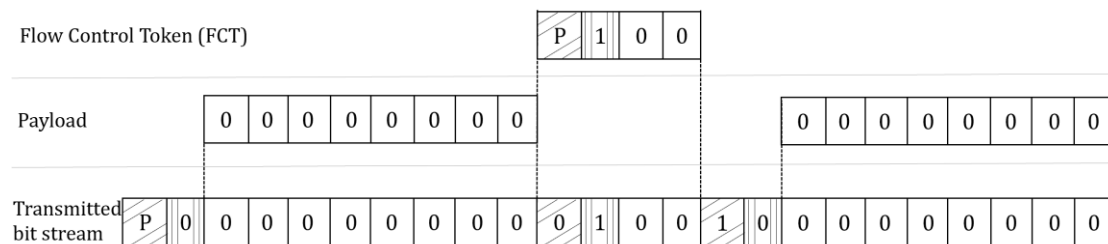


Figure 3-15. Example of a 2-byte packet, with an FCT transmitted in between the two bytes.

If the payload length is large enough, the values for any header (destination address) and the termination control character are negligible and the bit stream corresponding to the packet, consists predominantly of zeros. Additionally,

consecutive “NULL” control codes are comprised of the same number of ones and zeros as illustrated in **Figure 3-16**.

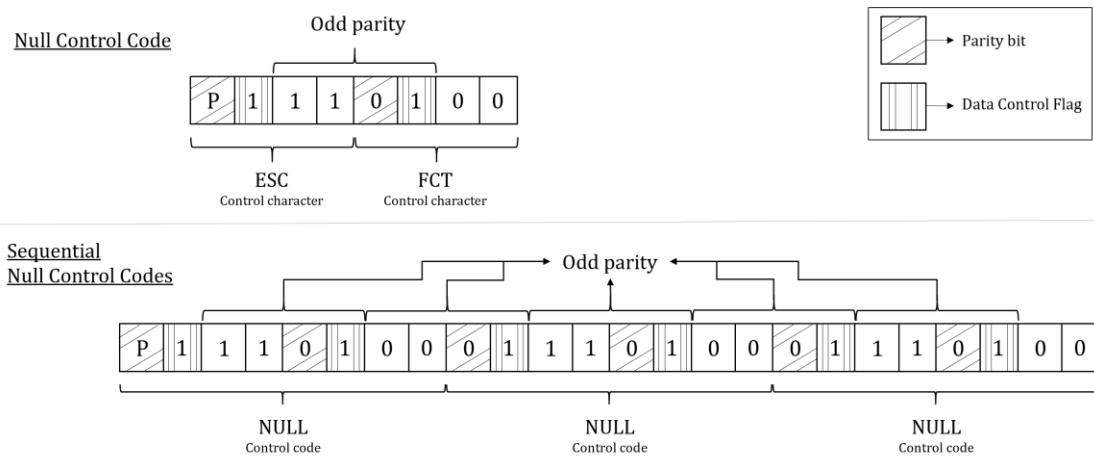


Figure 3-16. Bit stream of “NULL” control codes.

Even if between the repeating Nulls, FCT transmission occurs, the latter’s parity bit is set to zero, as presented in **Figure 3-17**, leading to a larger number of zeros compared to the number of ones.

Example of two Nulls with a interpolated FCT

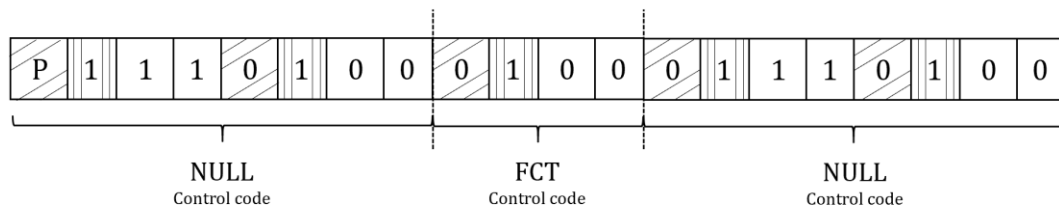


Figure 3-17. Bit stream of the sequence NULL-FCT-NULL.

As was described earlier in this clause, the repeating pattern in the current’s waveform consists of the packet’s duration and the delay between packets. The DC component of a periodic signal is equal to c_0 [3.4], which expresses the mean value of the signal for one period. For the delay between packets, where “NULL” control codes are sent, the waveform’s mean value will be very close to zero as there is approximately the same number of ones and zeros in this time span. On the contrary, for the packet’s duration, if the payload is comprised of only zeros, the mean value will be negative, especially for larger packets, as the data characters are also comprised mainly of zeros.

For random payload, a more uniform partition of zeros and ones is expected, thus the absolute mean value for one period, will be smaller. Therefore, for a payload of zeros, the signal's DC component is expected to be greater than that for a signal with random payload (**Figure 3-18**). Based on this theoretical prospect, the static parts of the measured fields will be compared for identical link characteristics and different payload types in **chapter 4**.

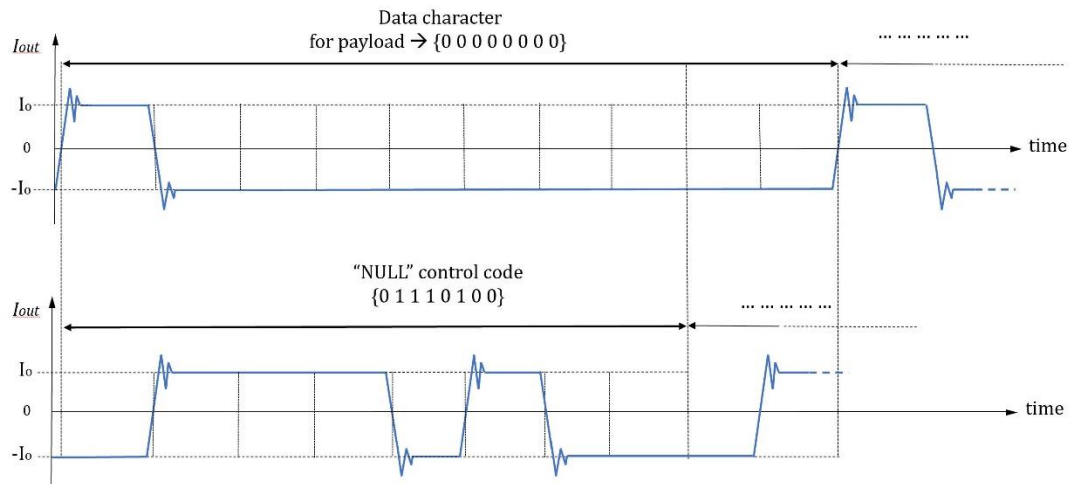


Figure 3-18. Current's waveforms for transmission of the data character [100000000] and a "NULL" control code with its parity bit set to zero.

As a final remark, it should be mentioned that the induced currents in the outer shield is only one of multiple potential emissions mechanism in the SpW link. Specifically, emissions can also be caused either by the connectors, due to their design or by the SpW ports which are also parts of the link. Whichever might be the case, it is considered very interesting and definitely worthwhile to examine the low frequency emissions spectrum of an operating SpW link.

4. Measurements Results

The purpose of the following chapter is to present the results of the performed measurements and attempt to explain the observed emissions, based on the mechanisms described in **chapter 4**. A thorough endeavor has been made to identify the worst-case scenario concerning the link's magnetic field emissions. For this reason, measurements have been performed for a great variety of link characteristics (link rates and packet sizes). The results displayed below have been verified by multiple tests, utilizing several layouts. For comparison purposes, a specific layout's measurements have been chosen to be presented. It is without saying that similar results occur for alternative layouts.

At this point, the measuring layout must be established. Specifically, in the following paragraph, the placement of the magnetic field sensors will be analyzed, with respect to the layout of the link, which has been extensively described in **clause 2-4**. The following figure (**Figure 4-1**) depicts the layout of the SpW link and the measuring equipment in the interior of the chamber.

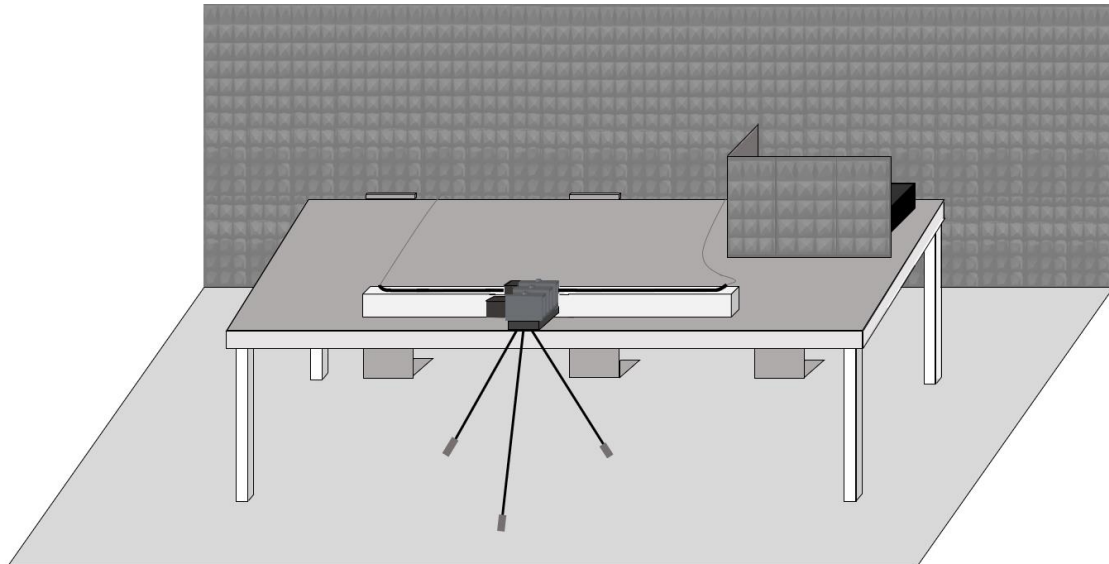


Figure 4-1. Overview of Measuring Layout.

1. Measuring layout

The two magnetic field sensors are placed on the outer cases of the 3D printed, plastic base (**Figure 2-3**) with the same orientation. The base is mounted on a tripod made of wood and plastic so as not to interfere with the measured field. The length of the base enables the inner magnetometer to be positioned closer to the link than the SpW cable's distance from the table's edge would otherwise allow. The magnetic field sensors are positioned in the middle of the linear part of the cable and they are oriented so that their largest dimension is parallel to it. The distance between a perpendicular to the table's surface plane, which includes the center of the cable and the center of the closest magnetometer, is 6cm, while between the centers of the two magnetometers, 15.2 cm. Both the magnetometers are positioned at a height of 8.2 cm over a tangent plane to the surface of the table. For the rest of this chapter the sensor closer to the cable will be referred to as magnetometer 1 (mag1) while the other sensor will be referred to as magnetometer 2 (mag2). The measuring layout as well as the orientation of the cartesian coordinate system used to display the measurement results are depicted in the following figures (**Figure 4-2** and **Figure 4-3**).

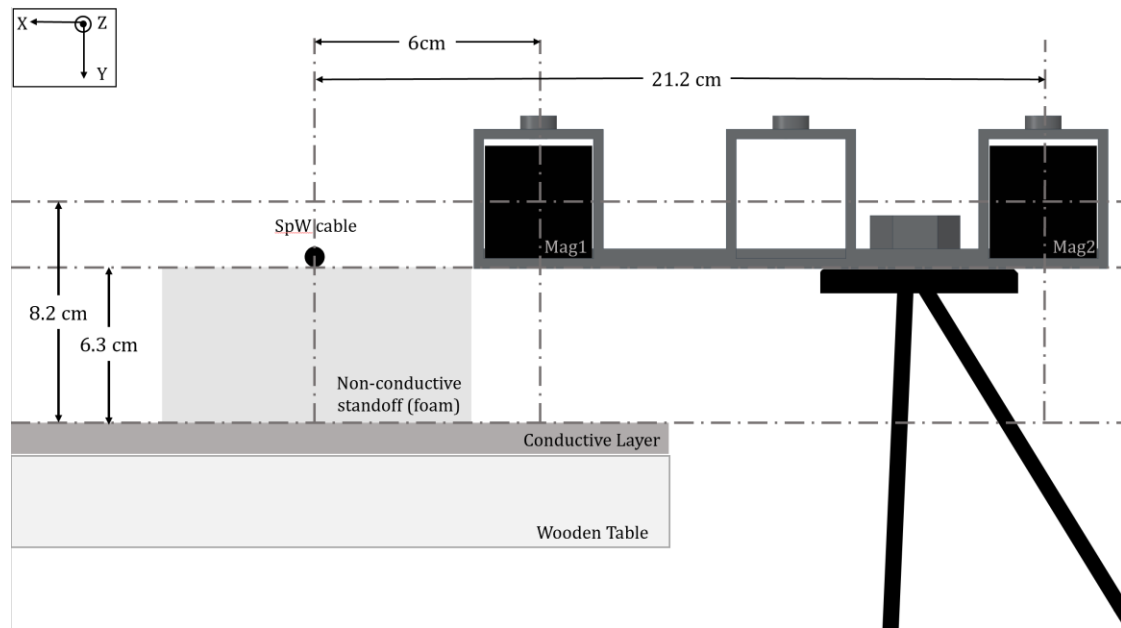


Figure 4-2. Side view of measuring layout [16].

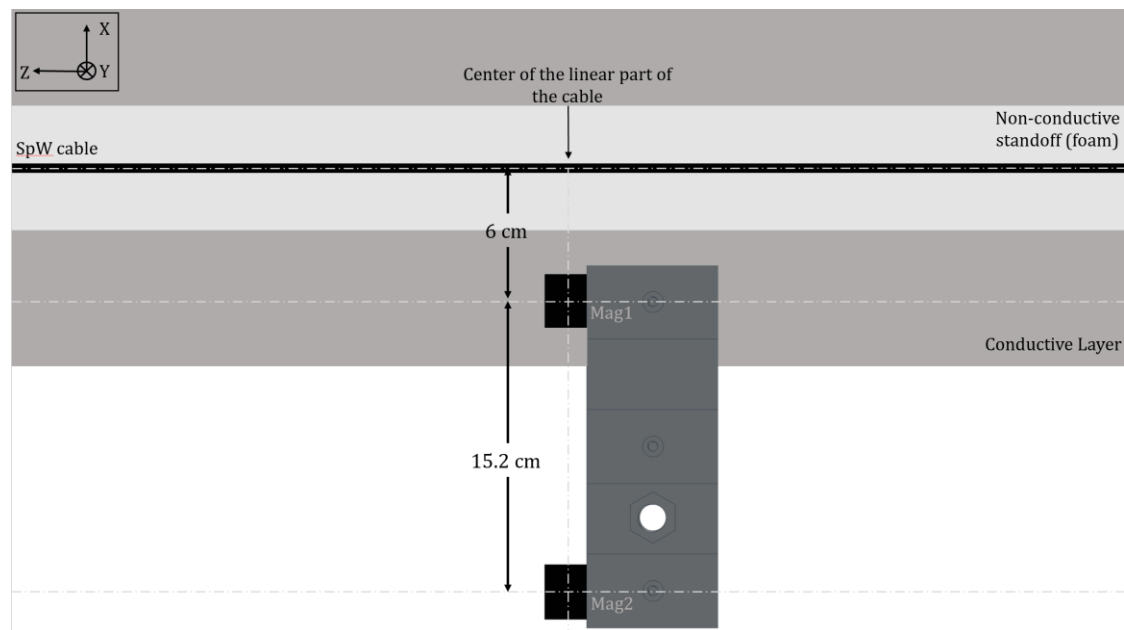


Figure 4-3. Top view of measuring layout.

The emissions analysis is divided into the static (DC) magnetic field emissions and the low frequency alternating (AC) magnetic field emissions. The signals produced by each magnetometer correspond to a triaxial time domain representation of the magnetic field for the duration of the measurement. Whereas the static magnetic field is obtained by calculating the mean value of the measured signal in the time domain, to examine the alternating magnetic field emissions, the frequency spectrum of the measured signal must be derived. For this purpose, the one-sided discrete Fourier transform of each measured signal, which represents its frequency spectrum, is computed using a fast Fourier transform (FFT) algorithm. By comparing the

static parts or frequency spectrums of the measurements for the operation of the link and the respective measurement for the ambient field, the contribution of the link, i.e. its emissions, can be obtained.

2. DC Magnetic Field Emissions

The first step in the measurement analysis is to examine any static magnetic field emissions produced by the operation of the link. As expected, the main source of static field in the measurements, is the Earth's magnetic field. The latter's measured amplitude, with respect to the coordinate system depicted in **Figure 4-3**, is around $4\mu\text{T}$ at x axis, $10\mu\text{T}$ at y axis and $11\mu\text{T}$ at z axis. Due to the presence of the Faraday cage, the field's amplitude is slightly altered from its expected value. The latter though, does not pose an issue to the measurements' accuracy as the exact value of the ambient magnetic field does not influence the background noise measuring technique. However, this is not the case for the slight fluctuations expected in the Earth's magnetic field between sequential measurements. Therefore, to ensure the reliable identification of any static field emissions, a set of measurements has been performed, without activating the EUT (SpW link deactivated and iSAFT shut down), in order to identify the range of the aforementioned fluctuations. In this measurement set, the delay between two sequential measurements is increased compared to the one achieved while measuring the link's operation, to simulate the worst-case scenario for the static field's variations.

After evaluating the measurement results, it is observed that the shift of the static part for most pairs of sequential measurements is confined to around 1.5 nT, nevertheless rarely it can be up to 4.5 nT (**Figure 4-4**).

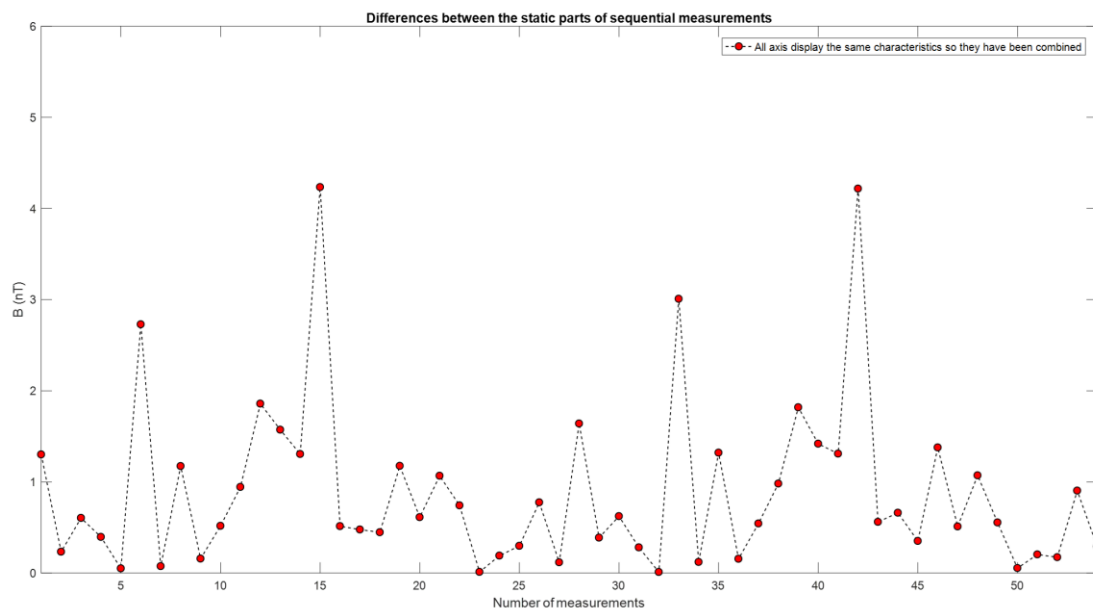


Figure 4-4. Absolute values of the differences between the static parts of sequential measurements.

An estimation of the power density function for the difference of two sequential background measurements' static fields is presented in **Figure 4-5**. By calculating the respective integral, it can be obtained that there is around 20% probability that the difference will be greater than 2nT. This means that lesser differences among the static parts of the ambient field and the link's operation measurements will not be considered as emissions caused by the link's operation. In addition, occasional and not repeatable differences at the range of 2 to 6 nT can be attributed to the probabilistic nature of the static field's fluctuations.

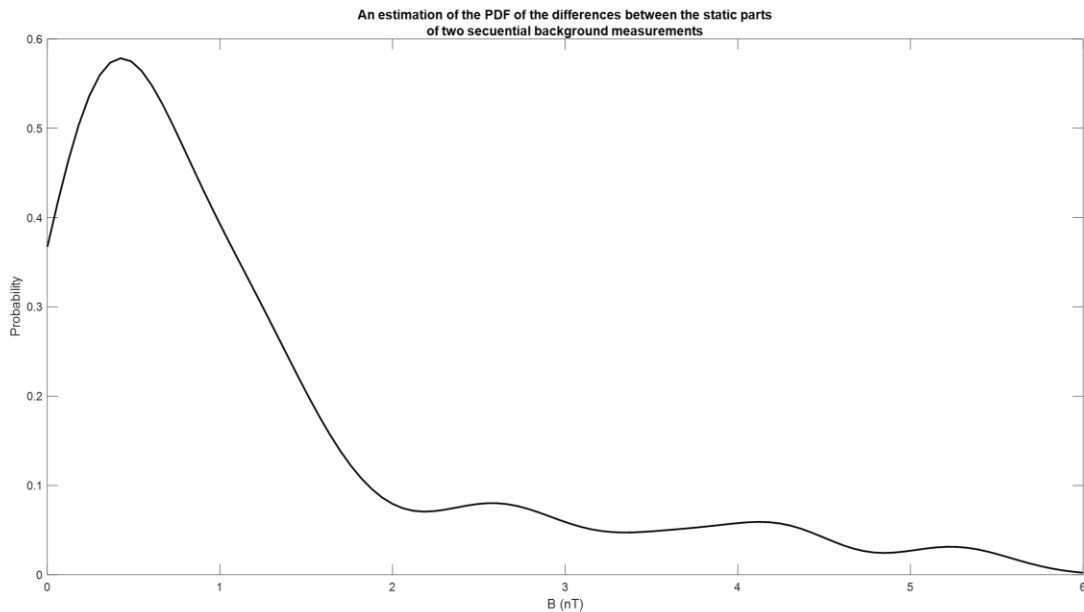


Figure 4-5. An estimation of the PDF for the absolute value of the difference between the static parts of two sequential measurements.

This can be additionally verified by a different group of measurements with the link active, in which for every set of link's characteristics two sequential measurements are performed, with little to no delay between them. It is observed that the static parts of the measurement pairs differ in a manner predicted by the derived power density function. As shown in **Figure 4-6** the difference is mainly less than 1.5 nT, while in a few cases it is around 2.5 to 3 nT. The somewhat improved behavior is due to the negligible delay between the measurements. It should be noted that the signals presented in the following figure are not denoised, therefore no comparison between different characteristics of the link should be made, only between the sequential measurements.

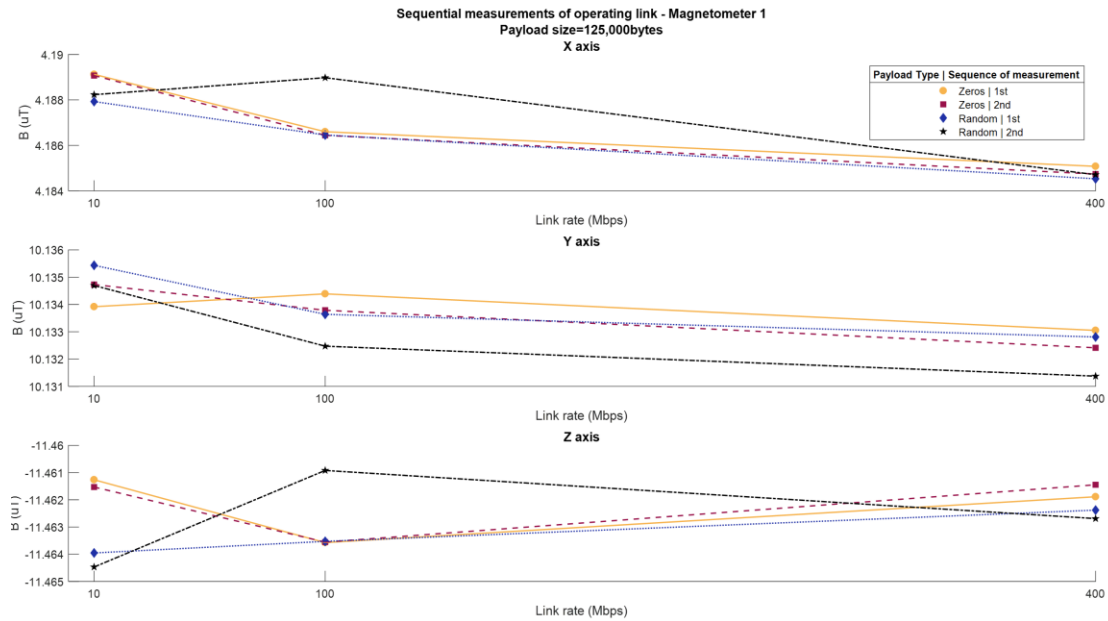


Figure 4-6. Sequential measurements of operating link – Link Rate
Magnetometer 1 - Payload size=125,000 bytes - “Zeros” and “Random” payload types.

Any static field emissions caused by the operation of the link, in contrast with the alternating field, are not produced by induced currents to the outer shield of the SpW cable. On the contrary, they would be caused directly by DC currents flowing through the twisted pairs. By design, the LVDS signalling method used does not produce DC currents through the pairs, though as was analysed in chapter 5.2 the repeating patterns created in the current’s waveform possess DC components in their frequency spectrum. Specifically, for packets comprised by a payload of only zeros, the DC component in the current’s spectrum is expected to have a greater amplitude than for packets with random payload.

The characteristics for the link’s operation utilized during the measurements included link rates of 10, 100, 200, 250, 300, 350 and 400 Mbps and payload sizes of 32, 512, 2048, 10,000, 50,000, 100,000 and 125,000 bytes. All measurements have been performed for both packets whose payload was a random sequence of bits and packets with a payload of only zeros. To produce the measurement results, the mean values of the signals derived from the ambient field and the operating link’s measurements are calculated and then subtracted. The results for various characteristics of the link are displayed in **Figure 4-7** to **Figure 4-11**.

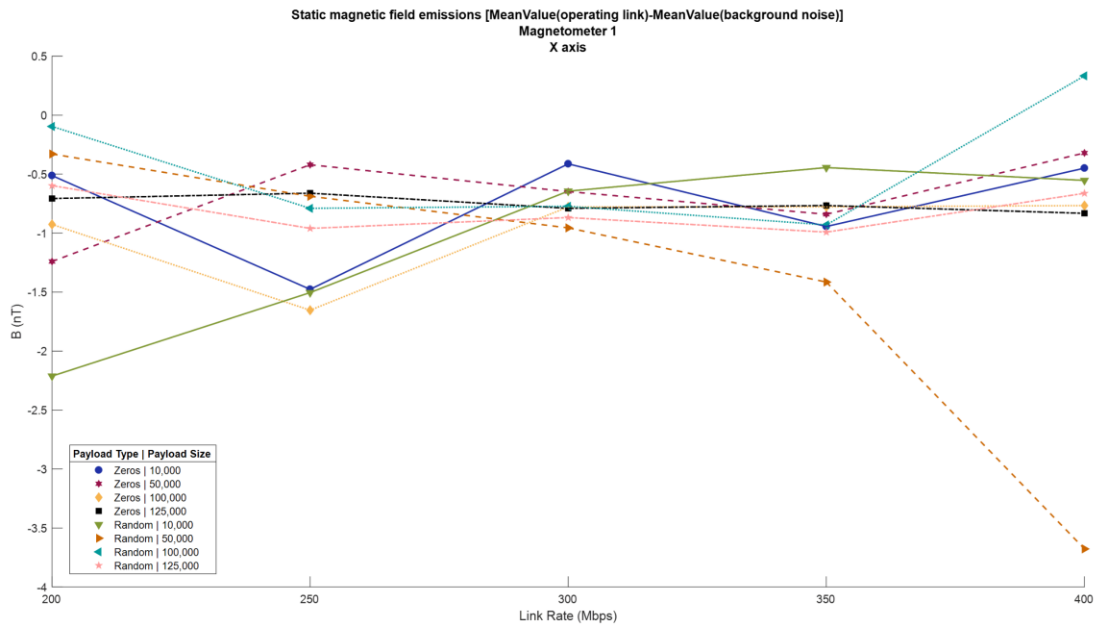


Figure 4-7. Static field emissions at x axis – Link Rate (Magnetometer 1)
Payload Sizes of 10,000, 50,000, 100,000 and 125,000 bytes – “Random” and “Zeros” payload types.

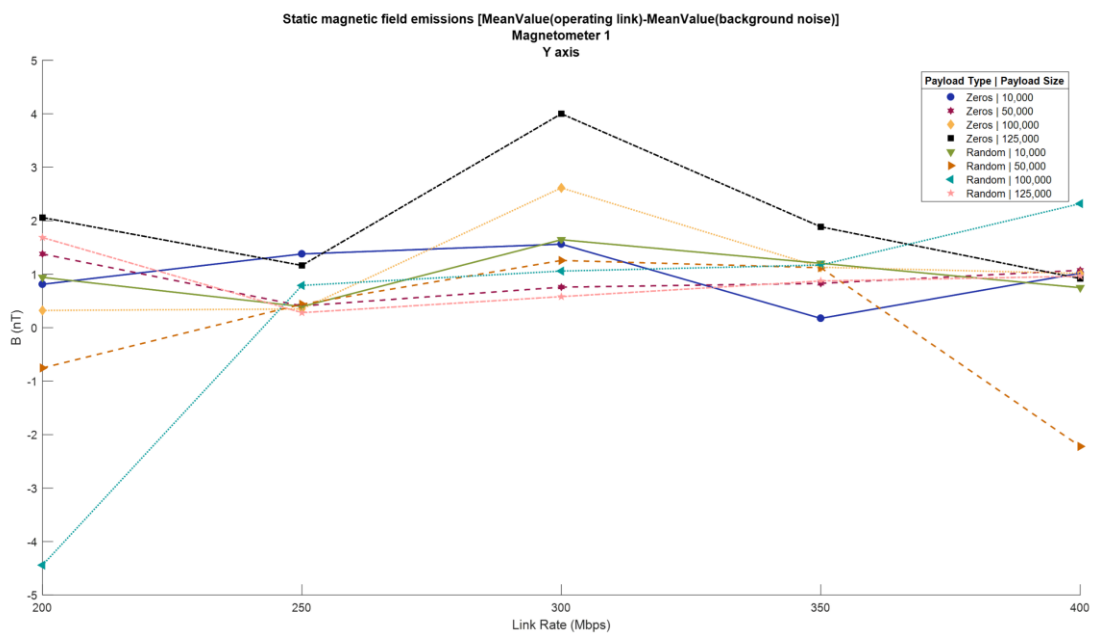


Figure 4-8. Static field emissions at y axis – Link Rate (Magnetometer 1)
Payload Sizes of 10,000, 50,000, 100,000 and 125,000 bytes – “Random” and “Zeros” payload types.

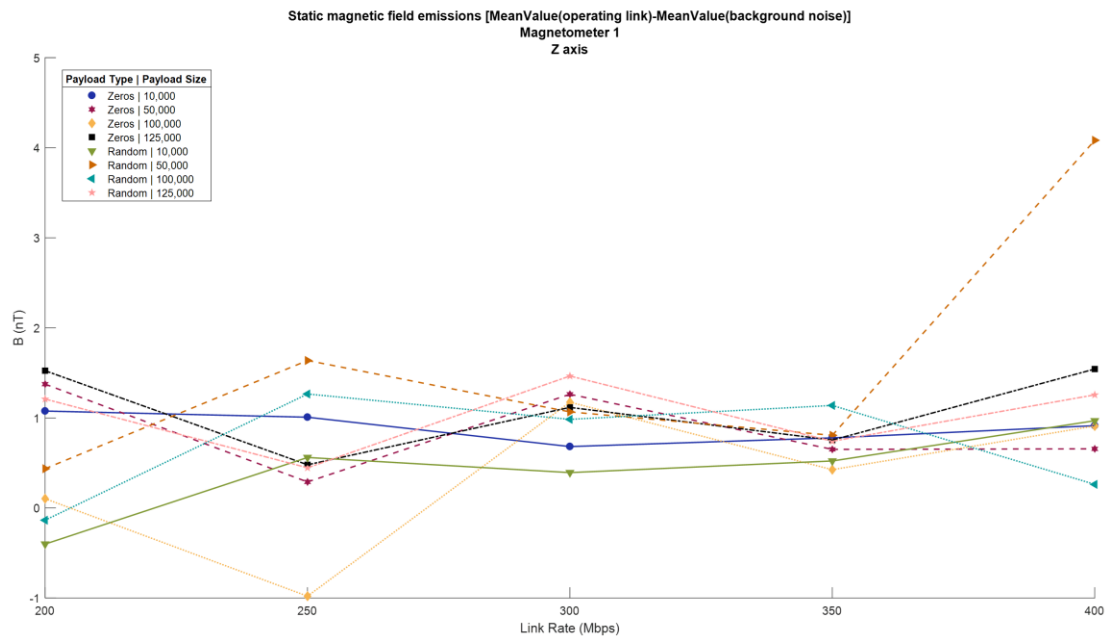


Figure 4-9. Static field emissions at z axis – Link Rate (Magnetometer 1)
Payload Sizes of 10,000, 50,000, 100,000 and 125,000 bytes – “Random” and “Zeros” payload types.

It is observed that no clear indication of magnetic field emissions caused by the operation of the link can be obtained from the measurements. Additionally, no remarkable differences exist between “random” and “zero” payload packets used. The rare occasion of relatively large difference between the static parts of the two measurements (4 to 6 nT) can be attributed to the worst-case scenario for the fluctuations of the ambient field. Furthermore, to reliably conclude that any results are caused by static emissions from the operation of the SpW link, a pattern would be expected to be observed. For instance, an increase of the measured difference when enlarging the packet size or when reducing the link’s rate for a particular packet size (**Figure 4-10** and **Figure 4-11**). The absence of such a pattern, combined with the lack of repeatability for certain sets of characteristics that are present in all measurement groups, are clear indications that these values are not related to the operation of the SpW link (**Figure 4-12**).

As a final remark, before concluding that the operation of a SpW link does not produce static magnetic emissions, it must be added that the differentiation achievable by the measuring equipment and the relatively large fluctuations of the static part of the ambient magnetic field, significantly limit the capability to identify static field emissions in the range of some nT.

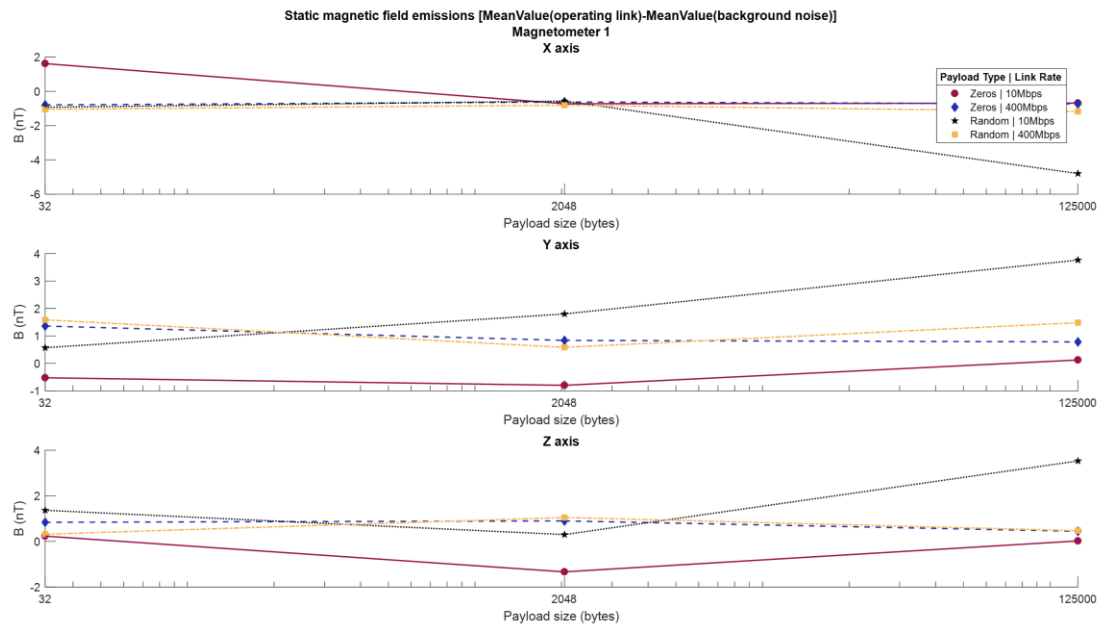


Figure 4-10. Static field emissions – Payload Size (Magnetometer 1)
Link rates of 10 and 400 Mbps – “Random” and “Zeros” payload types.

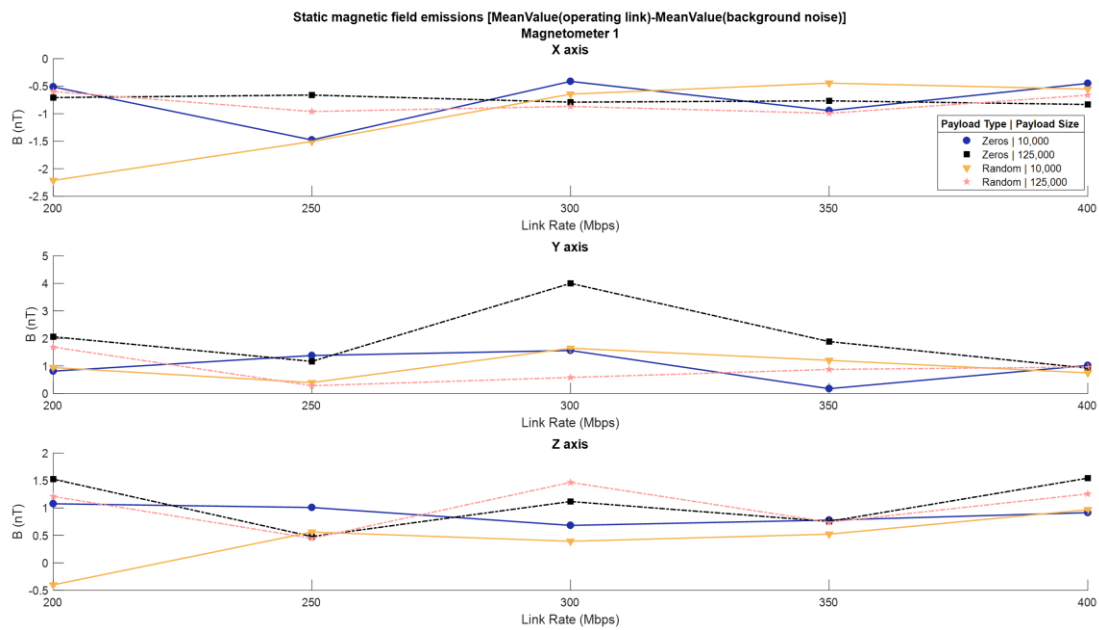


Figure 4-11. Static field emissions – Link Rate (Magnetometer 1)
Payload sizes of 10,000 and 125,000 bytes – “Zeros” and “Random” payload types.

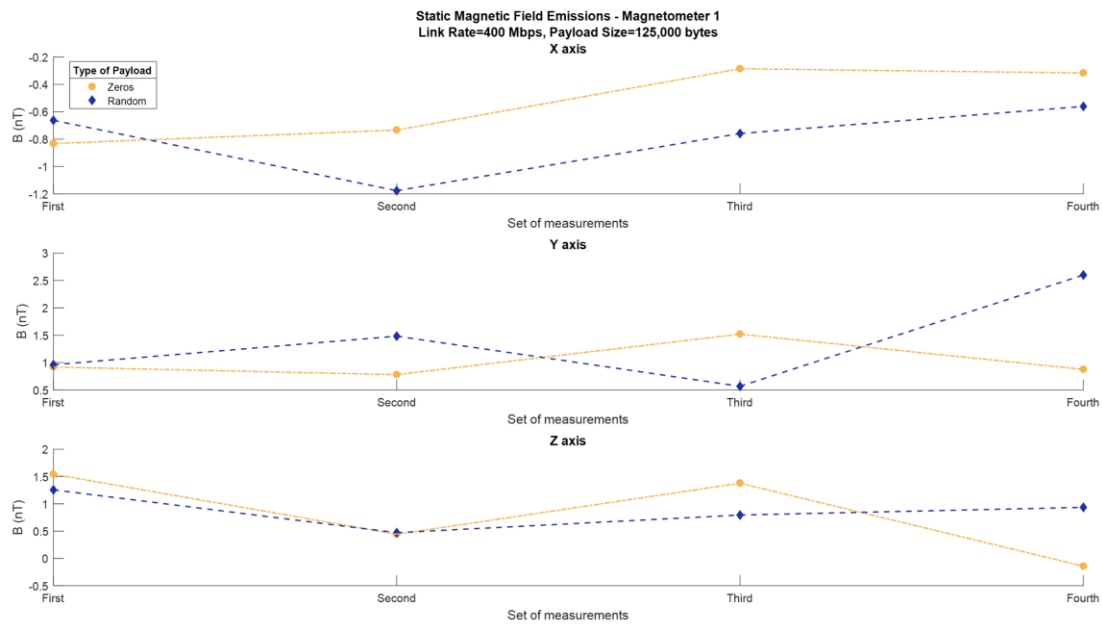


Figure 4-12. Static field emissions produced by four different sets of measurements, with the same characteristics (Magnetometer 1)
Payload Size=125,000 bytes, Link Rate=400 Mbps - “Random” and “Zeros” payload types.

Though no static emissions were observed from the operation of the SpW link, it is considered important to mention that in various situations this may not be the case. In particular, the setup used negates a significant drawback that is often present in many applications, namely, slight variations in ground potential between two connected instruments. As was thoroughly explained in **chapter 3**, the design of the cable assembly and specifically, the connection of the outer cable’s shield to local ground at both the cable’s ends, can lead to currents flowing through the outer shield. Therefore, the difference in ground potential between connected instruments can lead to DC currents flowing through the outer shield and thus produce static field emissions. This phenomenon can appear intensified in space missions due to the ambient space environment. Particularly, planetary and interplanetary space are plasma environments comprising of diverse densities of charged particles (ions and electrons). Such environments offer a plethora of physical mechanisms that can cause the electrical charging of a spacecraft’s surfaces (photoelectric effect etc.) and thereby lead to significant problems. Large conducting surfaces (mainly the spacecraft’s chassis) which are used to simulate electrical ground in spacecrafts are particularly vulnerable to those charging phenomena. Therefore, a mission design that utilizes multiple point ground, i.e. each instrument is grounded to a different point of the spacecraft’s conductive chassis [18], can have relatively large ground potential difference between interconnected units. Having said that, in the setup used, both ends of the SpW cable are connected to the same instrument (iSAFT), therefore there is no difference in the ground potentials between the two ends of the outer shield. In any case such emissions are not due to the operation but due to the physical design of the link.

3. AC Magnetic Field Emissions

In order to identify any low frequency emissions, the spectrums for the ambient field and the operating link measurements are calculated and compared. The sampling rate used for the digitalization of the analog measured signal, is 10,000 samples per second (sampling frequency $f_s=10$ kHz), which is enough to guarantee the absence of aliasing between the shifted spectral components comprising the sampled signal for frequencies up to 5kHz. For the purpose of staying well within the 3dB bandwidth of the magnetic field sensors, the examined frequency range will be up to 1.5 kHz. That being the case, the accurate reconstruction of the measured signal's frequency spectrum is ensured. The background noise measuring technique makes it easy to differentiate between background noise components and magnetic emissions caused by the operation of the link. As will be testified by the results presented in this chapter, any emission caused by the operation of the measuring equipment (DAQ, PSU) or in general any unrelated to the SpW link spectral components, will be present in both compared spectrums and thus will not be mistaken for magnetic emission produced by the link. Regarding the noise in the measurements, there is a level of random noise across all the examined low frequency range due to the thermal noise in the analog measured signal. In addition to this, several individual noise components can be identified by utilizing the background noise measuring technique. It is deemed necessary to briefly mention those noise components before analysing the magnetic field emissions of the link.

i. Discrete noise components in the low frequency range

To begin with, it is observed that certain noise components appear in all the measurements at around 1kHz. The existence of these components in both the ambient field and the operating link measurements makes it safe to assume that they are not relevant to the latter. For the ambient field's measurements, iSAFT is not shut down, only the transmission and reception of both ports is terminated. Therefore, to ensure that these components are not caused by any of iSAFT's operations, such as keeping the link active by sending Nulls over the link when there are no packets to be transferred, a specific set of measurements was performed where the link was deactivated and iSAFT was shut down. The results from these measurements can be observed in **Figure 4-13**. The unaltered presence of the aforementioned noise components signifies that they are unrelated to the SpW link. An educated guess is that they are caused by the operation of the measuring equipment, potentially the data acquisition unit (DAQ). In addition to these components, the noise caused by the electrical lines of the anechoic chamber can be noticed at the fundamental frequency of the electrical grid (50 Hz) and its third harmonic (150 Hz).

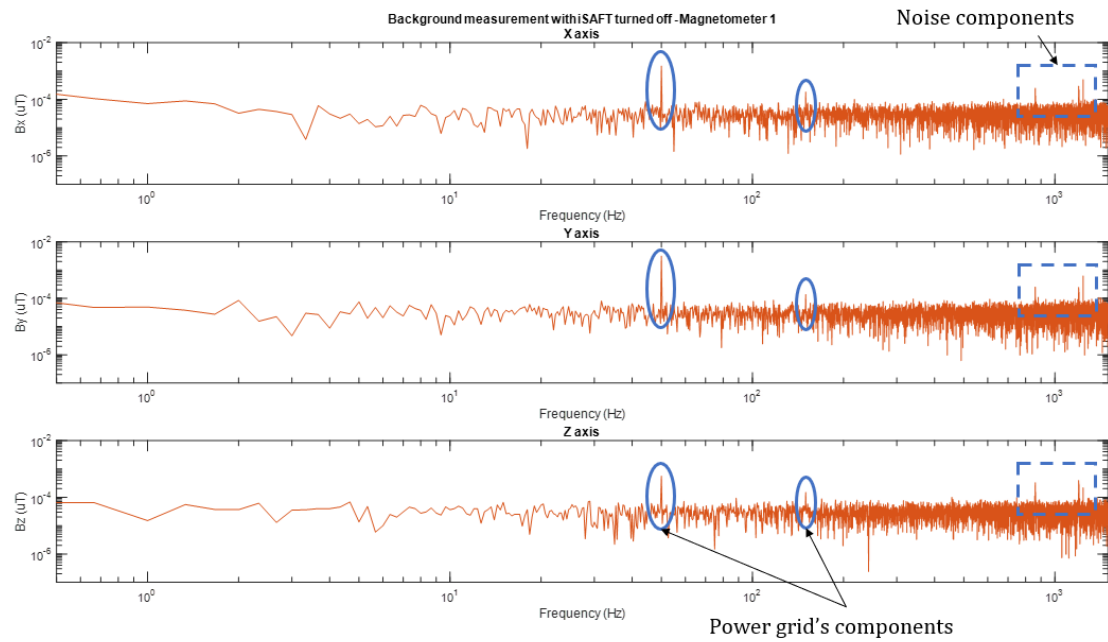
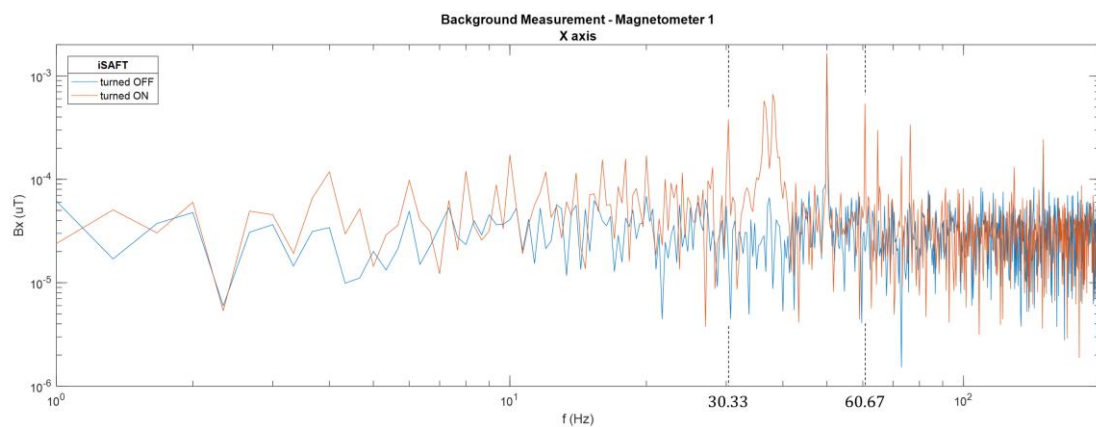


Figure 4-13. Ambient field measurement – Magnetometer 1, X,Y&Z axes.

Furthermore, by comparing background noise measurements with iSAFT turned on and off, the low frequency magnetic emissions caused by the operation of iSAFT can also be identified. Such low frequency components are located at the ranges of 30 Hz to 42 Hz and 60 to 130 Hz, as shown in **Figure 4-14** and can be recognized in all the measurements where iSAFT is turned on. Specifically, these components are stronger in x axis and more accumulated at the range 35-39 Hz, whereas discrete components exist at the frequencies of 30.33 Hz, 60.67 Hz, 64.67 Hz, 73 Hz, 76.33 Hz and 129.3 Hz. Moreover, the operation of iSAFT slightly increases the level of noise measured at the range of 4 to 30 Hz mainly at x axis. Two of iSAFT's discrete components whose origin will be thoroughly examined below, namely the components at 30 and 60 Hz, are labeled in the following figures.



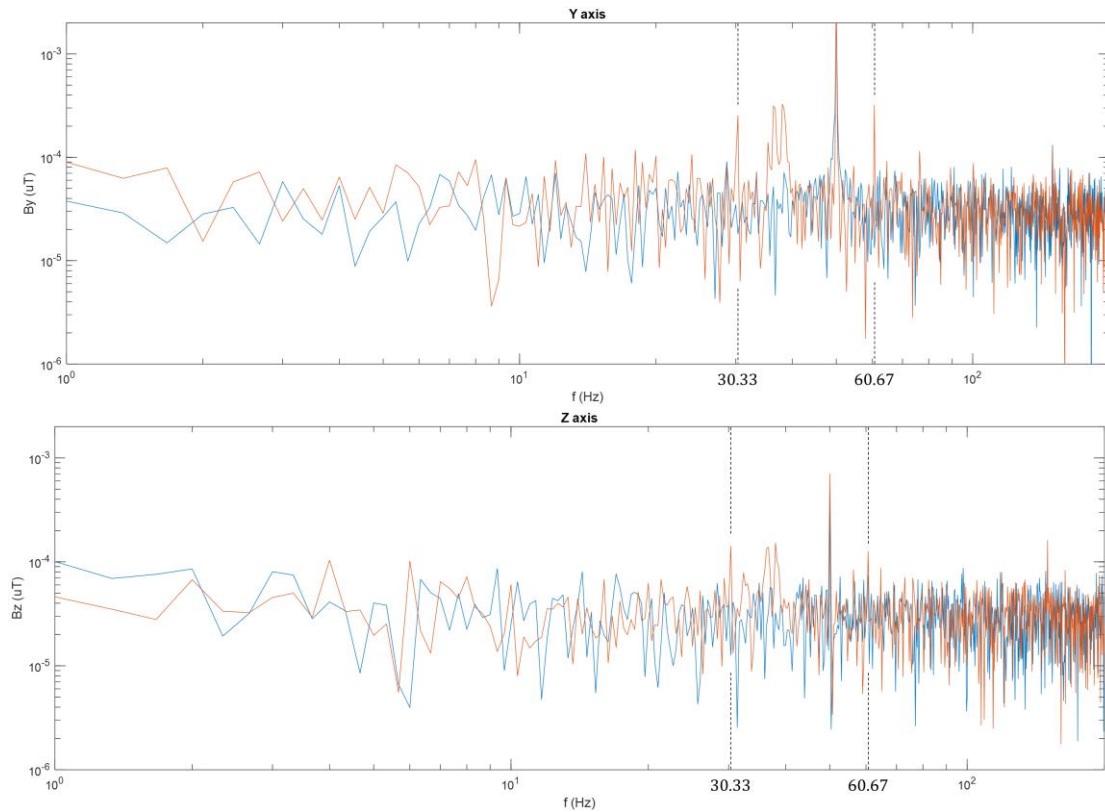


Figure 4-14. Background noise measurements with iSAFT turned ON and OFF - Magnetometer 1, X,Y&Z axes.

Having identified the existing noise components in the frequency range of interest as well as their potential sources, the magnetic emissions caused by the SpW link's operation can now be analyzed.

ii. SpaceWire link's low frequency emissions

As was already mentioned in the static field's analysis, the characteristics of the link modified to perform the measurements, are the packet size, the link's rate and the payload type. Magnetic emissions mostly appear when a combination of high data rate and large packet size is used, i.e. for data rates greater than 250 Mbps and payload sizes larger than 100,000 bytes. For alternative combinations of data rates and payload sizes, though no extensive emissions emerge, a very interesting behavior can be noticed in the spectrum. Specifically, two of the individual components caused by the operation of iSAFT, shift depending on the link's characteristics. These components correspond to a fundamental frequency and its second harmonic and when no transmission occurs, appear at the frequencies of 30.33 and 60.67 Hz respectively. The first component, initially at 30 Hz, shifts to slightly higher frequencies and many times becomes hard to distinguish due to the existing spectral components at 36-39 Hz. On the contrary, the second component, initially at 60 Hz, is shifted to the range of 61 to 77 Hz, an area without other noticeable emissions and can be clearly observed, as shown in **Figure 4-15**,

Figure 4-16 and **Figure 4-17**. In general, the distribution of the spectral power density of the emissions' spectrum in the respective axes, can indicate the physical mechanism responsible for the emissions. Nevertheless, in order to facilitate the desired observations, at this stage, only the results for x axis will be presented as at this axis the emissions are clearer. Similar observations can be made for the measurements in y and z axes.

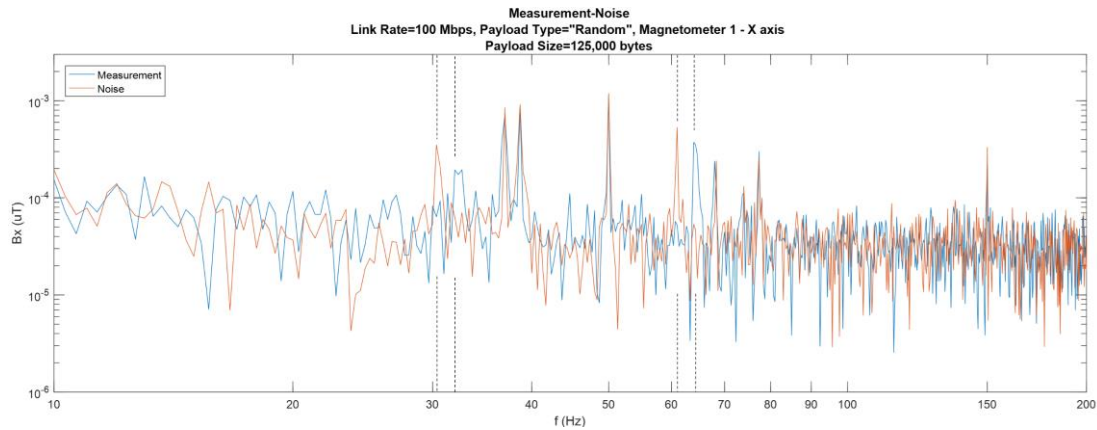


Figure 4-15. Background-noise and Operating-link measurements
 Magnetometer 1, X axis, Link Rate=100 Mbps, Payload Size=125,000 bytes, Payload Type="Random".

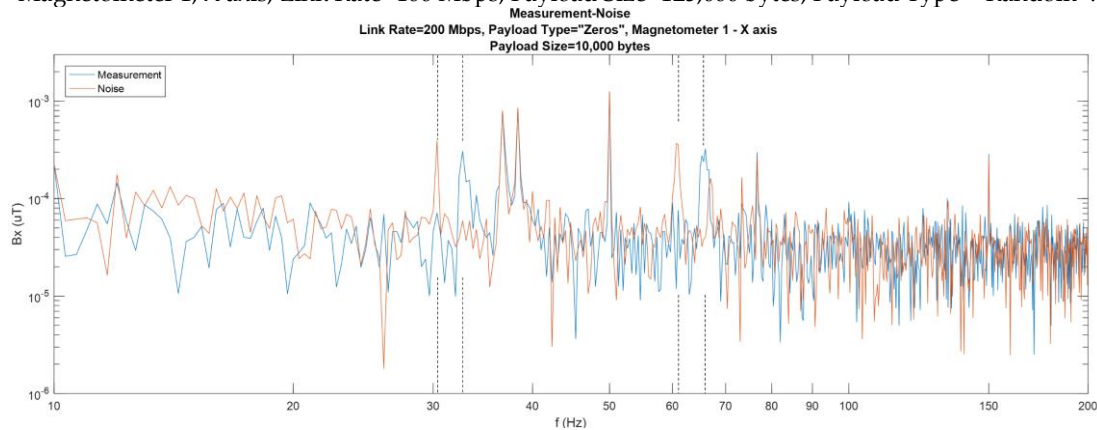


Figure 4-16. Background-noise and Operating-link measurements
 Magnetometer 1, X axis, Link Rate=200 Mbps, Payload Size=10,000 bytes, Payload Type="Zeros".

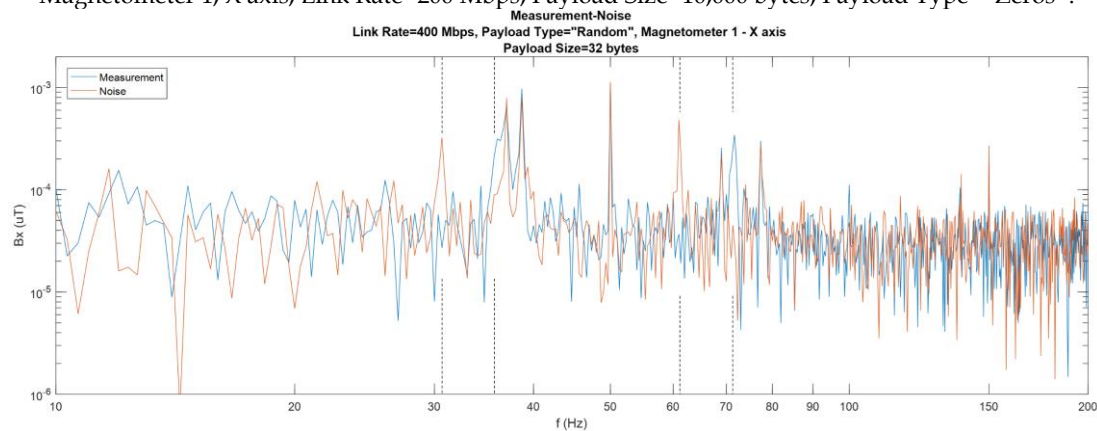


Figure 4-17. Background-noise and Operating-link measurements
 Magnetometer 1, X axis, Link Rate=400 Mbps, Payload Size=32 bytes, Payload Type="Random".

The rest of iSAFT's components do not significantly change when the transmission is activated, thus indicating that the two components of interest are somehow connected to the transmission. Therefore, their existence in the ambient field's measurements implies that there is some kind of transmission through the link before activating the transmission and reception in the two ports. In order to identify the nature of this potential transmission, the management of the SpW ports both from iSAFT and the operator must be examined.

For the purpose of altering the link's characteristics, the ports are disabled and re-enabled each time the link's rate needs to change. On the contrary, when only the transmitted packet needs to be changed, for example to modify its size or payload, the transmission and reception are disabled in both used ports and the ports remain enabled. The ambient field's measurement is performed before re-activating the reception and the transmission of both ports in the proper order. To justify a transmission during this time, the plausible assumption can be made, that when the reception and transmission are deactivated in a port, the link is not disconnected. In particular, this hypothesis states that the deactivation of the reception and transmission lead iSAFT to cease the storage of received data in the receive (RX) FIFO and the transfer of the transmit (TX) FIFO's data to the transmitter of the port. This behaviour is interpreted by the port's transmitter as an absence of N-Chars (packets) ready to be sent and therefore, following the sending priority of the standard when the link is running, Nulls are transmitted through the link to keep it active and avoid a disconnect.

Additionally, the components at 30 and 60 Hz are observed at the same frequencies in measurements where iSAFT is turned on and its ports are enabled, as can be observed in **Figure 4-14**. The latter indicates that simply enabling the ports causes some kind of transmission through the link. To explain this in accordance with the previous hypothesis, the operation of iSAFT can be considered as follows. When two connected ports are enabled through iSAFT's board configuration, the initialization of the link occurs. After a successful initialization, the link is ready to perform any user defined transmission and it remains active by sending Nulls until the transmission's parameters are specified and it is started by the operator. If the transmission is stopped, then the link is kept active until a new transmission is defined or the ports are disabled, in which case the link is disconnected.

Therefore, it is the authors' point of view that the component at 30 Hz and its second harmonic at 60 Hz are caused by the transmission of Nulls over the SpW link. The emissions can be either produced by induced currents to the outer shield of the cable or by the electronic circuitry of the SpW ports. If the latter is true, it must be considered that the distance of the magnetic field sensor

from the iSAFT's ports is much larger than that from the SpW cable, thus the components' small amplitude is misleading. At any case, both options are equally interesting as the ports are an inseparable part of any link and their emissions are of identical importance with the ones from the cable assembly.

Another evidence which verifies this hypothesis can be obtained by examining the emission's spectrum when the link is operating with 10 Mbps and a small packet size is used. Specifically, it is observed that the iSAFT's components are hardly shifted from their initial frequencies (**Figure 4-18**). Considering that a SpW link will operate at 10 Mbps if not specified otherwise, as mentioned in the SpW standard, it can be expected that when the packets are small and the packet to packet delay large, the transmission will be almost identical with only transmitting Nulls.

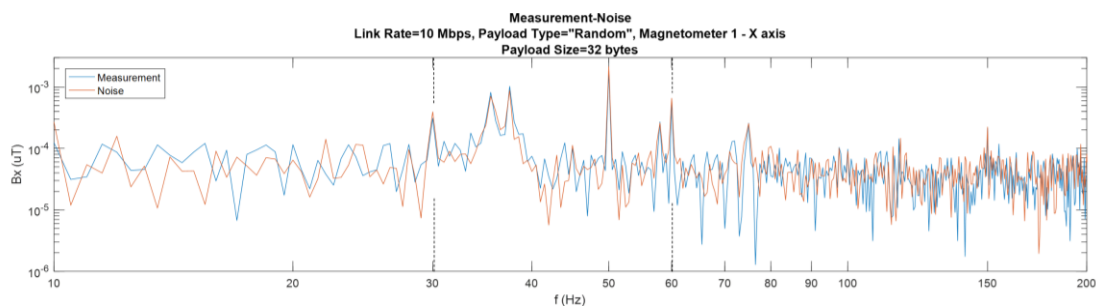


Figure 4-18. Background-noise and Operating-link measurements
 Magnetometer 1, X axis, Link Rate=10 Mbps, Payload Size=32 bytes, Payload Type="Random".

All things considered, no pattern can be distinguished for the shift of those components. Even when the same characteristics are used in the SpW link, for identical packets (zero payload packets), the components can appear at slightly different frequencies, as can be observed in **Figure 4-19**.

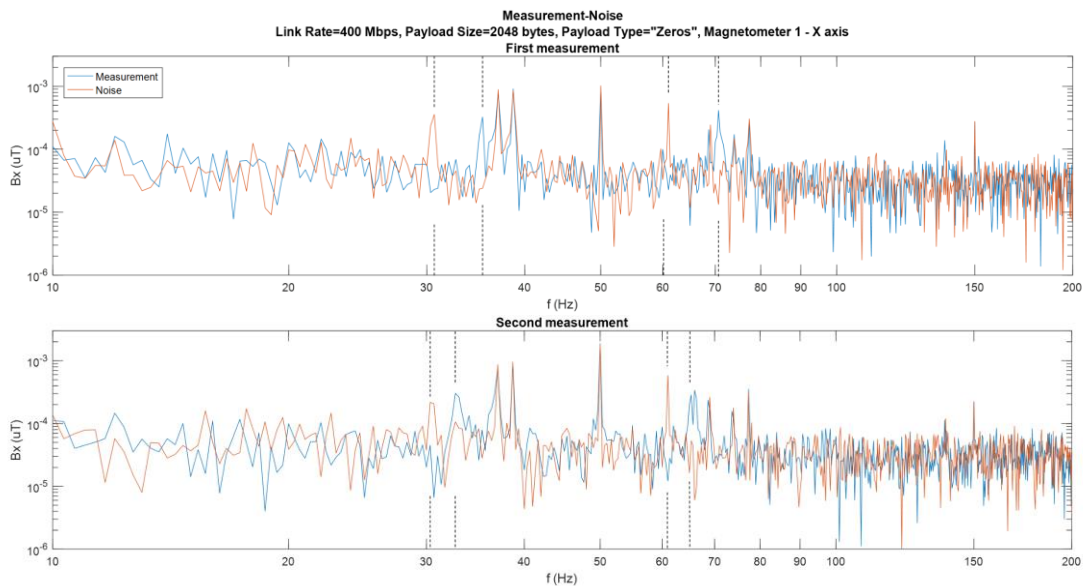


Figure 4-19. Two different measurements with the same link's characteristics
 Magnetometer 1, X axis, Link Rate=400 Mbps, Payload Size=2048 bytes, Payload Type="Zeros".

To conclude the analysis of these components, a final observation will be made which indicates that they are likely caused by currents flowing through the wire pairs and not by the port's circuitry. Specifically, they appear very concentrated at 30 and 60 Hz in the ambient field's measurement when no user defined transmission occurs which would signify an almost perfectly repeating pattern occurring in the measurement's duration. This can be explained by continuous Null transmission as the currents' waveforms would have an ideal periodic pattern. On the contrary, when traffic generation occurs, the current's waveform would be significantly more complicated, and any repeating pattern would surely not be present for the whole measurement's duration. This being the case, the components would be widened around their respective frequencies as can be clearly observed in the majority of the measurements. The results for a multitude of link's characteristics with an emphasis on the behaviour of these two components are represented in the following figures (Figure 4-20 to Figure 4-27). It should be noted that in order to have a clear depiction of these components, only the range from 10 to 200 Hz is represented.

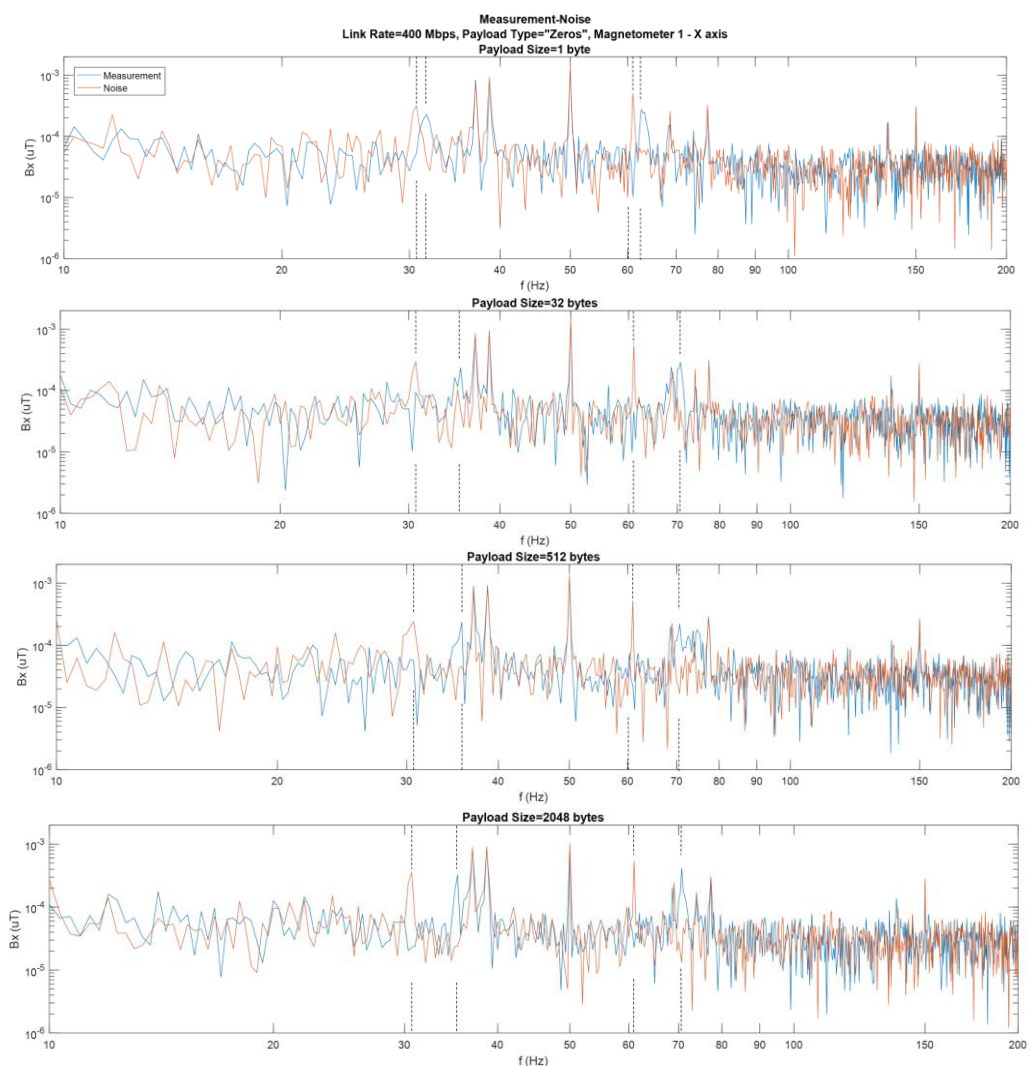


Figure 4-20. Background-noise and Operating-link measurements, Mag 1, X axis, Link Rate=400Mbps, Payload Type="Random", Payload Sizes=1,32,512,2048 bytes.

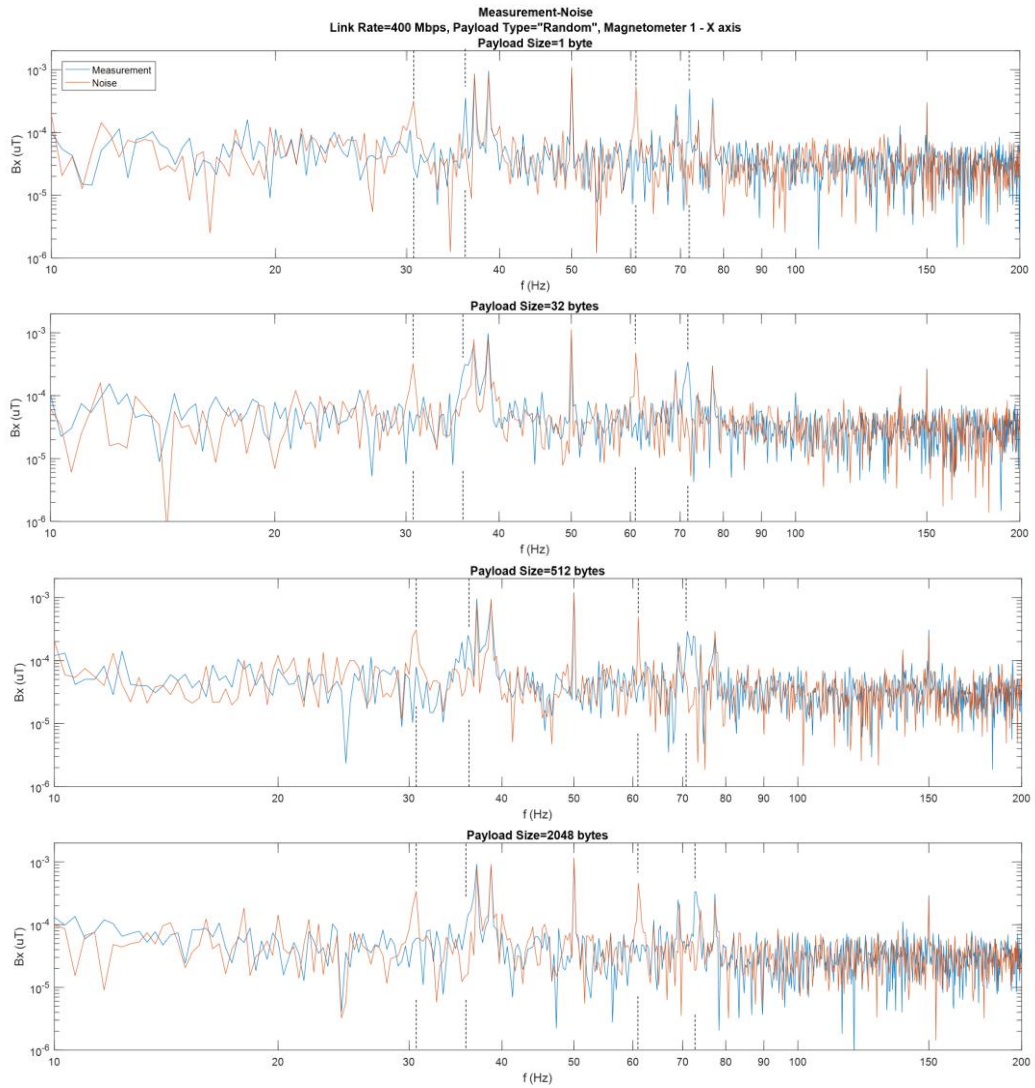
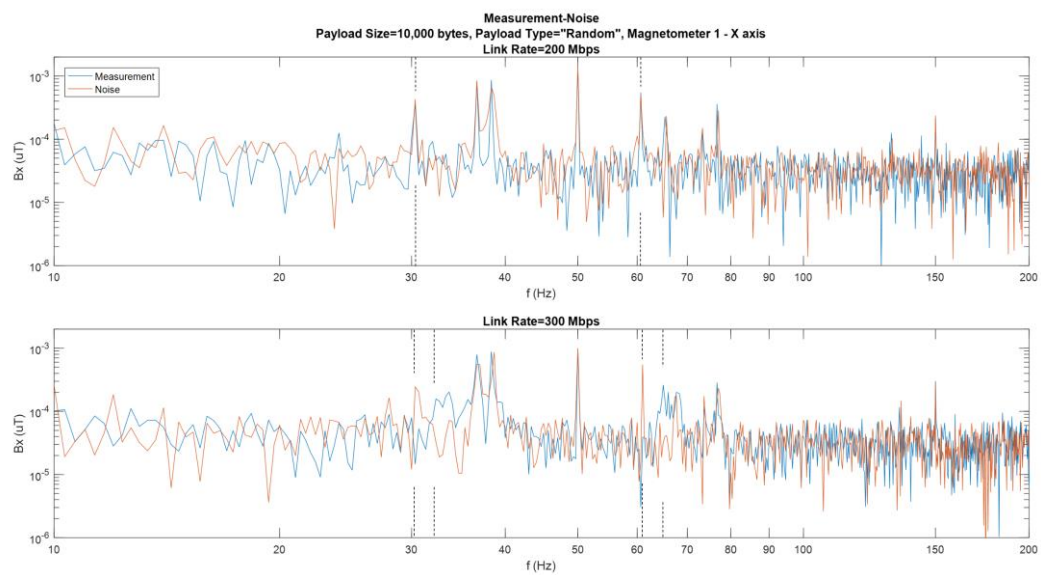


Figure 4-21. Background-noise and Operating-link measurements
Mag 1, X axis Link Rate=400Mbps, Payload Type="Zeros", Payload Sizes=1,32,512,2048 bytes.



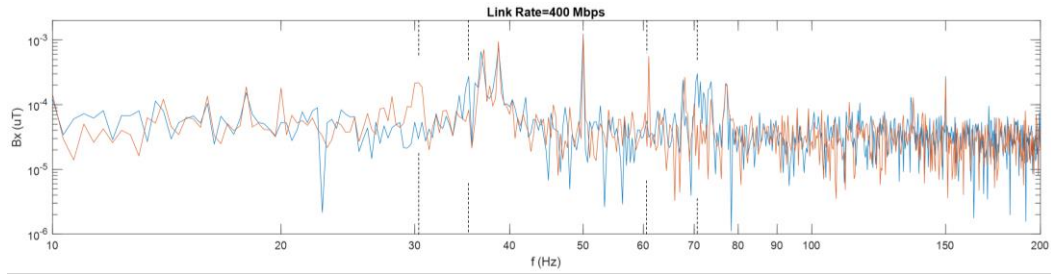


Figure 4-22. Background-noise and Operating-link measurements
 Mag 1, X axis, Payload Size=10,000 bytes, Payload Type="Random", Link Rates=200,300,400 Mbps.

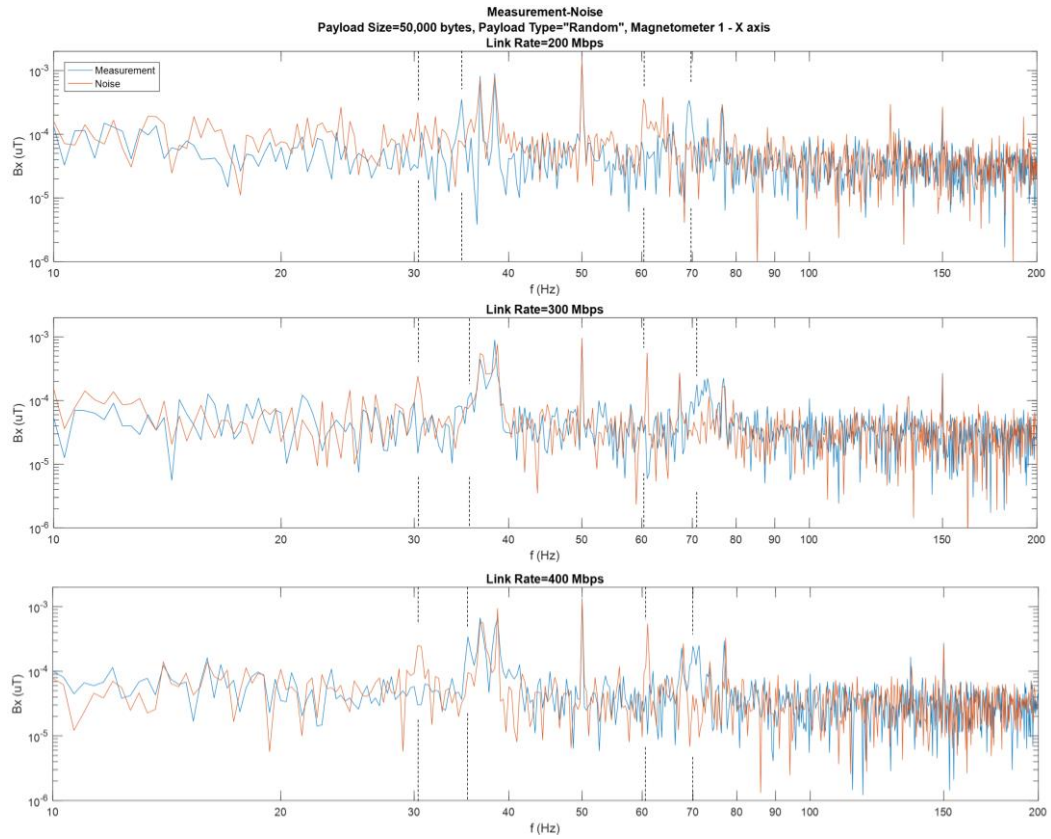
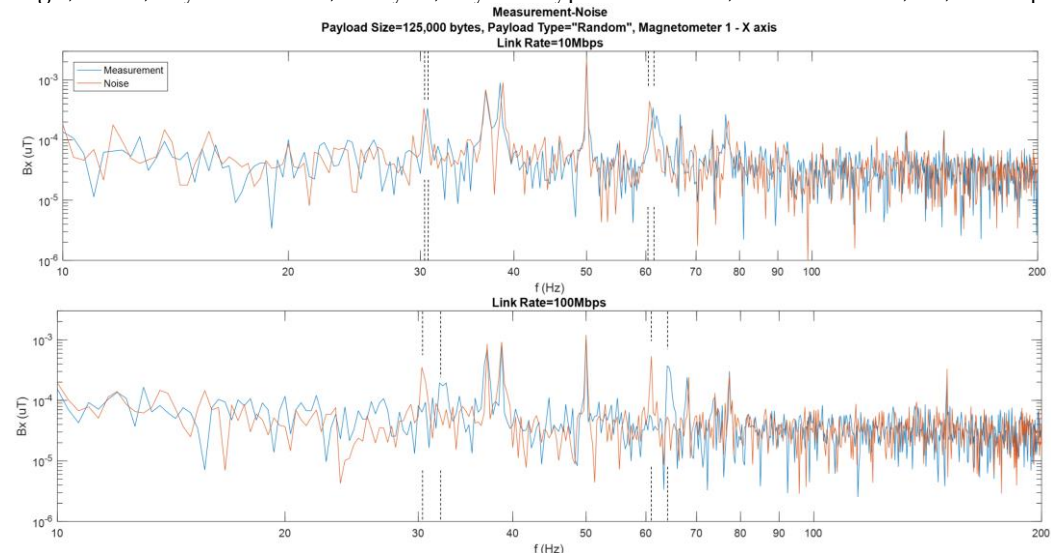


Figure 4-23. Background-noise and Operating-link measurements
 Mag 1, X axis, Payload Size=50,000 bytes, Payload Type="Random", Link Rates=200,300,400 Mbps.



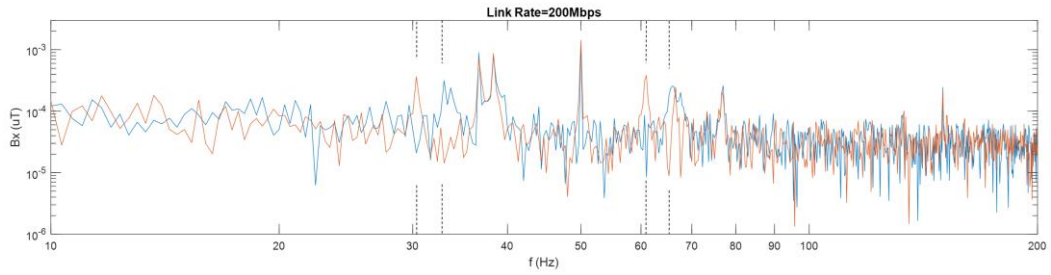


Figure 4-24. Background-noise and Operating-link measurements
Mag 1, X axis, Payload Size=125,000 bytes, Payload Type="Random", Link Rates=10,100,200 Mbps.

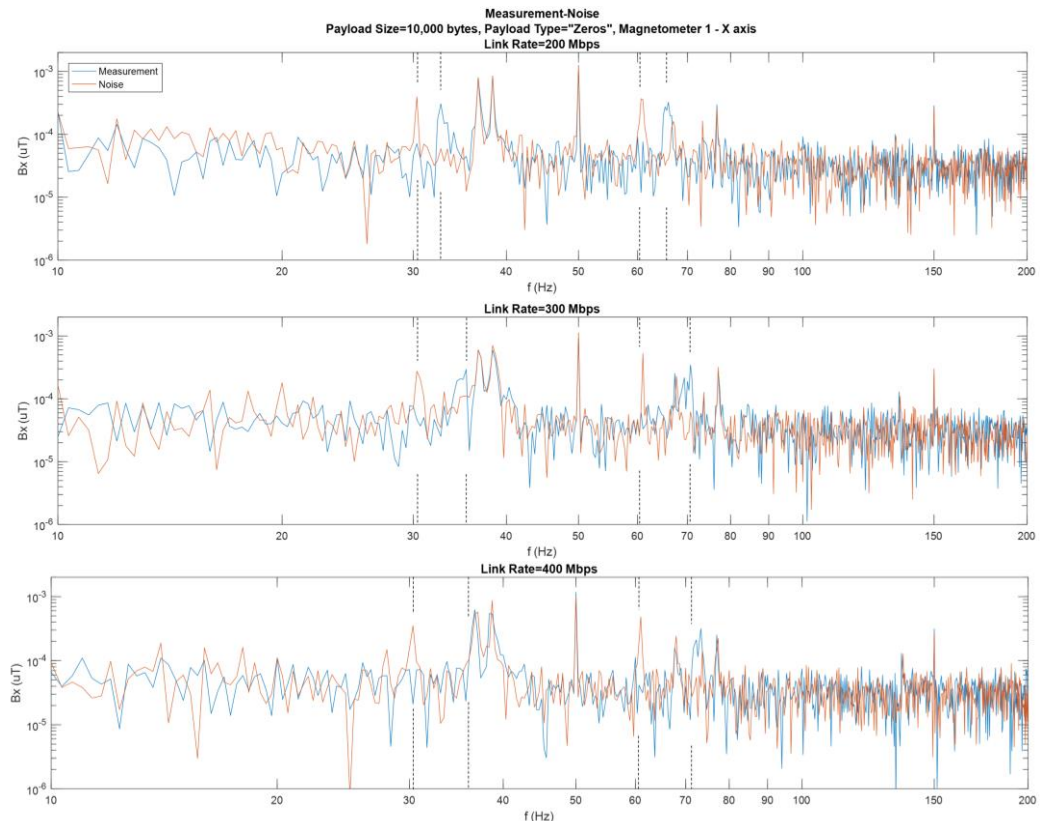
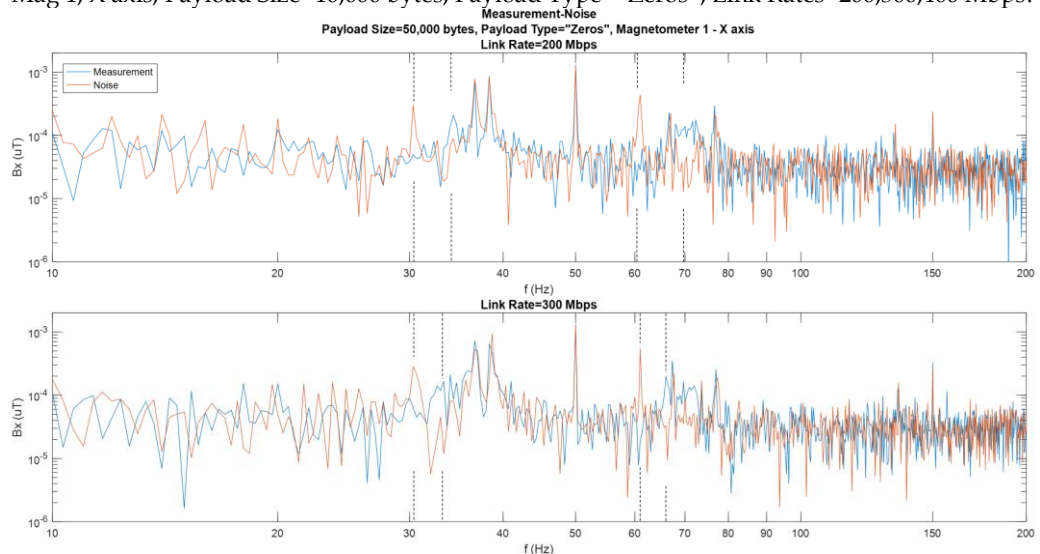


Figure 4-25. Background-noise and Operating-link measurements
Mag 1, X axis, Payload Size=10,000 bytes, Payload Type="Zeros", Link Rates=200,300,400 Mbps.



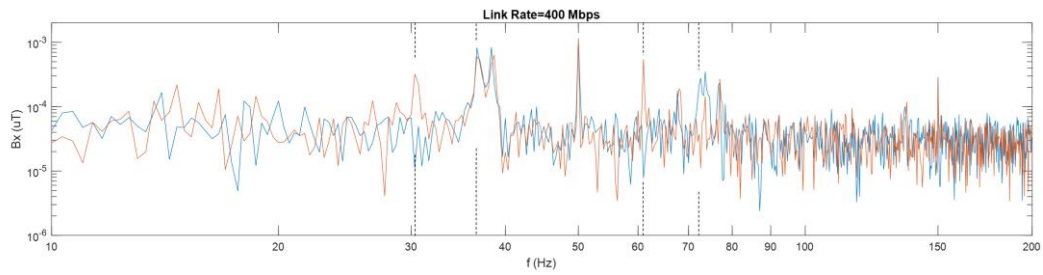


Figure 4-26. Background-noise and Operating-link measurements
 Mag 1, X axis, Payload Size=50,000 bytes, Payload Type="Zeros", Link Rates=200,300,400 Mbps.

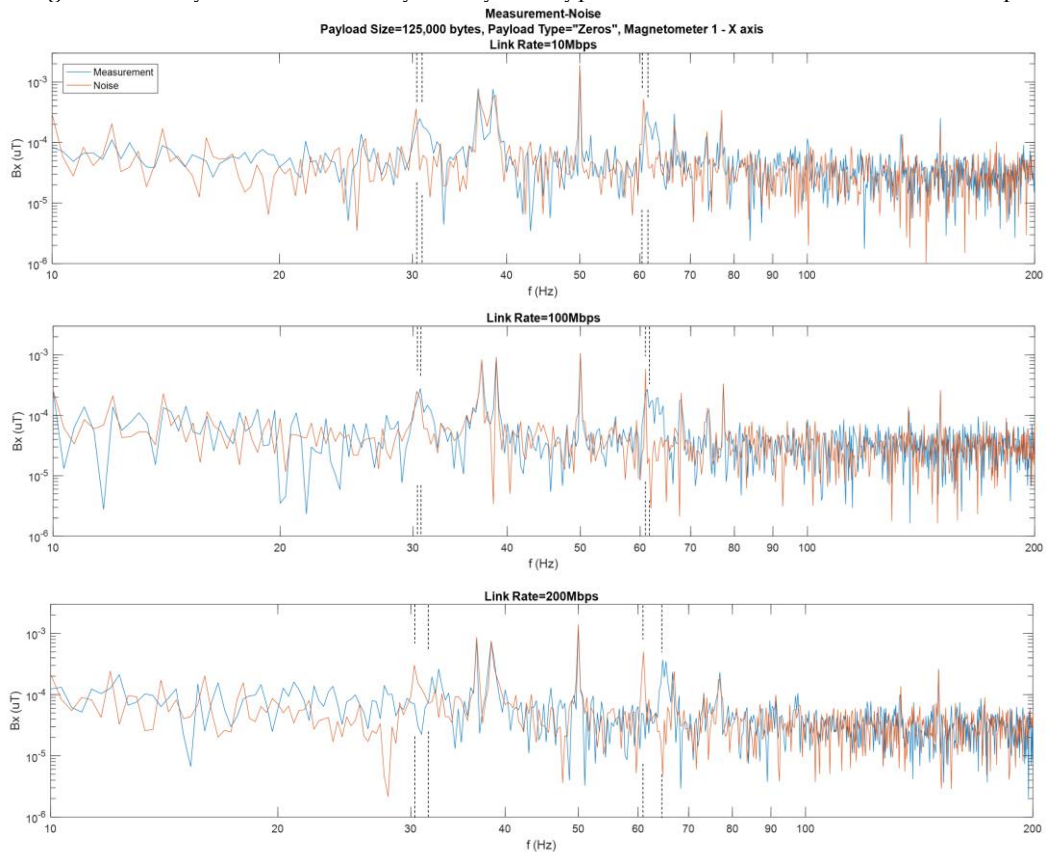


Figure 4-27. Background-noise and Operating-link measurements
 Mag 1, X axis, Payload Size=125,000 bytes, Payload Type="Zeros", Link Rates=10,100,200 Mbps.

As a final remark, it must be emphasized that the aforementioned hypothesis about iSAFT's port management, contains some assumptions based on the authors' understanding of the matter and might not be completely accurate. It is possible that the observed components at 30 and 60 Hz, when no transmission occurs, are caused by some electronic circuit of the iSAFT's port, and not by any transmission through the link despite the evidence to the contrary.

In the case of high link rate and large payload size being used, additional emissions arise. Specifically, for link rates higher than 250 Mbps and payload sizes greater than 100,000 bytes, emissions appear in a wider area of the spectrum. Though the amplitude of such emissions is not large, they are easily

identified, as the majority of the examined spectrum clearly rises in respect to the ambient field. As illustrated in **Figure 4-28**, their presence is more intense in x and y axes, however they are also noticeable in z axis. The example used to show the distribution of the spectrum in the three axes, corresponds to a link rate of 400 Mbps and a payload size of 125,000 bytes so the emissions are more than clear. It should be noted that in order to have a crisp representation of the emissions, only the range from 0.5 to 500 Hz is depicted.

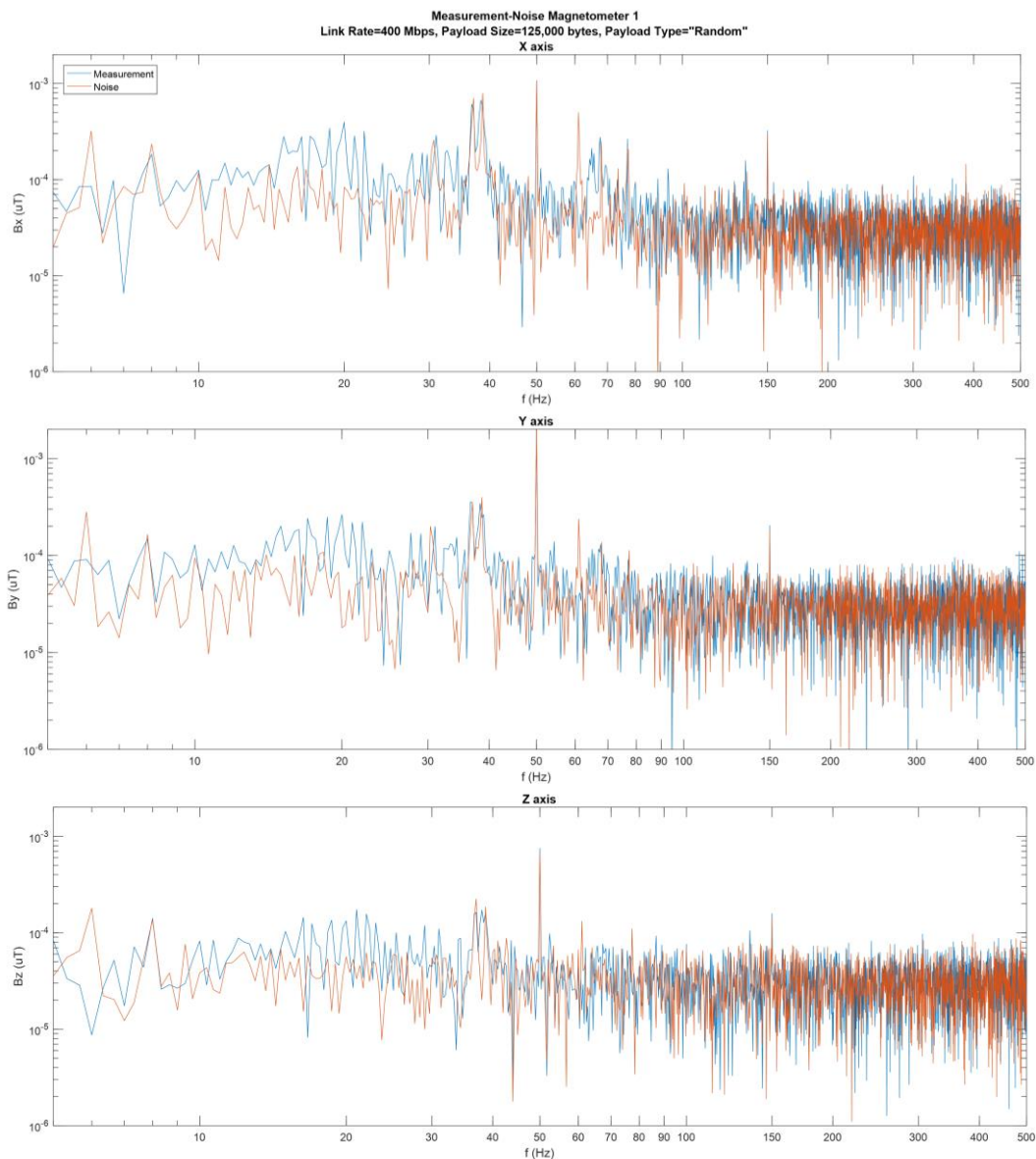


Figure 4-28. Background-noise and Operating-link measurements
 Mag 1, Link Rate=400Mbps, Payload Size=125,000 bytes, Payload Type="Random", X,Y&Z axes.

The frequency range where the emissions occur is approximately from 10 to 75 Hz. In particular, the range from 10 to 35 Hz is the one affected the most by the operation of the link, while in the range from 40 to 60 Hz, although additional emissions are noticed, their amplitude is markedly lower than of those at 10 to 35 Hz. Additionally, the component that appears in the range

from 60 to 75 Hz is considered as the second harmonic of the respective component at the range of 30 to 37 Hz, as was thoroughly discussed earlier in this chapter. The latter is not currently distinguishable, as it is muffled by the emissions that overall occur in this frequency range. The following figures (Figure 4-29 to Figure 4-32) depict the spectrums of the background-noise and operating-link measurements, while payload sizes of 100,000 and 125,000 bytes and link rates of 250, 300, 350 and 400 Mbps are used, for both “random” and “zeros” payload types.

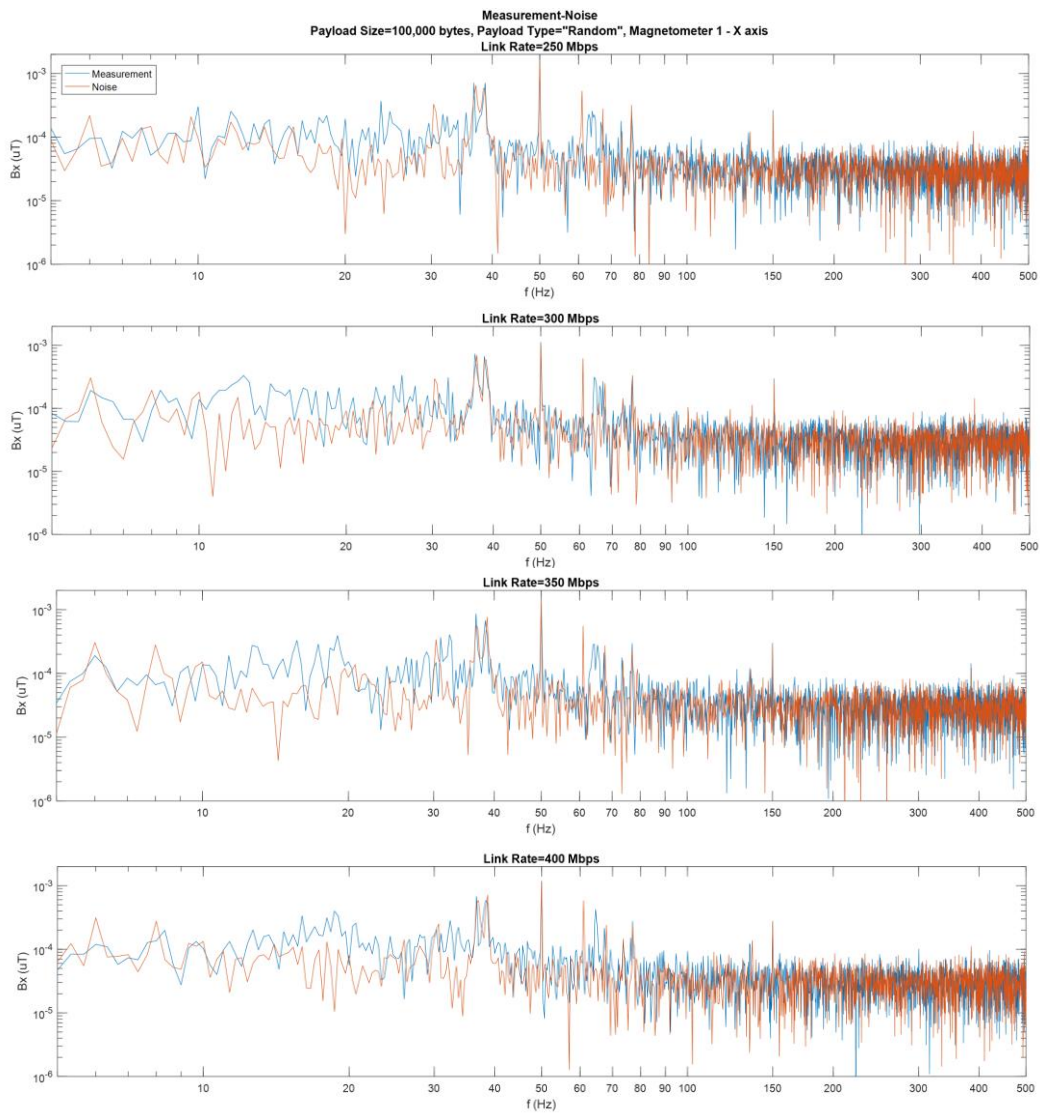
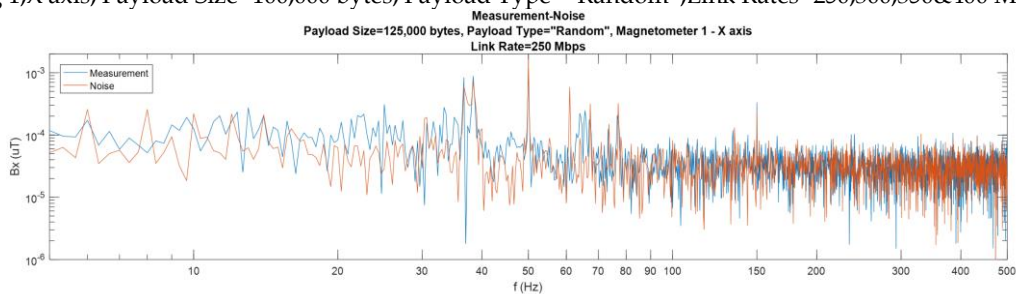


Figure 4-29. Background-noise and Operating-link measurements
 Mag 1,X axis, Payload Size=100,000 bytes, Payload Type="Random", Link Rates=250,300,350&400 Mbps.



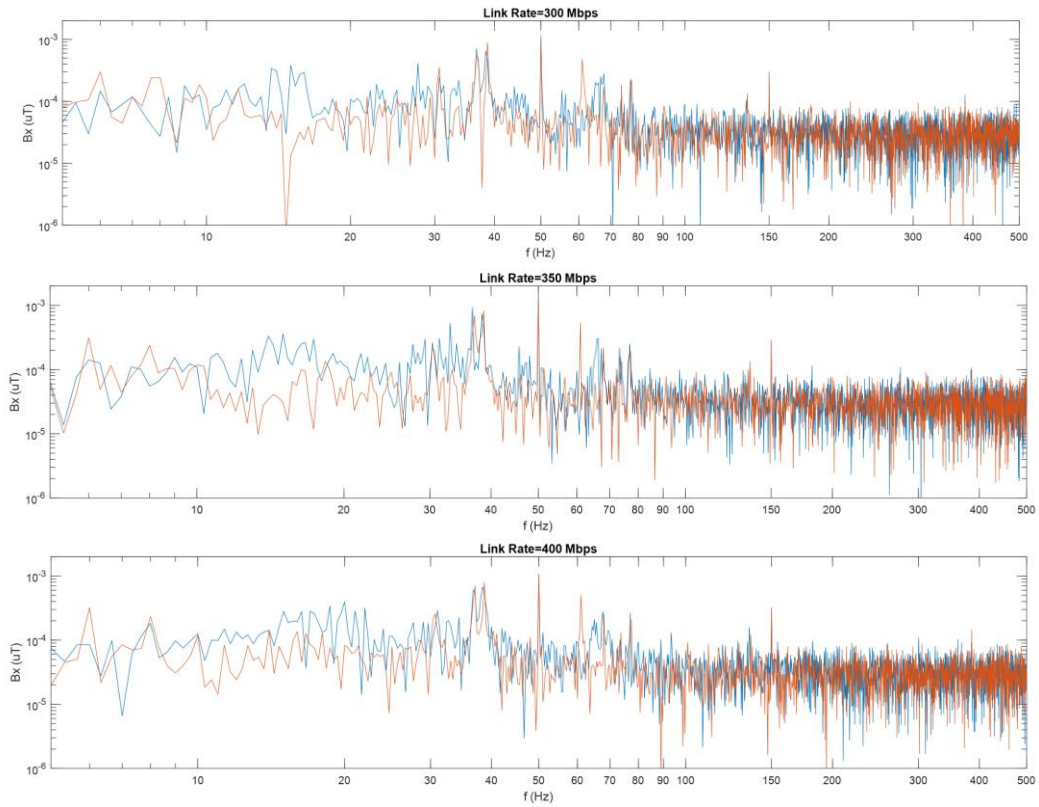
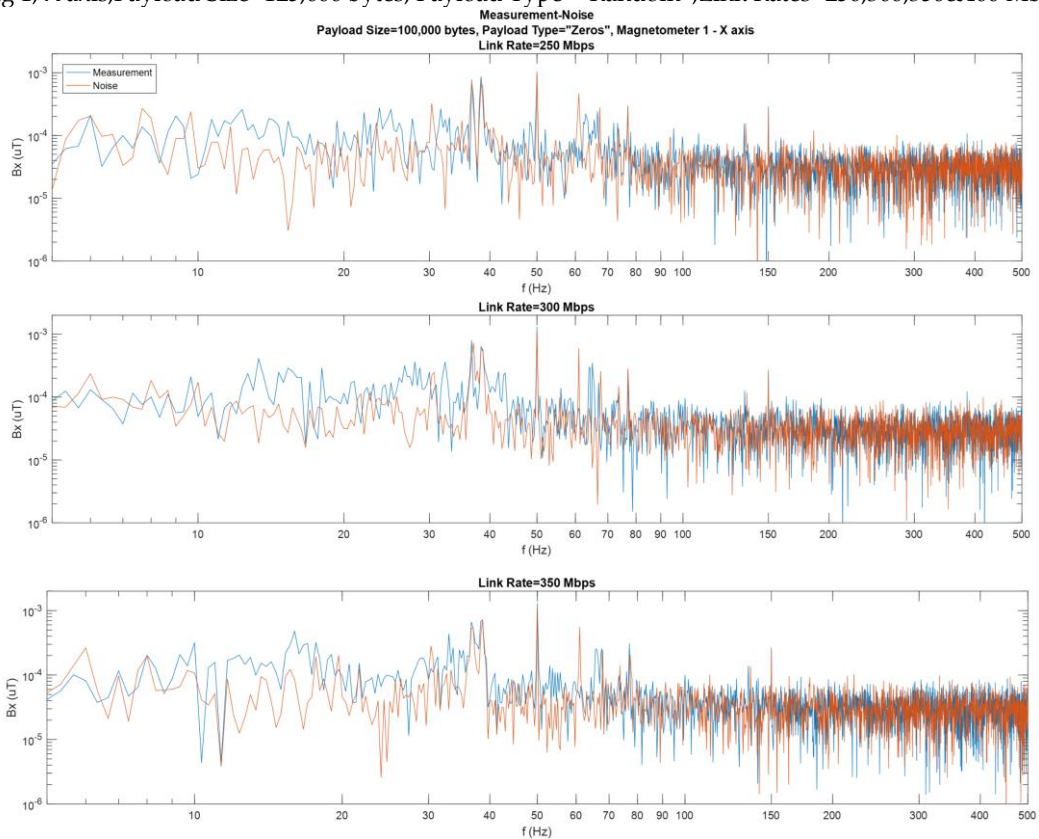


Figure 4-30. Background-noise and Operating-link measurements
 Mag 1, X axis, Payload Size=125,000 bytes, Payload Type="Random", Link Rates=250,300,350&400 Mbps.



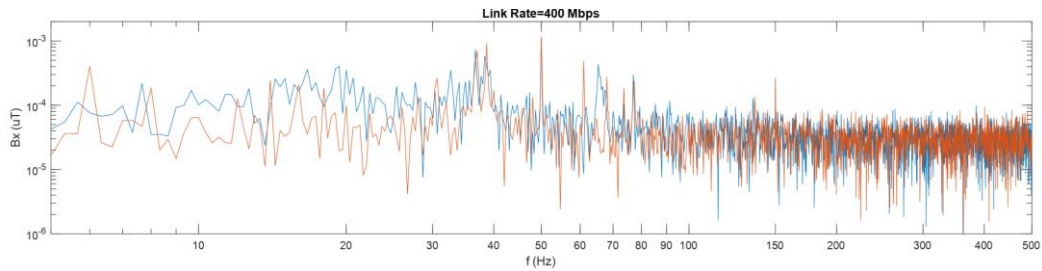


Figure 4-31. Background-noise and Operating-link measurements
 Mag 1, X axis, Payload Size=100,000 bytes, Payload Type="Zeros", Link Rates=250,300,350&400 Mbps.

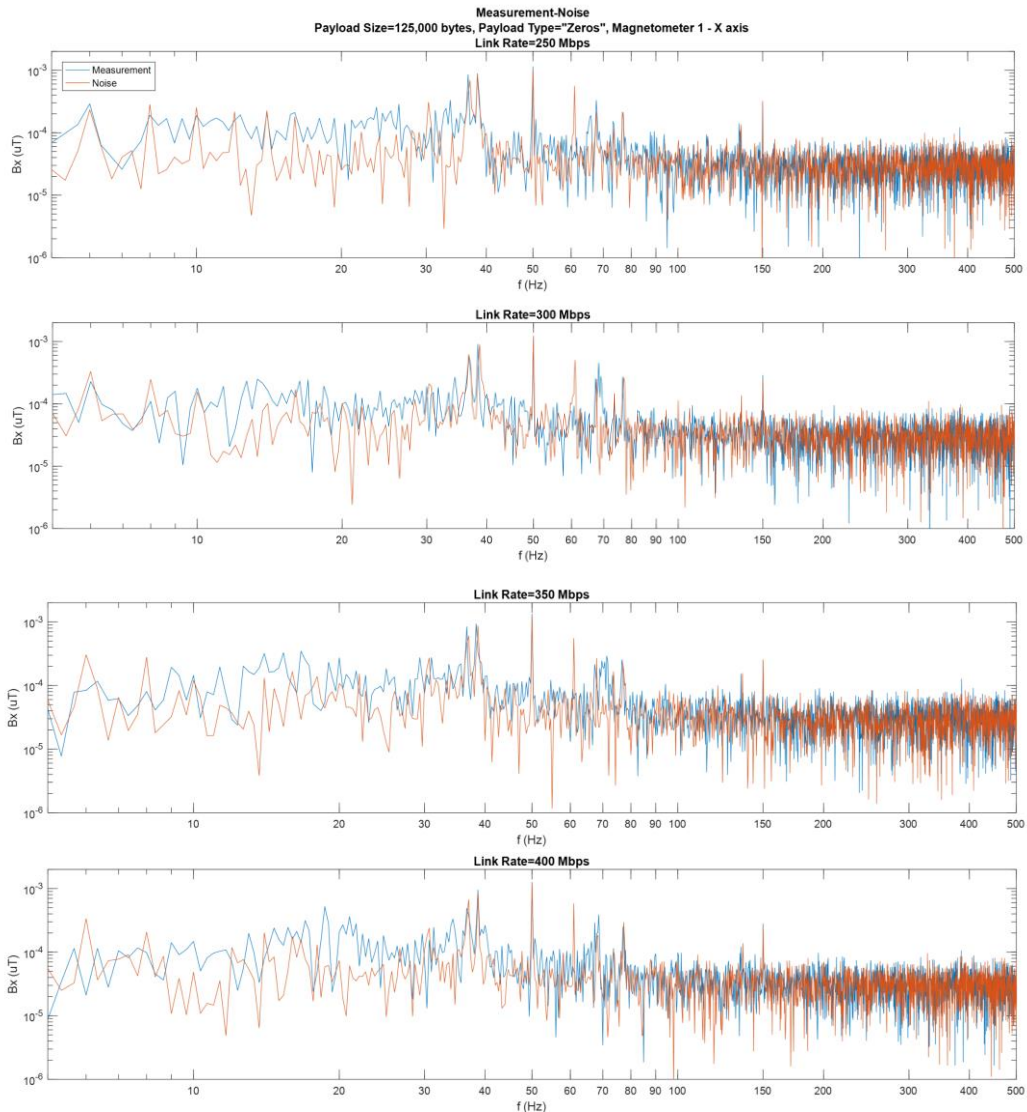


Figure 4-32. Background-noise and Operating-link measurements
 Mag 1, X axis, Payload Size=125,000 bytes, Payload Type="Zeros", Link Rates=250,300,350&400 Mbps.

As a conclusion, the higher the link's rate and the larger the packet's size, the more intense the emissions appear. The different payload types used, i.e. "random" and "zero" payloads, do not seem to greatly alter the described behavior of the emissions. In particular, although slight differences can be noticed for the two payload types, it is not clear if the payload has a significant impact, as similar differences also appear in sequential measurements with

identical packets, for example “zero” payload packets as shown in **Figure 4-33** and **Figure 4-34**. Overall, no other emissions are observed in the frequency range up to 1.5 kHz.

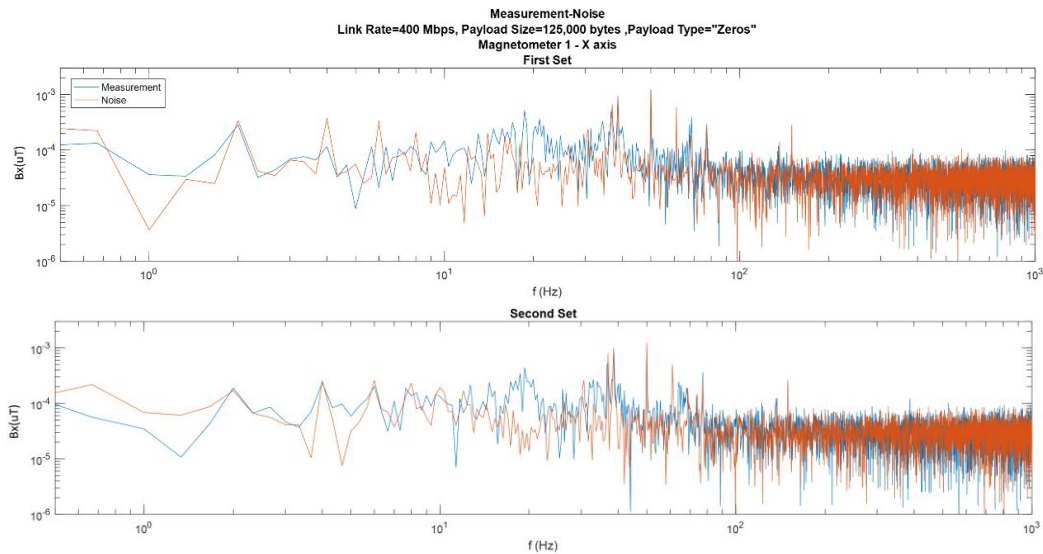


Figure 4-33. Background-noise and Operating-link measurements

Two sets of measurements with the same characteristics

Mag 1, X axis, Link Rate=400 Mbps, Payload Size=125,000 bytes, Payload Type=“Zeros”.

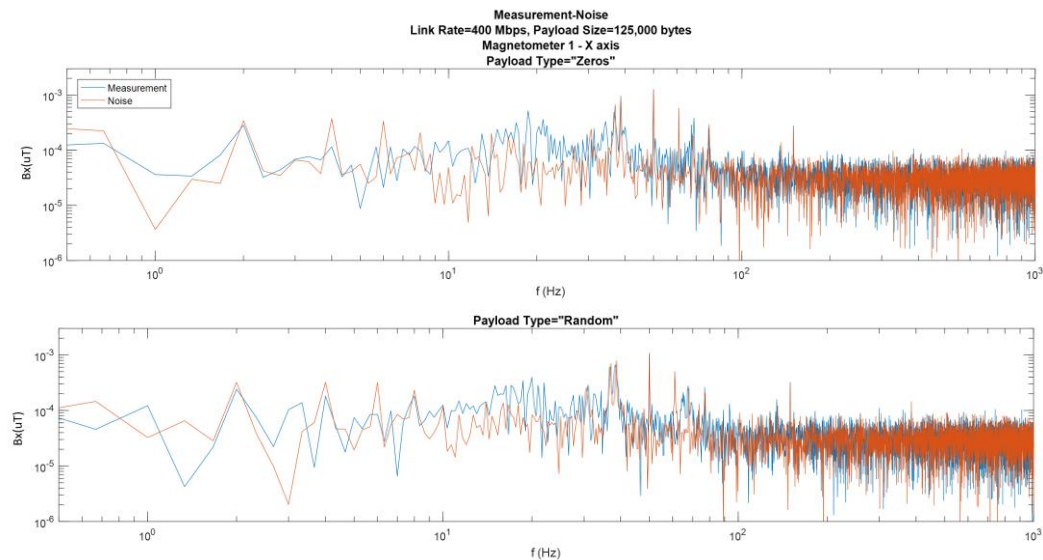


Figure 4-34. Background-noise and Operating-link measurements

Payload Types “Zeros” and “Random”

Mag 1, X axis, Link Rate=400 Mbps, Payload Size=125,000 bytes.

To facilitate the observations, until this point, only the emissions at x axis were presented. At this stage, in order to make some interesting remarks about the distribution of the emissions’ spectral power density, all axes will be examined.

iii. Spectral power density axial distribution

Magnetic emissions caused by the operation of a SpW link appear in all axes in the aforementioned ranges but not with the same intensity. Specifically, they are stronger in x axis, a bit dampened but still observable in y axis and greatly reduced in z axis. Similar behavior is noticed in iSAFT's components which were mentioned in an earlier clause. The axial distribution of the spectral power density can be an indication about the nature of the currents causing the emissions.

Another very interesting observation can be derived by comparing the measurements of the two magnetic field sensors. In particular, one may expect that due to the proximity of mag1 to the EUT, the measured field at this sensor will be greater for all axes. This assumption is justified when considering the modeling process for the magnetic emissions of a SpW link [19]. Namely, the latter can be replaced by a finite number of magnetic sources (linear currents, magnetic dipoles etc.) whose positions, orientations and magnitudes are calculated by complex stochastic algorithms with the aim of minimizing the difference between the measured and estimated fields. When modeling for the static field emissions, this procedure can be performed once. On the contrary, to model alternating field emissions, this method must be performed for each frequency of interest. This way, a set of magnetic sources is produced for each frequency which are then handled as phasor representations, producing magnetic sources varying sinusoidally with time. The final model of the EUT is derived with the superposition of all the magnetic sources for the examined frequencies. In any case, the area where these sources can be positioned, consists of the area covered by the EUT. When conductive or magnetic surfaces exist near the equipment, their contribution to the measured field must be accounted for. For example, in the case of this setup, due to the table's surface being covered by a conductive layer, if modeling is desired, the latter must also be considered. If for simplification purposes the conductive layer is regarded as infinite, the SpW link could be modeled by a finite number of magnetic sources in the area covered by the link (iSAFT and SpW cable) as well as the equivalent sources under the conductive layer. Considering that in such a case any magnetic source would be closer to the nearest sensor (mag1), it can be expected that the measured field at this sensor will be greater at all axes. Although this is the case for x and z axes, in y axis both magnetic field sensors measure exactly the same field, as illustrated in the following figures (**Figure 4-35** to **Figure 4-37**). Such a behavior can also be observed in the noise measurements, and specifically in iSAFT's components.

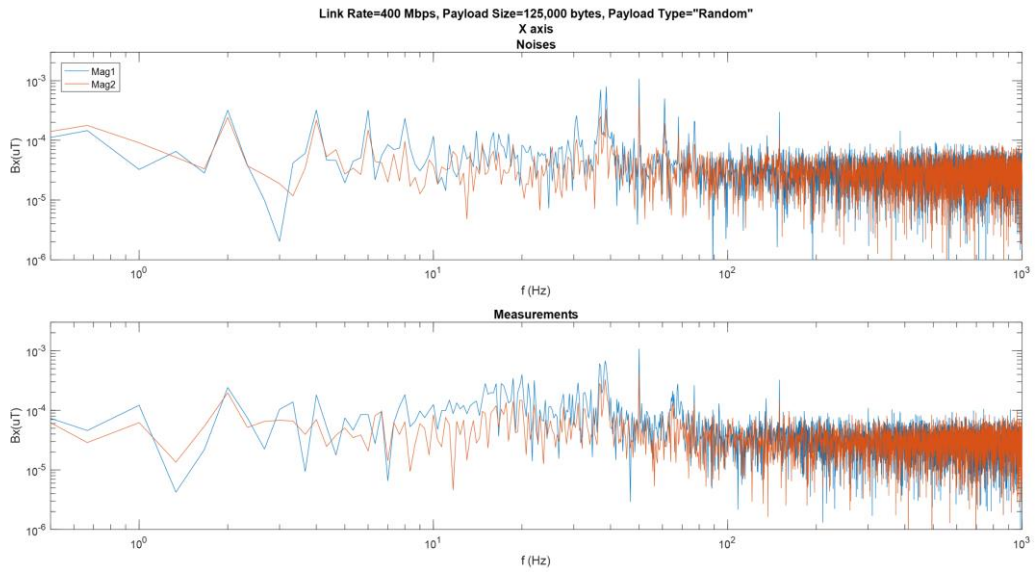


Figure 4-35. Comparison of Background-noise and Operating-link measurements of magnetometers 1 and 2 in X axes

Link Rate=400 Mbps, Payload Size=125,000 bytes, Payload Type="Random".

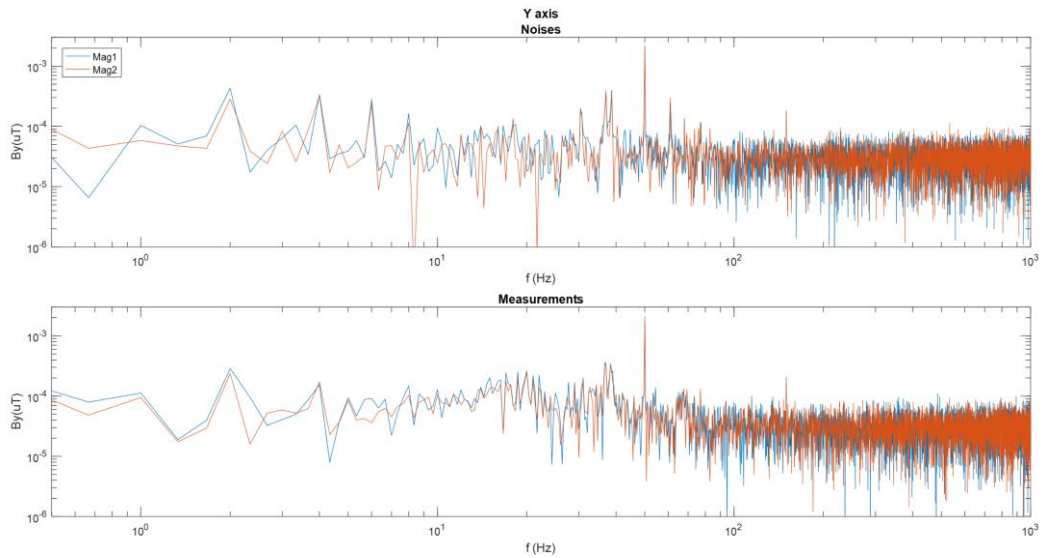


Figure 4-36. Comparison of Background-noise and Operating-link measurements of magnetometers 1 and 2 in Y axes

Link Rate=400 Mbps, Payload Size=125,000 bytes, Payload Type="Random".

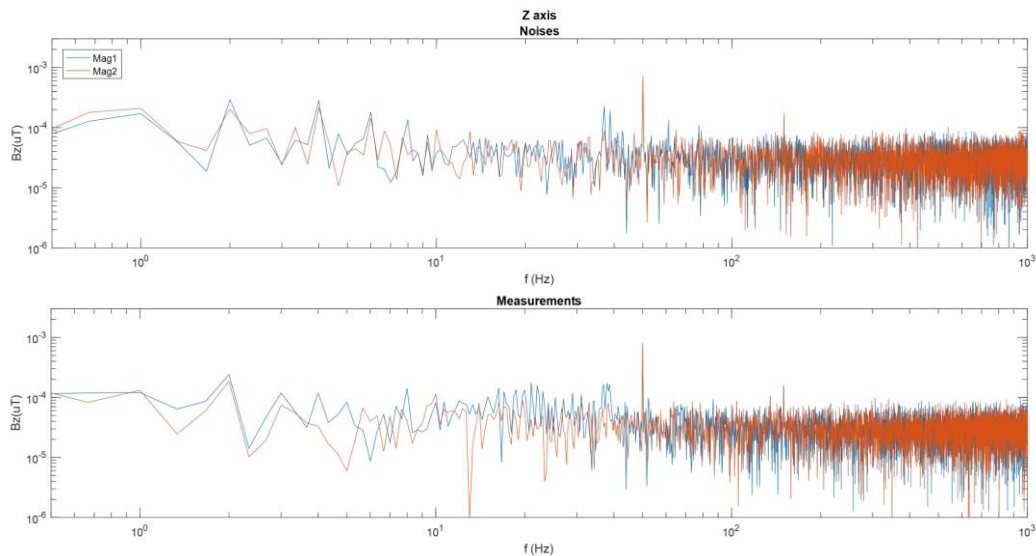


Figure 4-37. Comparison of Background-noise and Operating-link measurements of magnetometers 1 and 2 in Z axes

Link Rate=400 Mbps, Payload Size=125,000 bytes, Payload Type="Random".

Though unexpected, this observation may be due to the table's surface not being covered by an infinite conductive layer. Specifically, the linear part of the cable as well as the magnetic field sensors, are close to the table's edge. Therefore, the conductive layer's contribution to the measured field cannot be derived applying a simple method of images; a much more complex electromagnetic analysis is required where the phenomena caused by the table's boundaries are taken into account.

iv. Emission Amplitude

Regarding the amplitude of the emissions, though seeming negligible, it can be considered significant for missions with very strict magnetic cleanliness requirements. Lately, more and more missions implement stricter limits for the allowed level of interference in the magnetic field sensor's position, due to the need for studying more weak or distant magnetic phenomena and therefore even such levels of emissions can be detrimental.

Conclusion

To summarize, the design of the SpW cable assembly, namely the differential signalling and low voltage level used as well as the twisting of the wire pairs and the additional twisting of the four twisted pairs, provides the link with an almost ideal behavior regarding ELF magnetic field emissions. In particular, no significant emissions are noticed within the frequency range from 100 Hz to 1.5 kHz. Nevertheless, the appearance of spectral components within the ranges of 30-37 Hz and 60-74 Hz, regardless the transmission's characteristics, can cause significant interference, especially to instruments sensitive at those frequencies. Another aspect that should not be neglected when considering the wiring's contribution to the Electromagnetic Compatibility of a spacecraft's design, is the emergence of emissions between 10 and 100 Hz for certain combinations of link's characteristics. In addition to the latter, the relatively small amplitude of the presented emissions, in conjunction with the proximity of the magnetic field sensors to the linear part of the cable can be misleading. For instance, the magnetic field emissions may not be caused by currents flowing through the outer shield of the cable but produced either by the design of the connector or by the port's circuitry. In the two former cases, the distance of the emerging magnetic field sources from the sensors, is significantly larger than the one between the sensors and the linear part of the cable, indicating the potential existence of a larger-magnitude source than otherwise anticipated. Concerning static field emissions, the presented setup could not produce definite results due to the fluctuations of the ambient static field. The only conclusion that can be drawn is that no static emissions stronger than around 10nT are caused by the operation of the link. This topic has much to gain from the implementation of specialized magnetic shielding which will increase the differentiation achievable by the measuring layout. Moreover, the utilized link's setup, i.e. the relative positioning of the SpW link and the ground plane which simulates the spacecraft's conductive enclosure, is but one possible layout that can emerge in a spacecraft's design. Therefore, to definitively assess the ELF magnetic field emissions caused by a spacecraft's wiring, further tests must be performed with alternative link layouts and additional transmission characteristics modified, such as the packet to packet delay. As a final remark, it is the authors' conviction that the presented results can encourage further research on this topic, which is deemed necessary for a complete Electromagnetic Compatibility analysis of any spacecraft's design.

Bibliography

- [1] ECSS, Standard ECSS-E-50-12A "SpaceWire - Links, nodes, routers and networks", Noordwijk, The Netherlands: ECSS Secretariat, ESA-ESTEC, Requirements & Standards Division, 24 January 2003.
- [2] ECSS, Standard ECSS-E-ST-50-12C "SpaceWire - Links, nodes, routers and networks", Noordwijk, The Netherlands: ECSS Secretariat, ESA-ESTEC, Requirements & Standards Division, 31 July 2008.
- [3] ECSS, Standard ECSS-E-ST-50-12C Rev.1 "SpaceWire - Links, nodes, routers and networks", Noordwijk, The Netherlands: ECSS Secretariat, ESA-ESTEC, Requirements & Standards Division, 15 May 2019.
- [4] ESCC, Detail Specification No. 3902/004, ESA, European Space Components Coordination, October 2014.
- [5] ESCC, Detail Specification No. 3902/003, ESA, European Space Components Coordination, June 2008.
- [6] N. Hadjigergiou, M. Sophocleous, E. Hristoforou and P. Sotiriadis, "Magnetic Sensors for Space Applications: Development and Magnetic Cleanliness Considerations," in *Electromagnetic Compatibility for Space Systems Design*, C. D. Nikolopoulos, Ed., IGI Global, 2018, pp. 248-283.
- [7] Mag690, Low Cost Three-Axis Magnetic Field Sensor (DS2604/12), Bartington Instruments.
- [8] Operation Manual for PSU1 Power Supply Unit (OM2443/4), Bartington Instruments.
- [9] NI 6351/6353 Specifications, National Instruments.
- [10] Product Flyer, Multifunction I/O, National Instruments.
- [11] iSAFT SpaceWire Simulator Operation Manual Version 1.7, Athens, Greece: TELETEL S.A., March 2018.
- [12] ECSS, SpaceWire protocol identification ECSS-E-ST-50-51C, Noordwijk, The Netherlands: ECSS Secretariat, ESA-ESTEC, Requirements & Standards Division, 5 February 2010.
- [13] ECSS, Standard ECSS-E-ST-50-52C "SpaceWire - Remote memory access protocol", Noordwijk, The Netherlands: ECSS Secretariat, ESA-ESTEC, Requirements & Standards Division, 5 February 2010.

- [14] ECSS, Standard ECSS-E-ST-50-53C "SpaceWire - CCSDS packet transfer", Noordwijk, The Netherlands: ECSS Secretariat, ESA-ESTEC, Requirements & Standards Division, 5 February 2010.
- [15] Standard MIL-STD-461G "Requirements for the control of Electromagnetic Interference characteristics of subsystems and equipment", Department of Defence Interface Standard, 11 December 2015.
- [16] A. D. Bechrakis-Triantafyllos, A. P. Mavropoulou, C. D. Nikolopoulos, A. T. Baklezos and C. N. Capsalis, "EMC Assessment on SpaceWire Link ELF Magnetic Behavior for Modelling Purposes," in *IEEE International Conference on Applied Mathematics and Computer Science*, Athens, Greece, 2020.
- [17] H. W. Ott, *Electromagnetic Compatibility Engineering*, New Jersey: John Wiley & Sons, 2009.
- [18] NASA, Handbook NASA-HDBK-4001 "Electrical Grounding Architecture For Unmanned Spacecraft", February 17, 1998.
- [19] S. Spantideas and N. Kapsalis, "Magnetic Dipole Modeling for DC and Low Frequency AC Magnetic Fields in Space Missions," in *Electromagnetic Comatibility for Space System Design*, C. D. Nikolopoulos, Ed., IGI Global, 2018, pp. 71-114.
- [20] C. R. Paul, *Introduction to Electromagnetic Compatibility*, New Jersey: John Wiley & Sons, 2006.
- [21] C. R. Paul, "Representation of Nonperiodic waveforms," in *Introduction to Electromagnetic Compatibility*, Second ed., New Jersey, John Wiley & sons, 2006.